STUDIES ON SUBLIMED GaAs FILMS, ANODIC Al_2O_3 FILMS AND Al_2O_3/GaAs INTERFACES

by

GEORGE YAN

B.A.Sc., University of British Columbia, 1965

A THESIS SUBMITTED IN PARTIAL FULFILLMENT OF THE REQUIREMENTS OF THE DEGREE OF

DOCTOR OF PHILOSOPHY

in the Department of

Electrical Engineering

We accept this thesis as conforming to the required standard

Research Supervisor.....

.....

Members of the Committee.....

.....

.....

.....

Acting Head of the Department.....

Members of the Department

of Electrical Engineering

THE UNIVERSITY OF BRITISH COLUMBIA

June, 1970

In presenting this thesis in partial fulfilment of the requirements for an advanced degree at the University of British Columbia, I agree that the Library shall make it freely available for reference and study. I further agree that permission for extensive copying of this thesis for scholarly purposes may be granted by the Head of my Department or by his representatives. It is understood that copying or publication of this thesis for financial gain shall not be allowed without my written permission.

Department of Electrical Eng.

The University of British Columbia
Vancouver 8, Canada

Date 2 July 1970

ABSTRACT

The structural and electrical properties of sublimed GaAs films, the dielectric properties of anodic Al_2O_3 films and the electrical properties of Al_2O_3/GaAs interfaces are of interest from the viewpoint of using GaAs and Al_2O_3 films in thin-film integrated circuits.

A new method, the close-spaced sublimation (CSS) method, was developed and used to deposit GaAs films on sapphire. The effects of growth conditions on the structural properties of the films were investigated using optical and electron microscopy, an electron microprobe and X-ray diffraction techniques. Crystallites increased in size with increasing substrate temperature, from about 0.7μ to 20μ for substrate temperatures from 480 to 670°C. The degree of preferred orientation of crystallites in the films increased with increasing substrate temperature. The films exhibited <111> textures when substrate temperatures were above about 600°C. Single-crystal diffraction patterns were obtained from films deposited on substrates held at 630 to 640°C. Electron microprobe analysis indicated that the ratio of Ga to As in the films was stoichiometric to less than 2 wt %.

The as-grown heteroepitaxial films were p-type with room-temperature hole Hall mobility up to 42 cm^2/V-sec. The room-temperature resistivity ranged from 0.6Ω -cm to 1.6 x 10^5Ω-cm. The resistivity of higher resistivity films was more temperature dependent than that of lower resistivity films. The electrical properties of the films are discussed in terms of the effects of space charge regions in the grains, potential barrier at the grain boundaries, deviation from stoichiometry, and compensation of impurities. Conductivity-type conversion of the as-grown films to n-type was done by postdeposition dopant diffusion. A room-temperature electron Hall mobility of 77 cm^2/V-sec was obtained.

While transistor action and rectification characteristics were observed in thin-film insulated-gate field-effect transistors and Au-Schottky barrier

diodes made with GaAs films, better films are required before devices with characteristics competitive with bulk devices can be fabricated.

An n-type homoepitaxial film was deposited by using the CSS method. The film's electron Hall mobility varied with temperature as $T^{3/2}$, which is the form predicted by the Brooks-Herring formula for ionized impurity scattering. The room-temperature electron Hall mobility was 219 cm^2/V-sec.

A.c. bridge and step response methods were used to study the dielectric properties of anodic Al_2O_3 films. Metal/Al_2O_3/Al capacitors were made using evaporated Al films on glass which had been anodized in ammonium pentaborate dissolved in ethylene glycol. The dielectric constant and loss tangent of anodic Al_2O_3 decreased with increasing frequency over the range from 0.5 to 100 kHz. Step response currents followed a t^{-n} law. For linear dielectric response, this corresponded to $\varepsilon''(\omega)$ varying as ω^{n-1}.

Electrical properties of Al_2O_3/GaAs interfaces were studied using the metal-insulator-semiconductor (MIS) capacitance technique. Theoretical curves relating the capacitance of metal/Al_2O_3/GaAs capacitor to the d.c. voltage applied across the capacitor were calculated and plotted. These capacitance-voltage (C-V) curves then served as a basis for the interpretation of experimental C-V curves. "Fast" surface state densities greater than $10^{12}/cm^2$-eV were obtained.

TABLE OF CONTENTS

LIST OF TABLES

LIST OF ILLUSTRATIONS

ACKNOWLEDGEMENT

I am most grateful to my supervisor, Dr. L. Young, for his invaluable guidance and supervision during the course of my work. I especially thank him for the unwavering personal support and encouragements he gave me.

Grateful acknowledgement is given to the National Research Council for scholarships which allowed me to carry out this work. The research was supported, in part, by Defense Research Board contract #T79 and a National Research Council Grant #A3392.

Helpful cooperation and assistance from Dr. L.C. Brown, Dr. B. Hawbolt and Mr. A. Lacis of the Department of Metallurgical Engineering, U.B.C., is gratefully acknowledged. I also thank Mr. R. Halliwell of the Physics Department, U.B.C., for his help in obtaining Laue diffraction pictures and Mr. J. Mercier, of the Physics Department, S.F.U., for his help in doing the Talysurf measurements.

I thank Mrs. J. Larcher, Messrs. G. Anderson, H. Black, V. Loney, A. Mackenzie, E. Voth and especially Mr. J. Stuber for their valuable technical assistance and to Miss B. Harasymchuk for typing this thesis.

Finally, I thank my fellow graduate students in the Solid-State Electronics Group and my brother, James, for innumerable useful discussions and for proof-reading my thesis.

1. INTRODUCTION

Recent developments in integrated circuits have been principally on monolithic silicon, hybrid and thin-film integrated circuits. In a monolithic silicon integrated circuit, the circuit elements are connected to each other by unwanted electrical paths through the silicon substrate. Reverse biased p-n junctions are commonly used to reduce the unwanted paths. The usefulness of this method is limited by undesirable high frequency capacitive coupling effects and d.c. leakage at the junctions. Dielectric isolation is another method used. Circuit elements of an integrated circuit are electrically isolated from each other and from the polycrystalline silicon substrate by using a layer of SiO_2. This technique involves many process steps.

Good electrical isolation between circuit elements is achieved in hybrid circuits. In a hybrid circuit, discrete active elements are mounted on an insulating substrate which has thin-film or thick-film passive elements deposited on its surface. The disadvantages of hybrid circuits are increased assembly cost due to the handling of many separate components and lower reliability due to the increased number of interconnections.

Thin-film circuits with both active and passive elements deposited on the same insulating substrate have the advantages of simpler fabrication techniques and ideal isolation between circuit elements. Sputtered tantalum thin-film circuits have been successfully made and are used in increasing numbers in telephone systems. The use of thin-film circuits has been limited by the lack of an adequate thin-film active device. The most promising thin-film active device is the thin-film insulated-gate field-effect transistor. The properties of the semiconductor film, the insulator and the insulator/semiconductor interface largely determine the performance of a thin-film transistor. Thus, the study of the properties of materials and of materials processes used in device fabrication is vital to the improvement of device characteristics

and performance.

The following objectives were chosen for this thesis.

(1) To fabricate GaAs films on sapphire and study their electrical and structural properties;

(2) To study the dielectric properties of anodic Al_2O_3; and

(3) To study the interface properties of Al_2O_3/GaAs using the metal-insulator-semiconductor (MIS) capacitance technique.

CdS and CdSe have been most commonly and most successfully used in the fabrication of thin-film transistors (see, for example, Weimer 1961; Tickle 1969). At room-temperature, the electron mobility of bulk, single-crystal CdS and CdSe is about 300 and 500 cm^2/V-sec, respectively (Devlin 1967). In comparison, the room-temperature mobility of majority carriers in bulk, single-crystal n-type or p-type GaAs is 6000 or 400 cm^2/V-sec, respectively (Madelung 1964). Because of the higher carrier mobilities, devices fabricated using GaAs may have better high frequency characteristics and higher transconductances. Presently there is also interest in a new class of microwave (Gunn) devices made with bulk GaAs (Gunn 1963, Torrens 1969). The realization of thin-film microwave devices will further increase the importance of thin-film circuits. Up to now, not much information can be found in the literature on the properties of GaAs films deposited by using methods compatible with existing thin-film circuit fabrication techniques. A reason for this deficiency is that good quality GaAs films are difficult to make*. In this thesis, a different method, the close-spaced sublimation (CSS) method, is developed. This method offers several advantages over other vacuum techniques reported

---

* Since the initiation of this project (1967), significant advances in the fabrication of homoepitaxial GaAs layers have been made (1968 Symposium: GaAs). Unfortunately, the methods used are not compatible with existing vacuum techniques used in thin-film circuits (see Chapter 2).

in the literature. These techniques and the CSS method are discussed in Chapter 2.

The electrical properties of the CSS films are the most relevant to the characteristics of any device fabricated using these films. Since the structure of the films affects their electrical properties, further insight into the electrical properties of the films can be gained if information on their structural properties is available. Hence the structural and electrical properties of the CSS GaAs films are considered in Chapters 3 and 4, respectively. Included in Chapter 4 is a discussion on the postdeposition doping of CSS GaAs films on sapphire and the growth of homoepitaxial GaAs on semi-insulating GaAs. The fabrication of thin-film transistors and Au-Schottky barrier diodes using GaAs films on sapphire is also discussed.

The methods used in and the reasons for studying the dielectric properties of anodic Al_2O_3 are given in Chapter 5. The advantages and disadvantages of using Al_2O_3 as an insulator in semiconductor devices are compared with those of SiO_2.

The metal-insulator-semiconductor (MIS) capacitance technique, as used in the study of the properties of insulator/semiconductor interfaces, is a well established technique. It is simple and can be used to obtain information required to evaluate the merits of a particular insulator/semiconductor interface in so far as its field-effect properties are concerned. The use of the MIS capacitance technique to study the Al_2O_3/GaAs interface has not been seen reported in the literature. Such a study is presented in Chapter 6.

The main results of this thesis are summarized in Chapter 7. Areas for further research are also indicated.

2. CLOSED-SPACED SUBLIMATION (CSS) OF GaAs FILMS

2.1 Introduction

One of the important points that must be considered in the fabrication of compound semiconductor films is the maintenance of a stoichiometric ratio between the elements of the deposited film. Scanlon (1953) reported that non-stoichiometry in the lead-salt compound semiconductors affected their electrical properties. Similarly, the optical and electrical properties of II-VI compound semiconductors depend upon the stoichiometry of their constituent elements (Albers 1967, Devlin 1967). In the case of III-V compound semiconductors, previous work reviewed by Hilsum and Rose-Innes (1961) and Madelung (1964) indicated that no clear-cut evidence for nonstoichiometric behaviour has been observed in these compounds. Recently, however, Harris, Nannichi, Pearson and Day (1969) stated that their annealing experiments, photoluminescence data and contacting problems indicated that GaAs is not a stoichiometric compound. The concentration of Ga and As vacancies depends upon the growth conditions and the thermal treatment of the crystal after growth. Deviation from stoichiometry affects the electrical properties of GaAs. For example, a preponderance of As vacancies may change an initially low resistivity n-type sample into high resistivity n-type or into p-type.

From mass spectrometric and weight loss measurements, Arthur (1967) determined that at the melting point of GaAs (1238°C), the partial pressures of As_2, As_4, and Ga over GaAs are 0.328, 0.648 and 5×10^{-4} atm, respectively. Because of the disparate As and Ga partial pressures, the fabrication of GaAs films by evaporation from a molten source is complicated by problems of nonstoichiometry and the possible presence of excess Ga in the films. In attempting to circumvent these complications, some of the methods that have been used are:

1. Flash Evaporation Method,

2. Diode Sputtering,

3. Liquid Phase Epitaxy,

4. Vapour Phase Epitaxy and Close-Spaced Transport Method,

5. The "Three Temperature" Method, and

6. Near-Equilibrium Sublimation in Ultra-High Vacuum.

The essential features of each method will be briefly described.

2.1.1 Flash-Evaporation Method

Small grains of GaAs are continuously fed into a heater, situated inside a vacuum chamber, hot enough to volatilize completely each individual grain as it comes in contact with the heater. As will evaporate first because it is more volatile than Ga. However, if the grains are sufficiently small or if the source-to-substrate distance is sufficiently large, Ga and As vapours can condense in alternate monolayers on the substrate and recombine to form GaAs, provided the substrate is held at an appropriate temperature. For structurally good films, the substrate temperature must be high. But it must not be higher than the temperature at which As begins to re-evaporate. For Ge and GaAs substrates, this temperature was 475°C and 535°C, respectively (Richards 1963, 1966)*

2.1.2 Diode Sputtering

Sputtering as a method of making thin films is an established technique (Holland 1956). Sputtering can be either "reactive" or "physical", depending upon whether the bombarding gas ions and the cathode target chemically react with each other or not. There are many variations of the sputtering technique, with diode sputtering being the simplest (Campbell 1966). Briefly, the cathode (in this case, GaAs) is sputtered in a low pressure (10^{-2}Torr) Ar

---

* Recently, Farukhi and Charlson (1969) reported that mobilities near 0.01 cm^2/V-sec were obtained from films made by using the flash-evaporation method.

atmosphere by applying a 1 to 3 kV potential difference between the cathode and the (usually grounded) anode, where the substrate is situated. Positive Ar ions created by the discharge are accelerated toward and impinge on the surface of the cathode, ejecting atoms which eventually condense on the substrate. Molnar, Flood and Francombe (1964) sputtered GaAs on CaF_2, vitreous SiO_2 and single crystal Ge substrates. NaCl substrates were used by Evans and Noreika (1966). Electrical properties of sputtered GaAs films were not reported by any of these authors.

2.1.3 Liquid Phase Epitaxy

Two types of solution growth systems have been used in the liquid phase epitaxy of GaAs. They are the horizontal tilt tube system (Nelson 1963; Bolger, Franks, Gordon and Whitaker 1966) and the vertical steady-state system (Kang and Greene 1968). In the former method, a GaAs substrate is clamped at one end of a suitable boat (either graphite or silica) while a Sn-GaAs (or Ga-GaAs) mixture is placed at the other end. The boat is placed inside a constant temperature furnace which is tilted so that the source is lower than the substrate. The temperature inside the furnace is raised to about 640°C (or 850°C for Ga-GaAs) while H_2 is passed continuously. The furnace is tipped so that the melt runs onto the substrate and covers it. The furnace is then cooled. As the temperature drops, GaAs comes out of solution both as a homoepitaxial deposit and as a polycrystalline solid which remains suspended in the solution. At temperatures lower than 500°C, the substrate may be taken out and any excess Sn or Ga wiped off. In the vertical method, a GaAs substrate is lowered vertically onto a Ga-GaAs solution. A thermal gradient between the source and the substrate is subsequently maintained by slowly increasing the source temperature. Due to the increased solubility of Ga at higher temperature, a concentration gradient is established across the Ga solution. This

causes the transport of As from the source to the substrate. Epitaxial layers may be grown at a constant temperature by using this method.

2.1.4 Vapour Phase Epitaxy and Close-Spaced Vapour Transport Method

The underlying physical mechanisms involved in the vapour phase epitaxial growth of GaAs films are described by the following chemical reactions.

$$Ga\,X_3 + 2GaAs \rightleftharpoons 3Ga\,X + \frac{1}{2}\,As_4 \quad (X=Cl,\ Br,\ L)$$

or

$$2GaAs + H_2O \rightleftharpoons Ga_2O + H_2 + As_2$$

The reactions proceed from left to right with increasing temperature and reverse upon cooling.

Both closed tube (Moest and Shupp 1962) and open tube (Tietjen and Amick 1966) systems have been used. In the closed tube system, a GaAs source and a suitable substrate were sealed in a quartz ampoule backfilled with HCl. The source was kept at a fixed temperature in the range from 600 to 850°C. The substrate was kept at a temperature 20 to 150°C below the source temperature.

The open tube system is similar to the closed tube system except that a continuous flow of transport agent from the source to the substrate is maintained. It was found that this provided a better control over the growth processes. Appropriate dopants can also be introduced during growth. Epitaxial GaAs films with electrical properties approaching that of bulk GaAs had been fabricated using the open tube system (Effer 1965, Tietjen and Amick 1966). A disadvantage of this method is its low deposition efficiency (typically a few percent) due to the transported material condensing on surfaces other than the substrate. Deposition efficiency is defined as the ratio of the substrate weight gain to the source weight loss.

One way of improving the deposition efficiency is by placing the source and substrate very close together. Nicoll (1963) and Robinson (1963)

deposited GaAs on GaAs and Ge substrates using the close-spaced arrangement with wet H_2 as the transporting agent. Deposition efficiencies of up to 98% were reported by Robinson.

2.1.5 The "Three Temperature" Method

Assume that the vapour phase inside a vacuum chamber consists of two components A and B. Further assume that the vacuum is sufficiently high such that collisions between the component gases are negligible in the vapour phase and that interactions between them occur only within the adsorbed layer on the substrate, giving a stable compound AB. Gunther (1966) showed that at a to-be-determined substrate temperature, which has a limited range, only the stable compound can be formed at the substrate provided that

$$p_e(\frac{i}{AB}) < p_{e_i} \quad (i = A, B) \tag{2.1}$$

as the incident fluxes of A, B, (N_{+A}, N_{+B}) are varied over a range between $N_{+A}N_{+B}$ = constant and $N_{+A} = N_{+CA}$, $N_{+B} = N_{+CB}$.

In the above equation,

p_{ei} = equilibrium pressure of the ith component over its solid form.

$p_e(\frac{i}{AB})$ = partial pressure of the more volatile component i over the solid AB

N_{+Ci} = critical incident flux, above which the ith component can condense in elemental form.

For GaAs, $p_{e_{As_2}} > p_e(\frac{As_2}{GaAs})$; hence eqn. 2.1 is satisfied. Davey and Pankey (1964, 1966, 1968) had deposited GaAs on sapphire, Ge and semi-insulating GaAs. From their thermoelectric power measurements, they concluded that all the films were p-type. The lowest resistivity values measured were between 20 and 30 Ω-cm. Hall measurements were attempted. However, they did not observe Hall voltages which could be unambiguously interpreted as above the noise level of

their measuring system.

2.1.6 Near-Equilibrium Sublimation in Ultra-High Vacuum

Hudock (1967) deposited GaAs on semi-insulating GaAs by subliming a powdered charge in an essentially closed quartz vessel under near-equilibrium conditions. He showed that epitaxial films can be obtained at substrate temperatures as low as 600°C when depositions were performed in background pressures of 5×10^{-10} Torr or less. He also reported that the room-temperature mobility of a homoeptiaxial layer was 4350 $cm^2/V\text{-sec}$.

2.2 Close-Spaced Sublimation (CSS) Method

2.2.1 Introduction

The technology of vacuum-deposited passive thin films is well established (see, for example, Holland 1956; Berry, Hall and Harris 1968; Chopra 1969). This knowledge may be put to full use in thin-film integrated circuits applications if high quality semiconducting films can be fabricated by using vacuum techniques. One of the purposes of this thesis is to investigate the methods of fabricating semiconducting films which are compatible with existing vacuum techniques. For practical reasons, such methods must be adaptable to large scale production and must be economical on starting material.

The close-spaced sublimation (CSS) method was developed for it was felt that none of the reported methods satisfied the above requirements. Liquid phase epitaxy and vapour phase epitaxy have been used with considerable success in the fabrication of high quality homoepitaxial layers (1968 Symposium: GaAs).* However, these methods are not compatible with existing vacuum techniques. An additional problem of "seeding" is also raised when the liquid phase epitaxy

---

* Recently Manasevit (1968) reported the deposition of single-crystal GaAs on insulating substrates using a chemical method.

method is used to fabricate heteroepitaxial films. Insulating substrates other than semi-insulating GaAs may be more attractive for the following reasons. GaAs is brittle; greater mechanical strength, hence reduced susceptibility of the finished devices to mechanical shocks, can be provided by substrates like sapphire. Furthermore, sapphire substrates have low dielectric loss, are inert to most chemicals and do not outgas, even at elevated temperatures. Also, at the present, single-crystal semi-insulating GaAs costs US $38.50 per gram (Monsanto) while sapphire substrates cost about US $5.00 each (1/2" dia, Adolf Meller).

2.2.2 Vapour Pressures in the GaAs System

Upon heating up to temperatures below the melting point of GaAs, it dissociates as

$$2GaAs_{(s)} \rightarrow 2Ga_{(g)} + \frac{1}{2} As_{2(g)} + \frac{1}{4} As_{4(g)} \qquad (2.2)$$

Arthur (1967) used mass spectrometric and weight loss measurements of the species effusing from a Knudsen cell containing GaAs to obtain the partial vapour pressures of Ga, As_2, and As_4 over GaAs for the temperature range 900°K to 1200°K. Thurmond (1965) had constructed a similar P-T graph using the mass spectrometric data of Drowart and Goldfinger (1958) and Gutbier (1961), total pressure measurements near the GaAs melting point taken by Richman (1963), and solubility data of Koster and Thomas (1955) and Hall (1963).

The point of interest in the P-T plot is the one which corresponds to the "congruent temperature". At this temperature, Ga and As sublimes congruently, that is $p_{Ga} = 2p_{As_2} + 4p_{As_4}$. Thus, Ga and As vapours exist in a stoichiometric ratio. Arthur found that the congruent temperature was 910°K as compared to Thurmond's estimate of 933°K.

2.2.3 Principles of Operation of the CSS Method

The principles underlying the operation of the CSS method are as follows. A wafer of source material is situated parallel and close to the substrate. The source is held at or near the congruent temperature. If

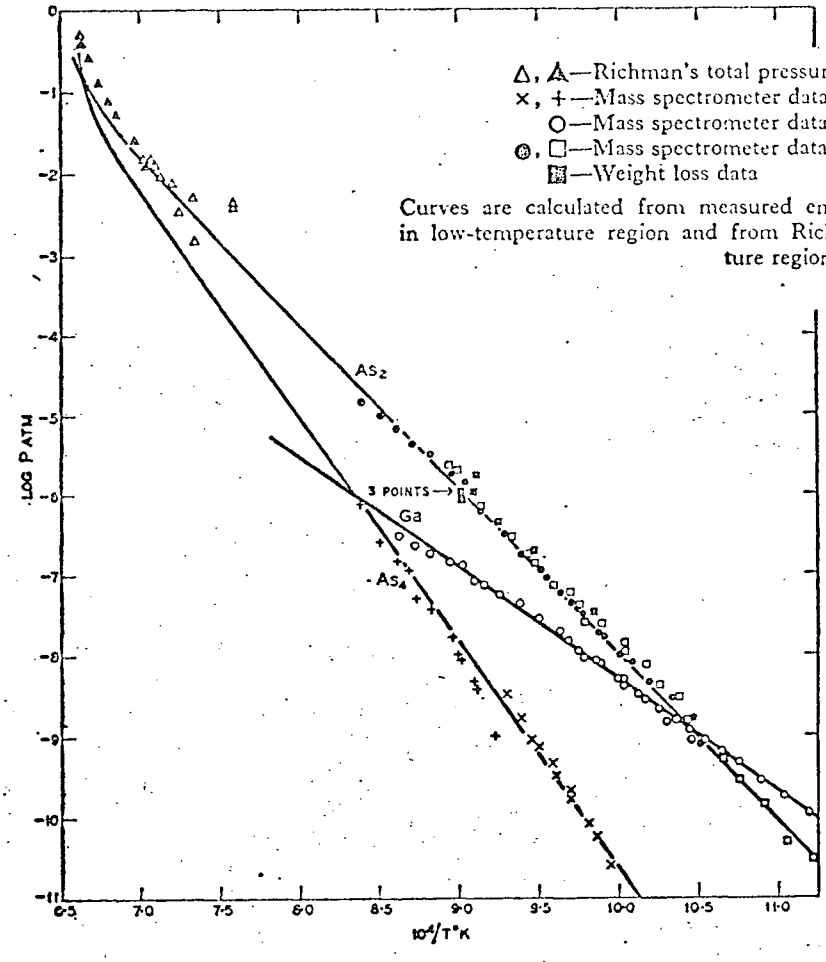

Fig. 2.1 Equilibrium pressures of As_2, As_4 and Ga over GaAs (from Arthur 1967).

a small temperature gradient is maintained between the source and the substrate, near equilibrium conditions prevail in the region bounded by them. Since Ga and As vapours exist in a stoichiometric ratio, they may condense stoichiometrically on the substrate.

Ga atoms were found to have a unity condensation coefficient on GaAs and GaP substrates, while As atoms have a condensation coefficient proportional to the Ga coverage of the substrate (Arthur 1968). Although no experimental data on the condensation coefficients of Ga and As on sapphire were found, it is reasonable to expect that the formation of GaAs on the cooler substrate surface is enhanced because of multiple collisions of Ga and As atoms with the substrate due to the close spacing, with a resultant increase in the

adatom density at the substrate.

2.2.4 Design and Fabrication of the CSS Apparatus

The following design criteria were adopted for the CSS apparatus.

(1) It must be made from materials compatible with existing high vacuum techniques.

(2) The source and substrate temperatures can be independently monitored and controlled.

(3) The heat sources must be "clean". That is, impurities emanating from the heaters must be kept to a minimum.

(4) A small spacing between the source and the substrate is desired.

(5) The source and substrate holders are to be independently supported and rotatable with respect to each other.

The last feature allows the in situ degassing of the source and substrate just prior to the actual deposition of a film. At the same time, multiple deposition on different substrates is possible.

Figures 2.2 and 2.3 show a close-up photograph of the CSS apparatus and a photograph of the CSS apparatus in the TNB vacuum system, respectively. Type 304 stainless steel, clear fused quartz and Ta sheets were used in the construction of the CSS apparatus. Two quartz iodide lamps (650 watts each, Sylvania type DWY) were used as radiant heat sources. Ta parabolic reflectors were used in conjunction with the heat sources. Temperatures were monitored by chromel-alumel thermocouples embedded in the quartz assemblies. The beads of the thermocouples were situated less than 3 mm. away from the source and the substrate. The all stainless-steel assembly can be externally rotated via a magnetically coupled drive and a 100:1 worm-gear arrangement. A cam assembly was used to achieve the close spacing which was less than 0.3 mm. The source-to-substrate distance was about 0.7 mm. when a quartz mask was used (Sec. 2.3.3).

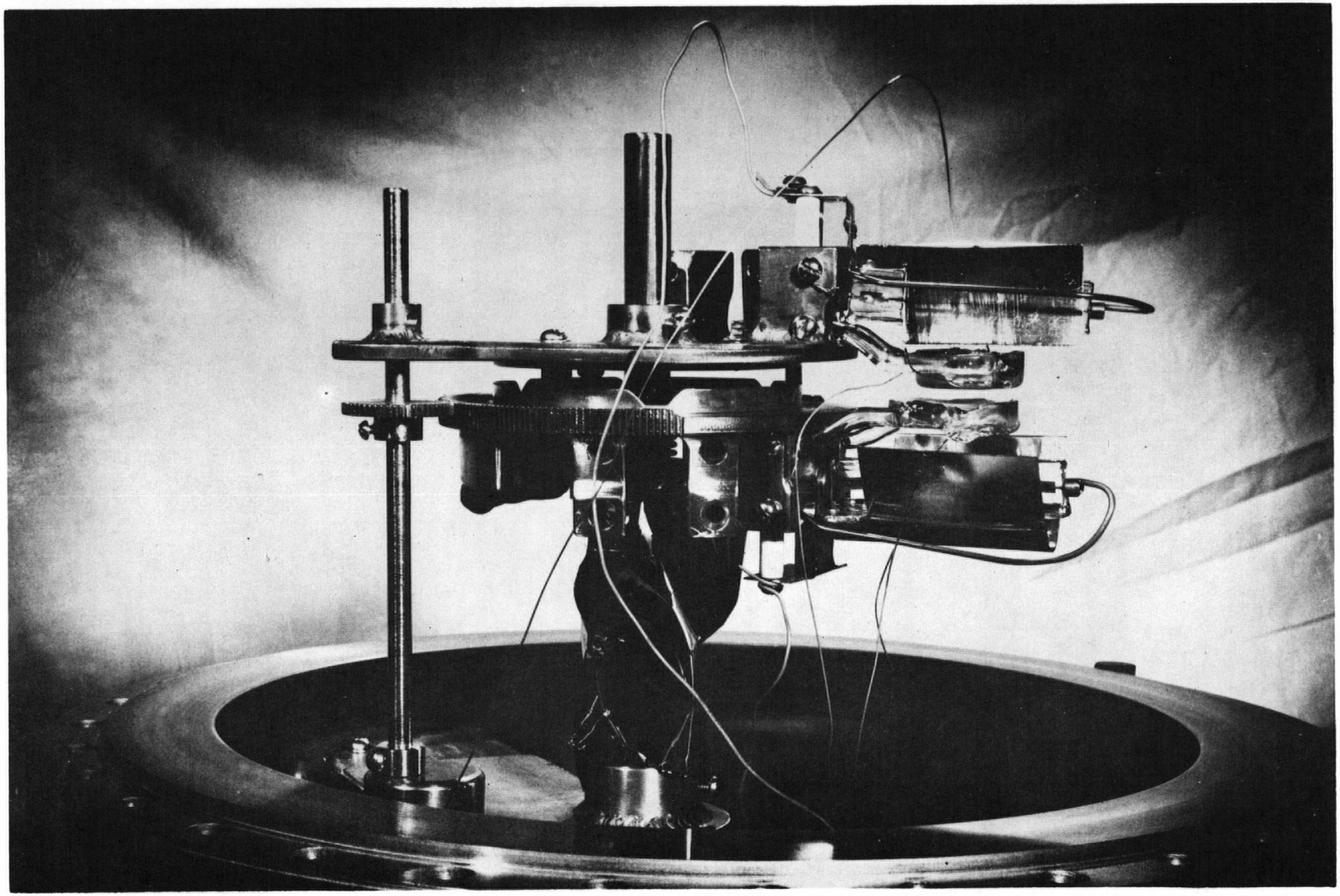

Fig. 2.2 A close-up photograph of the close-spaced sublimation (CSS) apparatus.

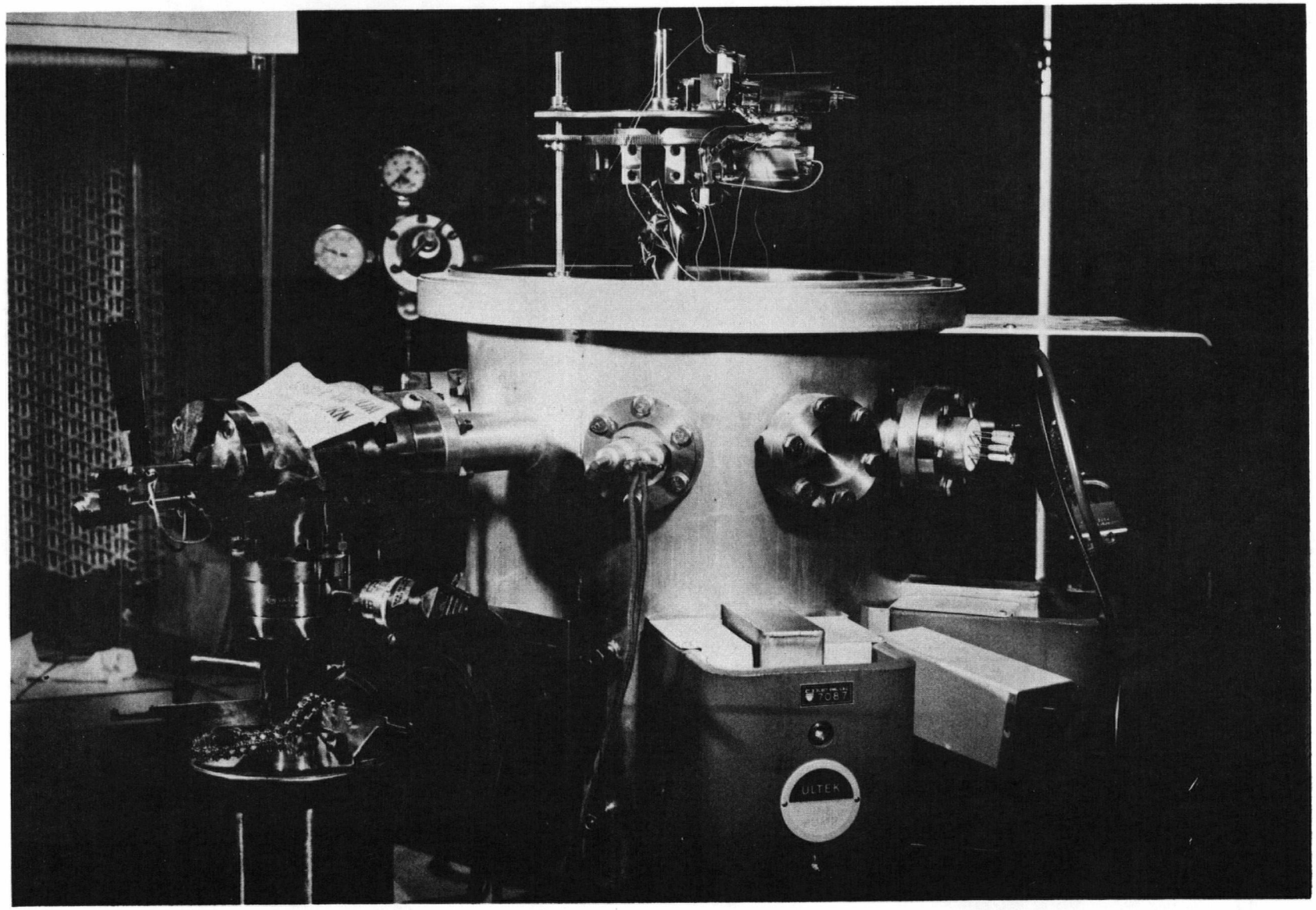

Fig. 2.3 A photograph of the CSS apparatus and the TNB vacuum system.

The CSS apparatus was mounted inside a Ultek TNB vacuum system. Roughing of the vacuum chamber was accomplished by using a molecular sieve sorption pump. This avoids hydrocarbon contamination of the chamber which is usually observed when a mechanical rotary pump is used. Final pumping was accomplished by two 50 lit/sec ion pumps plus a Ti sublimator pump, rated at 3600 lit/sec for air. Vacuum inside the chamber was monitored by using a Bayard Alpert ion gauge. Typical vacuum conditions during deposition are given in Sec. 2.3.3.

2.3 Experimental Procedures

2.3.1 Source Preparation

A wire saw was used to cut 0.5 to 1.2 mm thick slices off ingots of either mono or polycrystalline n-type GaAs crystals. The electrical properties of the sources are given in Table 4.2. Each wafer was lapped until the two faces were parallel. One face was mechanically polished, using Al_2O_3 powder, to a 0.3μfinish. Picien wax, used in mounting the sample during polishing, was dissolved away in a hot trichlorethylene bath. Just prior to loading into the vacuum system, the wafers were rinsed and ultrasonically agitated in hot trichlorethylene, hot acetone and hot propanol.* This was followed by vapour degreasing first in a Soxhlet extractor containing acetone and then in another containing propanol. The cleaning process following the hot trichlorethylene bath shall be called the standard cleaning procedure. After air drying, the wafers were chemically etched in 7 H_2SO_4(95%):H_2O_2(30%):H_2O by volume at 80°C (Northern Electric) for about 30 sec. Temperature of the etchant was maintained by using a water bath. Immediately after etching, the wafers were rinsed thoroughly in doubly-distilled water and finally placed inside a beaker containing reagent-grade propanol until ready for use.

---

* Low ultrasonic power must be used as GaAs is brittle.

2.3.2 Substrate Preparation

The effects of substrates on the quality of either homo or hetero-epitaxial semiconducting films have been extensively studied, with emphasis placed on the Si-on-sapphire technology. (See, for example, Filby and Nielsen 1967; Manasevit and Morritz 1967). A correlation was found to exist between the electrical properties of a Si film and the quality of the sapphire surface: better Si films can be grown on single crystal substrates with smooth, scratch-free surfaces. Similar results can be expected for GaAs films on sapphire.

Different methods of substrate preparation were investigated. Polishing of substrates by immersing in a 400 to 500°C orthophosphoric acid bath was attempted. A Pt cruicible was used to contain the hot orthophosphoric acid. The temperature of the acid was measured by using a thermocouple sheathed with Pt tubing and immersed in the acid. It was found that the dissolved Al_2O_3 redeposited on the sapphire surface, resulting in a rough surface finish. The polishing rate was also difficult to control.

Scheuplin and Gibbs (1960) found that while hot orthophosphoric acid removed the mechanically damaged layer successfully, even surfaces with the best orientations showed a pronounced orange-peel structure. The surface finish was difficult to reproduce, probably because the polishing action of orthophosphoric acid was temperature dependent (Filby and Nielsen 1967).

Robinson and Mueller (1966) polished sapphire using molten salt baths. They reported that at 1000°C, borax polished sapphire at the rate of about 10μ/hr. However, a film of residue was left behind on the sapphire surface. This residue was difficult to remove and degraded the electrical properties of the deposited Si layer.

Faktor, Fiddyment and Newns (1967) reported some preliminary results

on the polishing of sapphire using vanadium pentoxide at 900°C. Mechanically satisfactory surfaces were obtained. However, a pale violet film or bloom appeared on the sapphire surfaces after immersion in the V_2O_5 melt. This bloom was resistant to chemical etching. Heating in air at 1200°C for about 24 hours resulted in the disappearance of the bloom. It was not clear whether the bloom was evaporated away or diffused into the sapphire as weight changes on heating were insignificant. There is always concern that some residue is left behind on the surfaces which have been chemically polished. For this reason, chemical polishing of sapphire surfaces is undesirable (Filby and Nielsen 1967).

Hydrogen pre-firing of sapphire at about 1200°C for several hours was found to give excellent surface finish. Furthermore, the problem of residue left behind from chemical polishing is avoided. Robinson and Mueller (1967) obtained their best epitaxial Si layers on H_2 pre-fired sapphire substrates. In a private communication to Davey and Pankey, Manasevit also indicated that H_2 pre-firing of sapphire resulted in good surface finish (Davey and Pankey 1968).

Hart, Etter, Jervis and Flanders (1967) found that Si films with mobilities similar to those grown on chemically polished sapphire substrates were obtained when high quality mechanically polished substrates were used.

The substrates used in this study were Vernuille 0° sapphire (0.080" thick, 1/2" dia.; Adolf Meller) either in their as-received state or pre-fired in H_2 at about 1200°C for several (1.5 to 4.5) hours. The as-received sapphires were polished to a better than 200 Å finish (manufacturer's specifications). Prior to use, these substrates were subjected to the standard cleaning procedure.

Substrates were pre-fired in a 2.5" dia. quartz tube inside a JMC (115 volts 44 A) furnace. The temperature near the substrates was monitored

by using a chromel-alumel thermocouple sheathed with a fused quartz tube. Standard grade H_2 was introduced and monitored using a Roger Gilmart Inst. (RGI) flowmeter. The flow rate used was about 150 ml/min. The quartz tube was sealed and a positive pressure inside was maintained by venting H_2 through a Pyrex gas washing bottle containing H_2O. Substrates were cleaned following the standard cleaning procedure before H_2 pre-firing. The pre-fired substrates were introduced directly into the vacuum chamber for deposition of GaAs.

2.3.3 Sublimation of GaAs Films

Parameters which affect the films during growth are background pressure of the vacuum chamber, substrate temperature, contamination from outgassing of nearby materials and deposition rate. As a rule, the lower the background pressure, the less likely for the deposited material to getter impurities from its ambient surrounding. Typically, background pressures in the present experiments were 5 to 8 x 10^{-9} Torr, rising to 1 to 8 x 10^{-8} Torr during deposition. A possible contaminant was Si which may outgas from the quartz assemblies. However, quartz was still used for want of a better material. Because the heat lamps were sealed units, impurities emanating from the filaments may be expected to be excluded from the vacuum chamber. The vacuum gaskets and electrical leads used were made of Cu. There is always a possibility that Cu may contaminate the source material and the deposited film. This possibility was reduced by ensuring that Cu inside the vacuum chamber was not heated and away from the CSS quartz assemblies.

Source and substrate temperatures were varied between the ranges 640 to 740°C and 480 to 670°C, respectively. Their effects on the electrical and structural properties of the films will be discussed in the subsequent chapters.

The deposition rate is related to the source and the substrate temperatures and to the temperature gradient between them. Deposition rates were not monitored in situ due to experimental difficulties caused by the close source-to-substrate spacing. Nominal average deposition rate for each run was determined by measuring the total film thickness and the total deposition time. A typical deposition schedule is given in Table 2.1. A quartz mask was used to define the shape of the deposited film.

Time	Action taken and comments	Pressure (Torr)	Temperature of source (°C)	Temperature of Substrate (°C)
0_-	Source and substrate holders are initially misaligned.	5×10^{-9}	-	-
0_+	Heaters are turned on for outgassing of source and substrate.	8×10^{-9}	T_{sd} + 50	T_{sud}+100
15 min.	Heating power adjusted until source and substrate temperatures are near desired deposition temperatures.	8×10^{-9}	$\simeq T_{sd}$	$\simeq T_{sud}$
16 min.	Source and substrate holders are aligned. Source and substrate temperatures are set at deposition temperatures. Start sublimation.	8×10^{-9} to 5×10^{-8}	T_{sd}	T_{sud}
3 hrs.	Source and substrate temperatures are lowered at the rate of about 10 degrees per minute.		T_{sd} and T_{sud} are the source and substrate temperatures, respectively, chosen for the particular run.	
3.5 hrs.	Heating power turned off.			

Table 2.1 A typical CSS deposition schedule for GaAs films.

2.3.4 Film Thickness Determination

Three methods were used in determining the thickness of the deposited films. For films less than 0.2μ thick, a sloan Angstrometer (accurate to about ±150 Å) was used. A monochromatic light source (Na yellow, λ = 5890 Å) is used and Fizeau fringes of equal spacings are produced by multiple reflections from a highly reflecting surface. The reflecting surface was obtained by depositing a thin (about 1000 Å) layer of Al. The film thickness is determined by measuring the Fizeau fringe displacement across a film-substrate step and

$$t = \frac{d}{D}\frac{\lambda}{2} \qquad (2.3)$$

where

t = film thickness

d = fringe displacement

D = fringe step

λ = wavelength of monochromatic light

This is illustrated in Fig. 2.4.

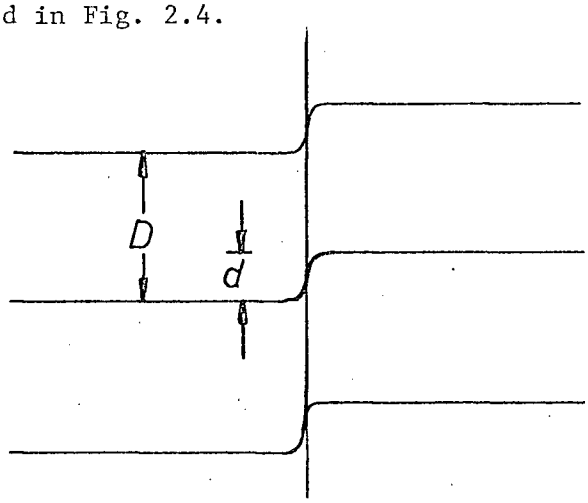

Fig. 2.4 Displacement of the Fizeau fringes due to a film-substrate step

The other two apparatuses used were the dial gauge and the Talysurf. They are primarily mechanical devices. The dial gauge is accurate to ±5μ. The Talysurf is, from the manufacturer's specifications, accurate to ±3% full scale for the ranges from 0.5 to 100μ full scale. This method consists of

simply measuring, with respect to a reference plane, the amplified mechanical movement of a stylus as it traverses a film-substrate step. Because the surface of the film and the reference plane are not necessarily coplanar, a correction procedure must be used to determine the true film thickness. This correction method has been described by Berry, Hall and Harris (1968). A limitation on the use of the Talysurf lies in that the thicknesses of a film at a distance greater than the stylus to heel distance (about 2 mm) from the film-substrate step cannot be measured accurately since the heel will ride on the film rather than on the substrate surface.

A typical Talysurf scan of GaAs films is shown in Fig. 2.5.

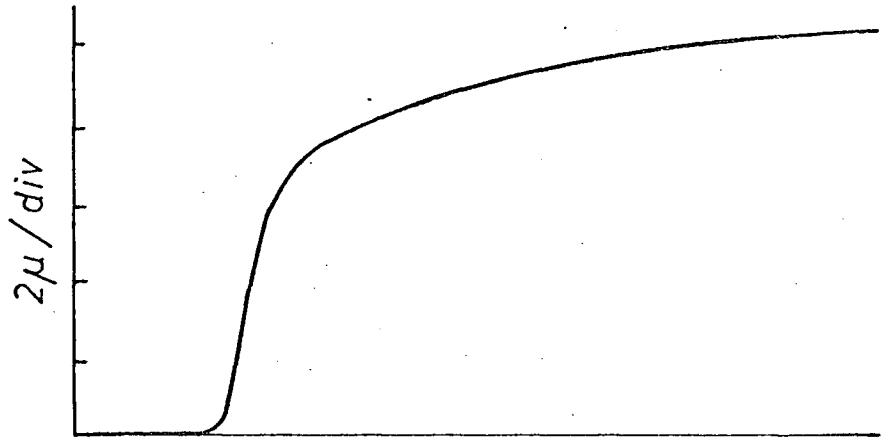

Fig. 2.5 A typical Talysurf scan across a GaAs-substrate step

3. STRUCTURAL PROPERTIES OF CSS GaAs FILMS ON SAPPHIRE

3.1 Introduction

The GaAs films were studied using optical and electron microscopy, an electron microprobe and X-ray diffraction techniques. The observed structural properties of these films are discussed and compared with the published results on sputtered films (Molnar, Flood and Francombe 1964, Evans and Noreika 1966), flash evaporated films (Muller 1964, Richards 1966), vapour phase epitaxial films (Joyce and Mullin 1966; Tietjen, Abrahams, Dreeben and Gossenberger 1968) and films produced by the "three temperature" method (Davey and Pankey 1964, 1966, 1968).

3.2 Optical Microscope Observations

Metallic droplets were observed at the edge of a 600°C film when the source-to-substrate distance was greater than about 1 mm. This is shown in Fig. 3.1. Their appearance suggests a lack of As at the substrate surface due probably to As vapour escaping from the region bounded by the source and substrate. The As loss left behind elemental Ga. Free Ga is a metal which may exist in the liquid state near room-temperature (melting point = 29.78°C). It adheres to the sapphire surface extremely well. Molnar, Flood and Francombe (1964) noticed that a mixture of Ga and polycrystalline GaAs was present on the surface of their sputtered films when substrate temperatures were higher than 580°C. This was a result of As loss at the films due to re-evaporation. To reduce the loss of As vapour from the source-substrate region in the CSS system, a source-to-substrate spacing of less than 0.7 mm was used in all subsequent runs. No evidence of liquid-like, rounded droplets was present in the films produced under the stated experimental conditions (see Sec. 2.3.3).

Joyce and Mullin (1966) reported that growth features, which look like "pyramids", were observed on homoepitaxial layers of GaAs. From electron

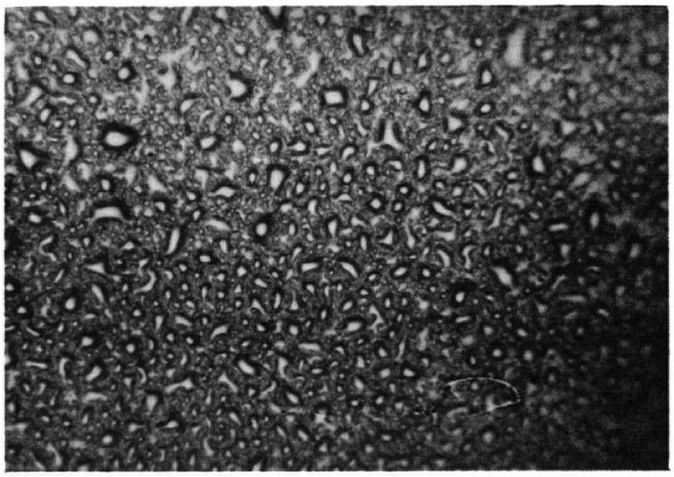

Fig. 3.1 Droplets of liquid Ga on a GaAs film.

microprobe studies, they found that the "pyramids" formed at the sites of free Ga droplets. Similar growth features were not observed in the CSS films. This would suggest that Ga droplets sufficiently large enough to initiate the formation of growth "pyramids" were not present at the substrate surface of the CSS films. Electron microprobe studies confirmed this observation (see Sec. 3.3.2).

Films obtained with substrate temperatures in the range from about 600 to 670°C were shiny and metallic grey in colour. Dull grey films were obtained when substrate temperatures were in the range from 480 to about 580°C.* The "shiny" films were composed of relatively large crystallites which were visible under low (x30) magnification. Faceting was well developed. The

---

* Due to the close spacing between the source and substrate, the actual surface temperature of the substrate depends on the intensity of radiation of the source heater. No sharp demarcation substrate temperature was found above which "shiny" films were produced and under which "dull" films were produced. The stated temperatures can only be taken as apparent rather than actual temperatures at the substrate surface and at the source material.

shininess of these films may be due to the high reflectivity of the facet faces. No surface features were discernible in the "dull" films under the same magnification. The surfaces of the "dull" films appeared to be smoother than the surfaces of the "shiny" films. It was quite evident that the particle size of the "shiny" films was larger than the particle size of the "dull" films. This is expected because the particle size of most films condensed from the vapour phase increases with increasing substrate temperature which increases the surface mobility of adatoms and clusters during deposition.

Microphotographs of both as-grown and chemically etched surfaces were taken using a Reichert metallurgical microscope. Not many surface features were seen on a 580°C film when magnified 1420 times. However, faceting was developed and was seen on films grown at substrate temperatures higher than 600°C. These are shown in Fig. 3.2. The crystallites were quite uniform in each CSS film. This would suggest that the temperature was fairly uniform across the substrate surface where the GaAs was deposited during each sublimation run. The grain size of the 580°C film was estimated to be about 0.4 to 2μ. The 600°C film had grains about twice as large. Twinning in some of the larger crystallites was evidenced by the presence of parallel lines within the grains. This is illustrated in Fig. 3.3, which is a photograph of an etched 670°C film. The as-grown film was mechanically polished to a 0.5μ finish and then etched for about 15 sec. in a freshly prepared grain-boundary-revealing etch. The composition of the etchant was $8H_2O$:H_2O_2 (30%): H_2SO_4 (95%) by volume (Cunnell, Edmond and Harding 1960). The parallel edges of the twin bands indicate that these were growth twins which arose probably due to stacking faults in the film during growth.

A 630°C film which manifested numerous "120°" growth features is shown in Fig. 3.4. This structure appears similar to the top view of an

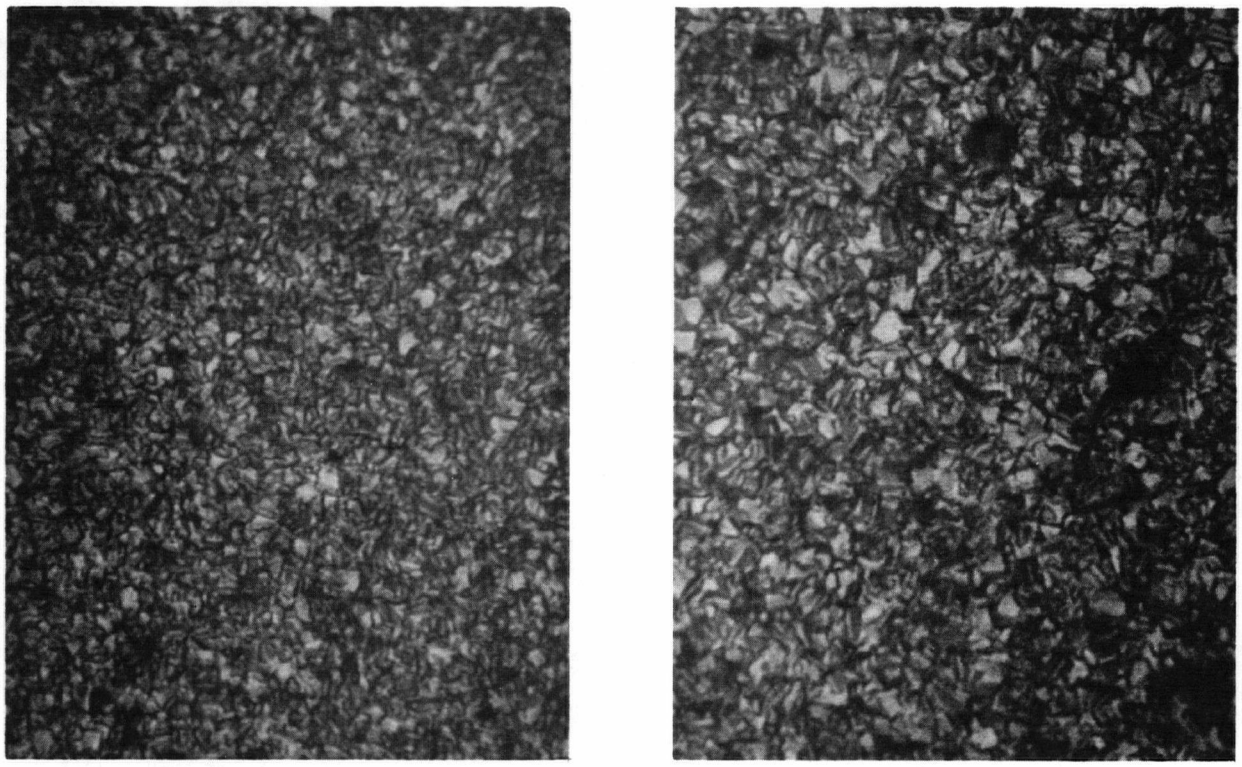

580°C (#2)

10μ

600°C (#4)

Fig. 3.2 Optical photomicrographs of GaAs films deposited at different substrate temperatures.

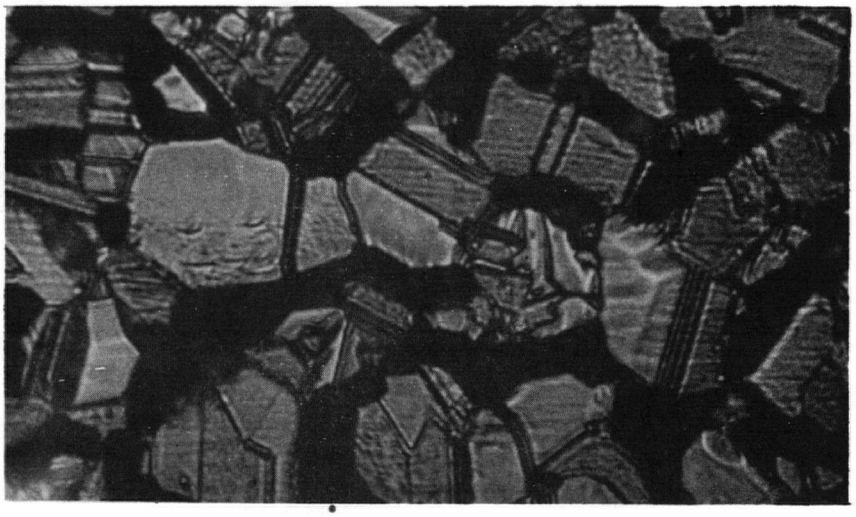

670°C (#42)

10μ

Fig. 3.3 Optical photomicrograph of an etched film.

equilateral tetrahedron which has its basal plane parallel to the plane of the photograph. Three lighter coloured ridges intersect at the apex and each two adjacent ones subtend a 120° angle. These growth features appear to possess a three-fold symmetry which would be consistent with the symmetry properties of the <111> direction of a zincblende structure.

630°C(#12) 10μ

Fig. 3.4 Optical photomicrograph of a film with "120°" growth features.

3.3 Electron Probe Microanalysis

3.3.1 The Electron Microprobe

The electron microprobe allows the X-ray spectrochemical analysis of small samples. (See, for example, McKinley, Heinreich and Wittry 1966; Castaing, Deschamps and Philibert 1965). Colby (1968) had analyzed and determined the stoichiometry of thin (>350 Å) dielectric films such as the oxides and nitrides of Si, Al and Ta. Kyser and Wittry (1966) studied the cathodoluminescence of GaAs using the electron microprobe. Lubkin and Sutkowski (1966) determined the composition of epitaxial layers of AlAs-GaAs. Joyce and Mullin (1966) used the electron microprobe to confirm the presence of Ga droplets at growth "pyramids"

on vapour phase epitaxial layers of GaAs.

A description of the electron microprobe was given by Birks (1963). The electron microprobe consists essentially of three systems. The first is an electron optics system, similar to that of an electron microscope, which focuses a beam of electrons (about 0.1 to 0.3μ in diameter) onto the surface of the sample. Due to the impinging electrons, the emission of X-rays and other physical processes occur. These processes, together with the methods of obtaining information from the specimen are depicted pictorially in Fig. 3.5. The second is an X-ray optics system which is used to analyse the X-rays emitted by the sample. Both qualitative and quantitative results can be obtained. The third is a viewing system which allows the operator to see and to choose the sample area under test.

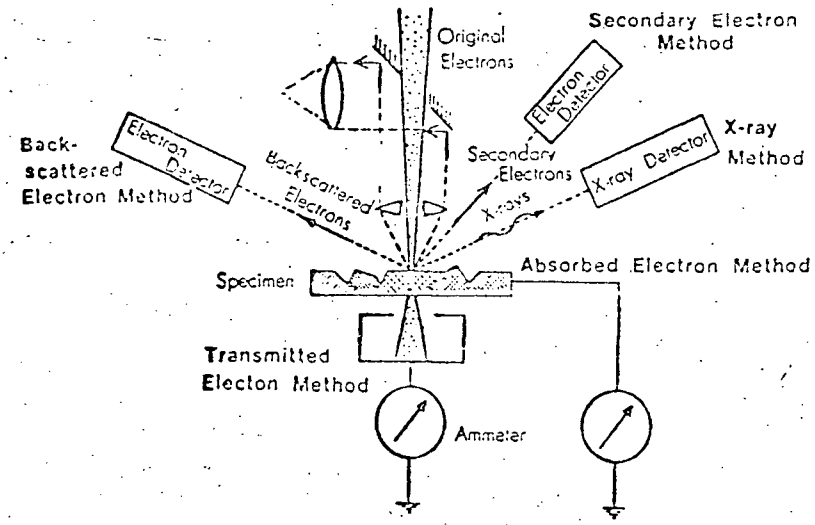

Fig. 3.5 Schematic illustration of methods used in obtaining information from a specimen using the electron microprobe

The electron microprobe was used to obtain X-ray counts and scans, and surface topographies of CSS GaAs films.

3.3.2 X-Ray Counts and Scans

Under ideal operating conditions, the detection sensitivity* of a probe

---

*The detection sensitivity is derived from statistical considerations. For significant results, 90% of the X-ray counts, for a typical peak to background count ratio of 1000 to 1, must lie within $N-3\sqrt{N}$ and $N+3\sqrt{N}$, where N is the number of counts.

is 0.03%. The practical detection sensitivity for elements with atomic numbers 11 to 21 and 33 to 37 is 0.1 to 1%, and is 0.01 to 0.1% for elements with atomic numbers 22 to 33, 38 to 74 and 82 to 92. The atomic numbers of Ga and As are 31 and 33, respectively. The accuracy* of the JX3-3A probe was placed at 1 to 2% (Dept. of Metallurgy, U.B.C.). The presence of trace impurities in concentrations of less than 1 part per 100 cannot be adequately detected by using the electron probe. However, gross inhomogeneities such as impurity inclusions, dust particles or Ga droplets with volumes $\geq 2\mu^3$ can be detected.

CSS films were polished to a 0.5μ finish and scanned. No gross inhomogeneities and impurities in concentrations greater than $10^{20}/cm^3$ were observed. All the identifiable peaks were due to Ga and As. For purposes of comparison, a single crystal GaAs standard was scanned. Quartz and mica crystals were used to detect the X-ray emissions of Ga and As, respectively.

An indication of the relative composition of Ga and As in the CSS films can be obtained by recording their respective X-ray counts and comparing them with those obtained from a GaAs standard. Correction factors due to matrix absorption, fluorescence and atomic number correction were assumed to be the same for both the CSS films and the GaAs standard. Correction due to the "dead time", t_D, of the proportional flow counters was taken into account by applying

$$C_{true} = C_{meas}/(1-C_{meas}\ t_D) \qquad (3.1)$$

where

c_{meas} = recorded counts per second

t_D = dead time of counter (4μ sec.)

c_{true} = true counts

---

* The accuracy of the probe is defined as

$$\%\text{accuracy} = \frac{\left|(\text{concentration of element A})_{actual} - (\text{concentration of element A})_{meas}\right|}{(\text{concentration of element A})_{actual}} \times 100$$

Assume that I_{Ga}, I_{As} and I°_{Ga}, I°_{As} are corrected (for dead time) average number of Ga and As counts of the film and standard, respectively. A number, r, can be defined as

$$r \stackrel{d}{=} (I_{Ga}/I_{As})/(I^{\circ}_{Ga}/I^{\circ}_{As}) \qquad (3.2)$$

where

$r = 1$ implies that Ga and As exist in a stoichiometric ratio in the film;

$r < 1$ implies that the film is Ga deficient;

and $r > 1$ implies that the film is As deficient.

One of the reasons for defining r as above is that it is not necessary to know the effects of matrix absorption, fluorescence and atomic number of the elements on the X-ray counts. Their effects all cancel out. The bounds on the values of r for the different cases, however, must be modified to take into account equipment and operator errors. As was mentioned, the accuracy of the probe is about 2%. Apart from this, X-ray counts depend on surface flatness. A 1% change in flatness results in a 3% change in the calculated weight percent (Brown, Dept. of Metallurgy, U.B.C.). Errors due to surface conditions can be reduced by using adequate preparation techniques and by taking the average of several consecutive counts at each area over several areas on the same sample. Errors due to instabilities in the probe is reduced by counting the standard before and after probing a film. Within the limits of the equipment, the modified bounds on r are 1 ± 0.02, $r < 0.98$, $r > 1.02$ for the cases of stoichiometry, Ga deficient and As deficient, respectively.

CSS GaAs films were examined, taking into account the precautions mentioned. All the films were found to be stoichiometric within the limits imposed by this method.*

---

* Apart from electrical measurements, a standard method of determining the presence of trace impurities in semiconductors is emission spectroscopy. The stoichiometry of most compounds can be determined by quantitative chemical analysis (Kroger 1964). These methods entail the destruction of the specimen under test.

3.3.3 Surface Topography

The surface topography of films grown with substrates held at different temperatures is shown in Fig. 3.6. The electron microprobe topographs revealed more surface features than the optical photomicrographs in Sec. 3.1. The "120°" growth features discussed in conjunction with Fig. 3.4 are apparent in Fig. 3.6c. Particle size of the films as a function of substrate temperature was estimated and tabulated in Table 3.1.

Sample	Substrate Temperature (°C)	Particle size (μ)	Obtained from
41	480	0.3 to 1	electron probe topograph
40	580	1 to 2.5	electron probe topograph
2	580	0.4 to 2	optical photomicrograph
4	600	1.5 to 4	optical photomicrograph
12	630	3 to 8	optical photomicrograph
39	650	3 to 10	electron probe topograph
42	670	16 to 20	electron probe topograph

Table 3.1 Particle size as a function of substrate temperature

3.4 Reflection Electron Diffraction Observations

Reflection electron diffraction (RED) photographs of CSS films were taken using a Hitachi HU-11B electron microscope. The camera constant, λL, was determined to be 2.3198 Å-cm at 50 kV and 1.6035 Å-cm at 100 kV. An evaporated gold film was used as the standard.

The degree of preferred orientation of crystallites in the films increased with increasing substrate temperature. Arcing in the Debye rings of

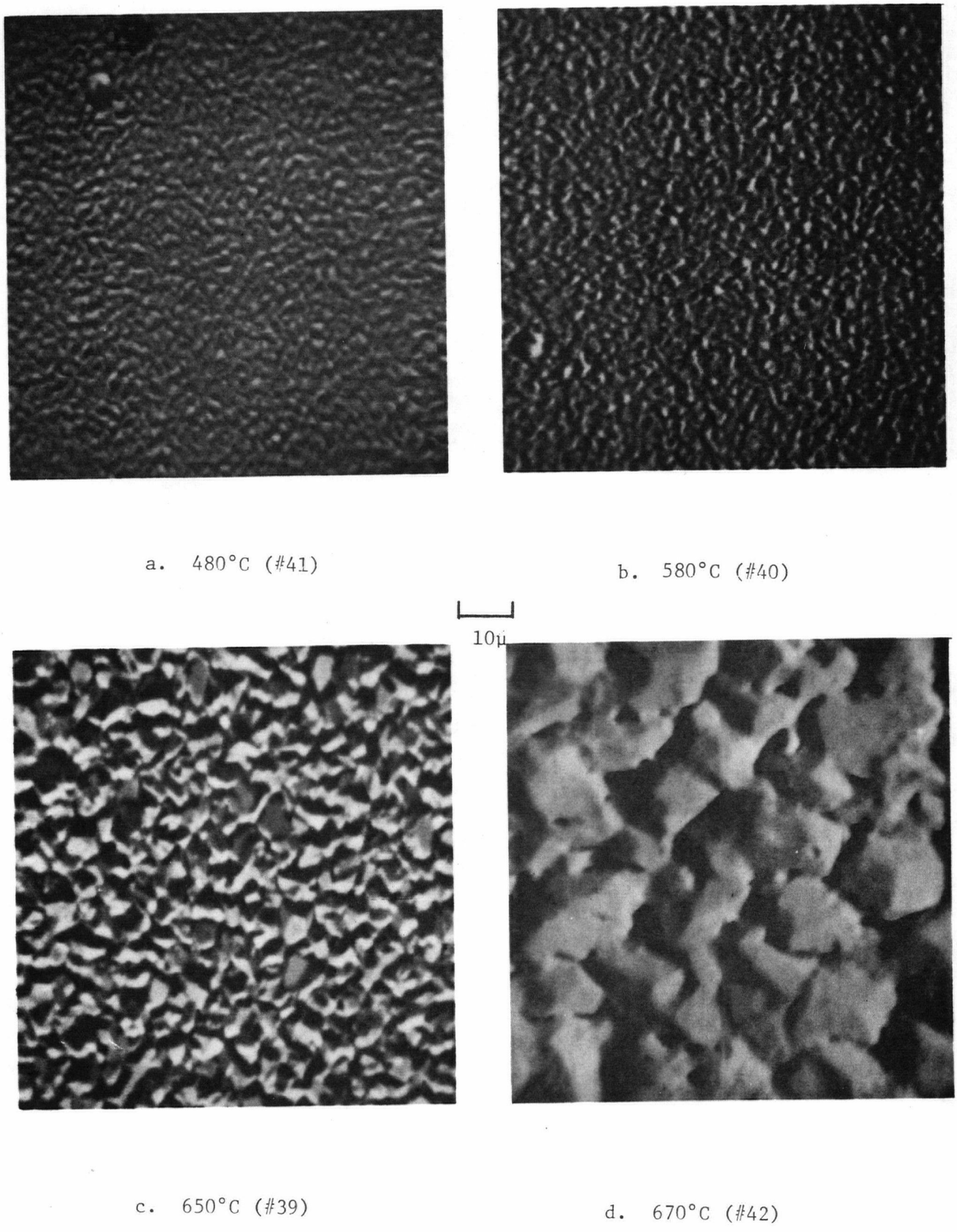

a. 480°C (#41)

b. 580°C (#40)

c. 650°C (#39)

d. 670°C (#42)

Fig. 3.6 Electron microprobe topographs of films deposited at different substrate temperatures.

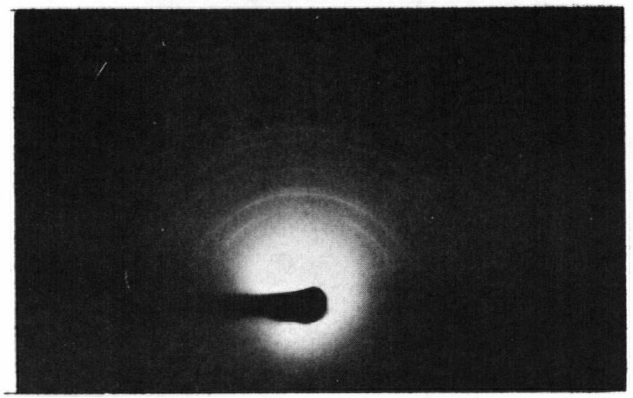

a. 580°C (#5)

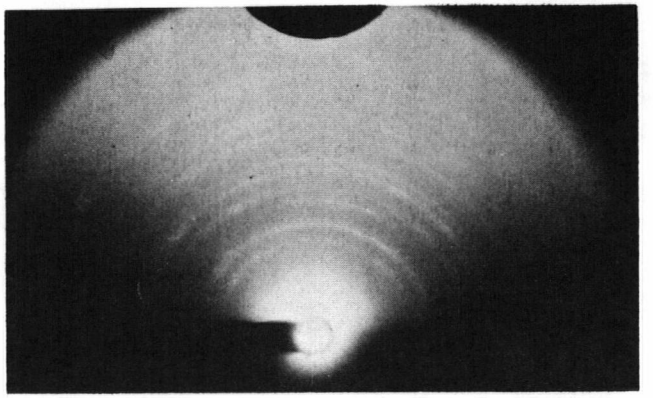

b. 600°C (#4)

c. 610°C (#15)

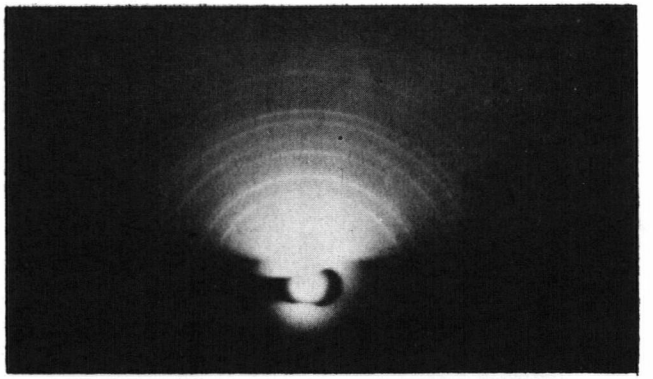

d. 620°C (#3)

Fig. 3.7 Reflection electron diffraction patterns of GaAs films deposited at different substrate temperatures.

films deposited at substrate temperatures higher than 600°C indicated that these films were preferentially oriented. Single crystal diffraction patterns were observed on 630 and 640°C films. Fig. 3.7 shows the RED patterns of CSS films deposited at different substrate temperatures. For purposes of comparison, line drawings of the RED patterns of fcc (face centred cubic) and hcp (hexagonal close pack) GaAs and free Ga are reproduced in Fig. 3.8.

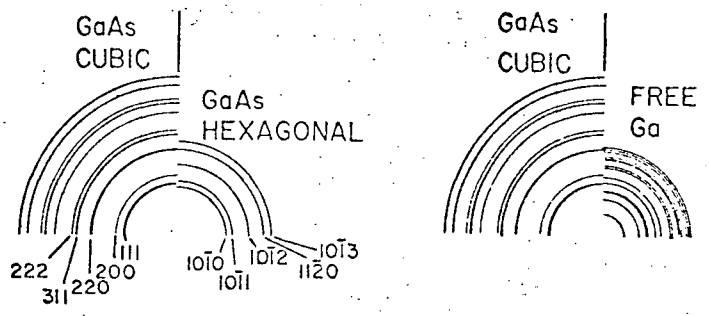

Fig. 3.8 Line drawings of RED patterns of fcc and hcp GaAs and free Ga (from Pankey and Davey 1966).

Debye rings found in the RED patterns were indexed using the relationship (Hall 1966)

$$\lambda L = r\, d_{hk\ell} \tag{3.3}$$

where

r = radius of Debye ring

$d_{hk\ell}$ = d spacing of the diffracting plane (hkℓ).

The d values for most of the lower order {hkℓ} planes are tabulated in ASTM standards. Alternatively, the d value for a specific (hkℓ) plane of a cubic crystal can be calculated from

$$d^2 = a^2/(h^2 + k^2 + \ell^2) \tag{3.4}$$

a = lattice constant of the unit cell. (For GaAs, a = 5.65 Å at room temperature).

Results of the indexed films are tabulated in Table 3.2.

Since GaAs has a zincblende structure, the diffraction spots were indexed by proceeding as follows (Howie 1965, Alderson and Halliday 1965)

Sample	Substrate temperature (°C)	Ring number*	d spacing
5	580	1	111
		2	(200)
		3	220
		4	311
		5	400
4	600	1	111
		2	220
		3	311
15	610	1	111
		2	220
		3	311
		4	331
		5	422
3	620	1	111
		2	220
		3	311
		4	(222)
		5	400

* Rings are numbered consecutively beginning with the first visible ring nearest the beam spot.

Table 3.2 The d-spacing of Debye rings

Three noncollinear spots, including the centre (beam) spot, were chosen. The lengths of the vectors $\bar{g}_1$ and $\bar{g}_2$, from the centre spot to spots 1 and 2, were measured. The d values were calculated using the relationship $\lambda L = d|\bar{g}|$, where λL is known. A total of 48 combinations of $(h_1\ k_1\ \ell_1)$ and $(h_2\ k_2\ \ell_2)$ are possible. The correct sets were obtained by comparing the measured and the calculated planar angle ϕ_{12}.

$$\cos \phi_{12} = \frac{\bar{g}_1 \cdot \bar{g}_2}{\sqrt{(\bar{g}_1 \cdot \bar{g}_1)(\bar{g}_2 \cdot \bar{g}_2)}}$$

$$= \frac{h_1h_2 + k_1k_2 + \ell_1\ell_2}{\sqrt{(h_1^2 + k_1^2 + \ell_1^2)(h_2^2 + k_2^2 + \ell_2^2)}} \qquad (3.5)$$

Having determined $(h_1\ k_1\ \ell_1)$ and $(h_2\ k_2\ \ell_2)$, the normal to the cross-grating $\bar{n} = [u, v, w]$ can be obtained from

$$\begin{aligned} \bar{g}_1 \cdot \bar{n} &= h_1 u + k_1 v + \ell_1 w = 0 \\ \bar{g}_2 \cdot \bar{n} &= h_2 u + k_2 v + \ell_2 w = 0 \end{aligned} \tag{3.6}$$

where $\bar{n}$, $\bar{g}_1$, $\bar{g}_2$ form a right-handed set of axes and

$$\begin{aligned} u &= k_1\ell_2 - k_2\ell_1 \\ v &= \ell_1 h_2 - \ell_2 h_1 \\ w &= h_1 k_2 - h_2 k_1 \end{aligned} \tag{3.7}$$

The RED pattern of a 630°C film is shown in Fig. 3.9. The dominant spots were indexed and are shown in the accompanying schematic drawing. The zone axis was $[0\ \bar{1}\ \bar{1}]$. This is one of the prominent cross-grating patterns of an fcc structure.

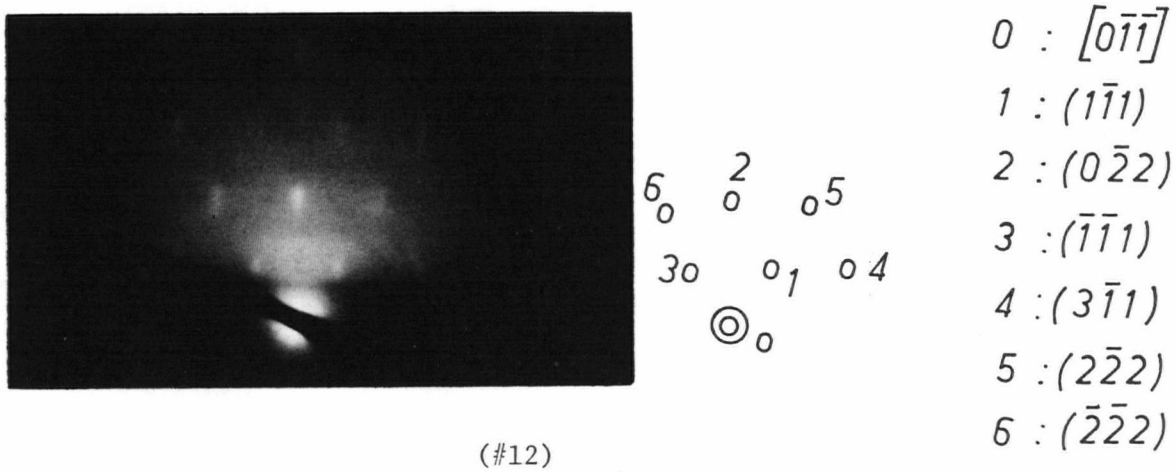

(#12)

Fig. 3.9 Single-crystal RED pattern of a 630°C film.

Kikuchi bands, which indicate that the film has a high order of angular perfection, were observed in the RED pattern of a 640°C film (see Fig. 3.10).

A hexagonal modification of GaAs was reported by Muller (1964) and by Davey and Pankey (1966, 1968). Precipitation of free Ga on Al_2O_3 was also reported by the latter authors. Extra diffraction lines which can only be indexed as due to free Ga were observed by them. Examination of the RED patterns of the CSS films did not reveal any lines other than those which belong to and were indexed as zincblende GaAs. Since wurtzite GaAs is metastable, its absence in the CSS

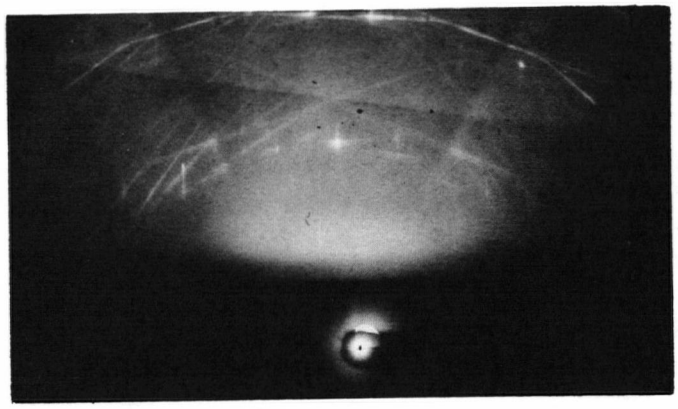

(#14)

Fig. 3.10 Kikuchi bands in a 640°C film.

films may be due to the following reasons. The substrate temperatures used were relatively high (480 to 670°C) compared to those used by Muller (410 to 500°C) and Davey and Pankey (450 to 500°C). The higher substrate temperatures result in higher surface mobility of adatoms thus preventing the formation of the metastable structure. Because of the small temperature gradient between the source and substrate, no sharp quenching occurs at the substrate surface. Quenching may occur if the deposition rate is sufficiently fast. This further minimizes the formation of the metastable wurtzite phase. Martinuzzi (1966) found reflections due to excess Ga in all the films he deposited at substrate temperatures above 470°C. Laverko, Marakhonov and Polyakov (1966) found that GaAs whiskers grown in an excess of Ga exhibited RED rings due to polycrystalline wurtzite GaAs. On the basis of these and their own observation that polycrystalline films deposited above 450°C exhibited extra RED lines due to free Ga and that GaP films and whiskers grown under excess Ga exhibited the wurtzite modification, Davey and Pankey stated that the existence of the wurtzite modification may be causally related to a non-equilibrium structure associated with an excess of Ga either in the deposition beam and/or due to special conditions at the substrate. As an

example of the latter case, free Ga may nucleate preferentially at scratches on the substrate surface. In the case of the CSS films, near-equilibrium conditions established in the region bounded by the source and substrate due to their close spacing may reduce the loss of As, resulting in less free Ga. Thus, the absence of the wurtzite structure in CSS films is consistent with electron microprobe and (see later) X-ray results that no free Ga was to be found in the CSS films.

3.5 X-Ray Diffraction Analysis

Information obtained from standard RED techniques is limited by the fact that only the surface layers of the films are characterized. Differences in geometrical arrangements between the RED and X-ray apparatuses and longer penetration depths of X-rays enable X-ray measurements to present a picture of the structure of the underlayers of the films.

3.5.1 Diffractometer Measurements

Diffractometer scans of the films indicated that the strength of the <111> texture increased with increasing substrate temperature. All the identifiable peaks were indexed to be those of zincblende GaAs. If a wurtzite modification is present, a weak $(1\ 0\ \bar{1}\ 0)$ peak should appear at $2\theta = 25.75°$ (Pankey and Davey 1966). Because of its weak intensity, this peak may be swamped by the background noise and its presence undetected when diffraction scans are taken at high speeds. Consequently, low speed (0.25°/min) scans were taken in the 2θ range between 24.5° and 27°. No $(1\ 0\ \bar{1}\ 0)$ peaks were seen. Since the $(1\ 0\ \bar{1}\ 0)$ reflection was absent, higher order reflections would probably be also absent. This was true for these films.

The ratio, I_r, of the intensities of the (111) and (220) reflections of a powdered GaAs sample is 1.1 (ASTM standards). For the CSS films, I_r ranged from 2.35 to infinity (i.e. 220 peak absent). I_r may be taken as an index of the extent of texturing in the films. In contrast with sputtered and "three temperature" films, which exhibited either <110> or <111> textures, depending upon

deposition conditions, only <111> textures were observed in the CSS films produced under the present experimental conditions. From the appearance of the GaAs growth form (Wolff 1956) and from calculations for the diamond structure (Stranski and Kaischew 1931), Molnar, Flood and Francombe determined that the GaAs (111) plane has the lowest specific surface energy. Occurrence of the <111> orientation may be explained by the theory of Kaischew and Bliznakow (1948) that crystals growing on a structureless base must present one of their equilibrium surfaces to the substrate. The crystal must be able to grow by two-dimensional nucleation in a plane parallel to the substrate. The initial layer arises as two-dimensional nuclei of the equilibrium face. Subsequent crystal growth will rest on such a face. Since the order of preference of the equilibrium faces does not appear to be temperature dependent, it is supposed that GaAs crystallites nucleate on inactive substrates {111} planes parallel to the surface. However, surface adsorption at the substrate may modify the order of importance of the equilibrium faces. Since the (110) face is also an equilibrium face of GaAs, the effect of adsorption may be sufficient to produce <110> orientations at lower substrate temperatures. The background pressure used in the CSS method was 5×10^{-9} Torr as compared with 10^{-6} and 10^{-7} Torr for the sputtering (Molnar, Flood and Francombe 1964) and "three temperature" (Davey and Pankey 1968) methods, respectively. The absence of <110> orientations in the CSS films may indicate that the substrates used in this work were "cleaner" than those used in sputtered and "three temperature" films.

The particle size, t, can be estimated by measuring the width, B (in radians), at $\frac{1}{2} I_{max}$ of the most intense peak of a diffractometer scan and applying the Scherrer formula (Cullity 1959)*

$$t = 0.9 \lambda/(B \cos \Theta_B) \qquad (3.8)$$

---

* Another method that is commonly used is a Fourier-Stokes type analysis (Warren and Averbach 1950).

where λ is the wavelength of the incident X-ray. For a Cu target, it is 1.54 Å. The corresponding Bragg angle is Θ_B. The particle sizes were estimated to range from about 250 Å to 770 Å for substrate temperatures in the range 480 to 600°C. Under normal operating conditions, no incident beam is perfectly parallel or monochromatic. These deviations from ideality and the mosaic structure of the films render the Scherrer formula, at best, a rough estimate of the true particle sizes. A better estimate can be obtained from optical photomicrographs or electron microprobe topographs. This was done in Sec. 3.3.

3.5.2 Back Reflection Laue

The Bragg angle, Θ_B, of a Debye ring in back reflection Laue pinhole photographs is given by (Cullity 1959)

$$\mathrm{Tan}(\pi - 2\Theta_B) = \frac{V}{2D} \qquad (3.9)$$

where V = diameter of the Debye ring

D = specimen to film distance (3.0 cm.)

Because of the position of the photographic plate with respect to the sample in the back reflection Laue method, only high angle reflections are recorded. This limits its usefulness in the analysis of texturing in the GaAs films. For polycrystalline samples, back reflection Laue pinhole photographs can give qualitative information regarding the relative "degree of crystallinity" of the films. The more crystalline the films, the less diffuse the Debye rings. Arcing of the Debye rings implies preferred orientation in the specimen. As the crystallites increase in size, the Debye rings become more "grainy". Fig. 3.11 show Debye rings of films deposited at different conditions. As expected, the Debye rings of lower substrate temperature (480 to 580°C) films were diffuse. "Grainy" Debye rings were observed in a 650°C film while arced rings were observed in a 660°C film.

A 630°C and a 640°C film exhibited single-crystal Laue patterns having most of the prominent spots consistent with those of the cross-grating of [111]

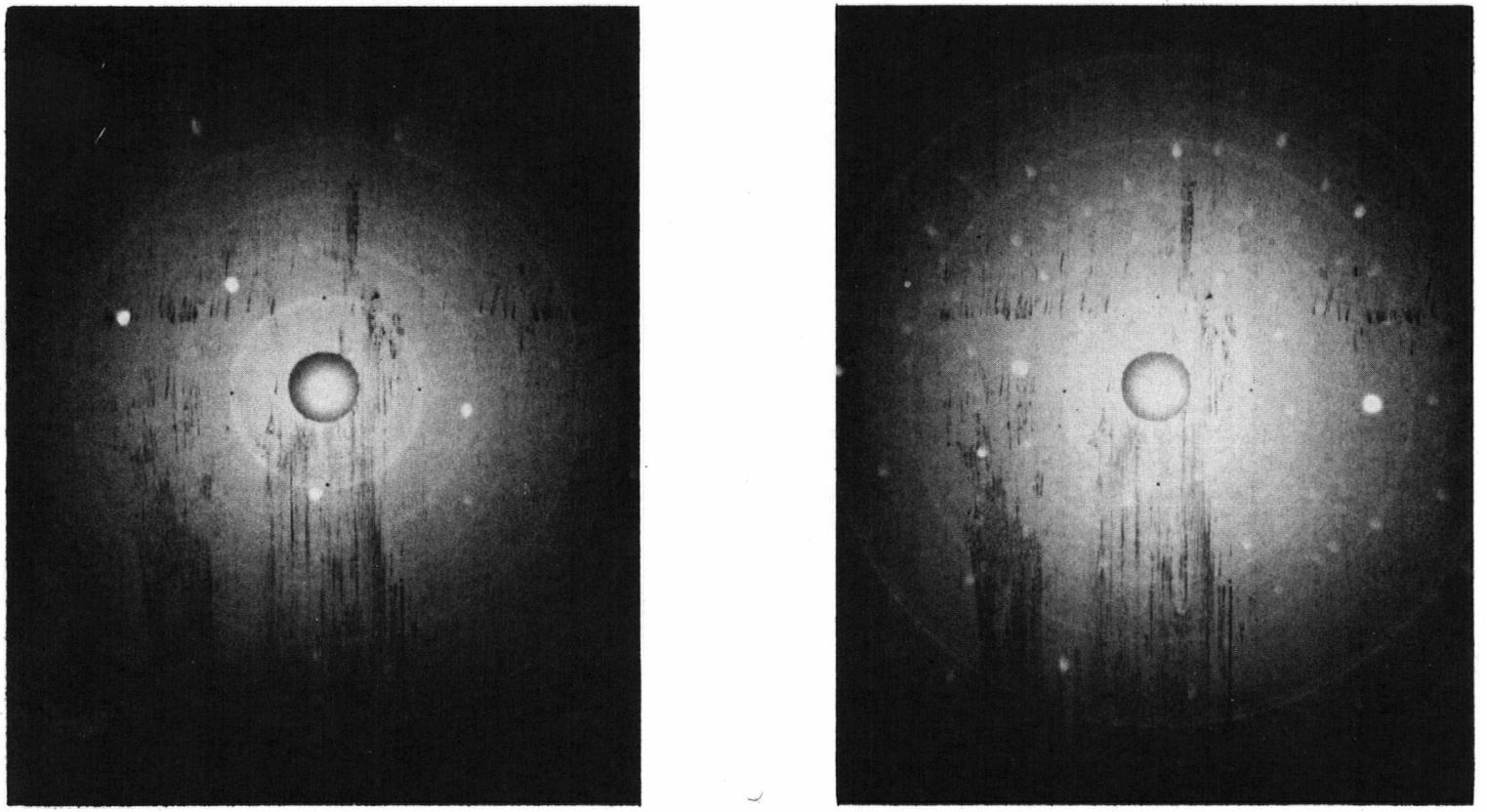

480°C (#41)

580°C (#40)

Fig. 3.11a Back reflection Laue diffraction patterns of GaAs films.

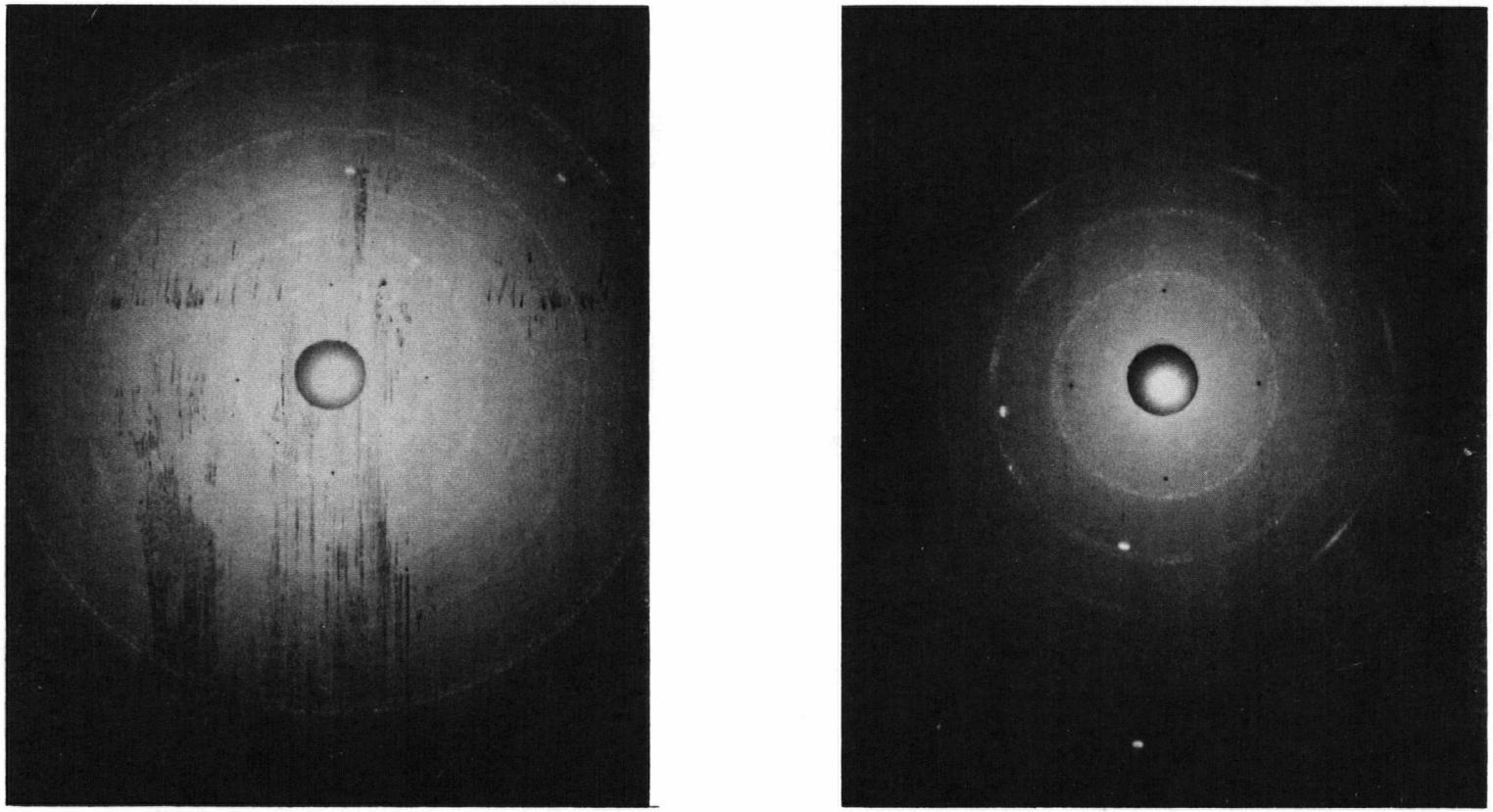

650°C (#39)

660°C (#24)

Fig. 3.11b Back reflection Laue diffraction patterns of GaAs films.

GaAs perpendicular to the substrate surface. These were compared with a [111] projection for GaAs adapted from Manasevit (1968) and are shown in Figs. 3.12a and 3.12b.

3.6 Summary and Discussion

Results from RED X-ray analysis indicated that texturing in the CSS GaAs films increased with increasing substrate temperature. <111> textures were observed in films deposited on substrates held at temperatures above 600°C. Single-crystal Laue patterns, with most of the prominent spots consistent with the pattern of a (111) GaAs plane parallel to the substrate, were observed on 630 to 640°C films. In contrast with GaAs films deposited using other vacuum techniques, only <111> textures were observed in the CSS GaAs films. An explanation for the occurrence of <111> textures is that it is energetically most favourable for {111} GaAs planes to form on a substrate since these planes have the lowest specific surface energy.

Because of the constraints imposed by the present CSS apparatus, the deposition rate cannot be varied independently nor monitored easily. For this reason, substrate temperature was the main parameter used to identify the different films. Crystallites ranged from 0.3 to 20μ wide. Larger crystallites were obtained with higher substrate temperatures. This is because higher substrate temperature lends itself to providing activation energy for adatoms to occupy postions of potential minima; enhancing recrystallization due to the coalescence of islands by increasing surface and volume diffusion; and lowering supersaturation which allows the adatoms sufficient time to reach equilibrium positions (Chopra 1969). Higher substrate temperature also aids in the desorption of adsorbed surface contaminants. All CSS films were deposited on substrates which had been outgassed in situ by raising the temperature about 100°C higher than the deposition temperature.

The abnormal wurtzite phase was not observed in the CSS films. Excess

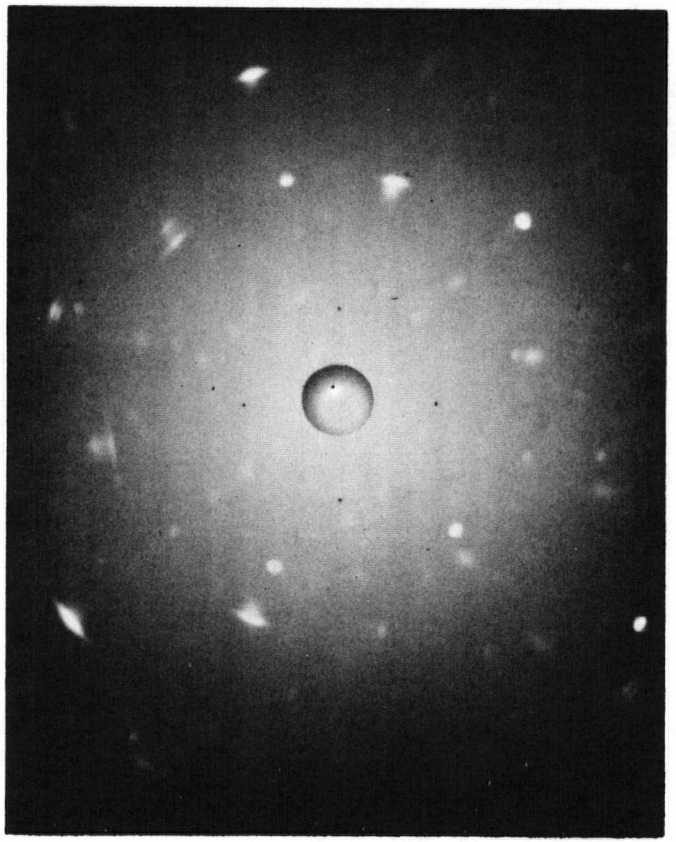

640°C (#21)

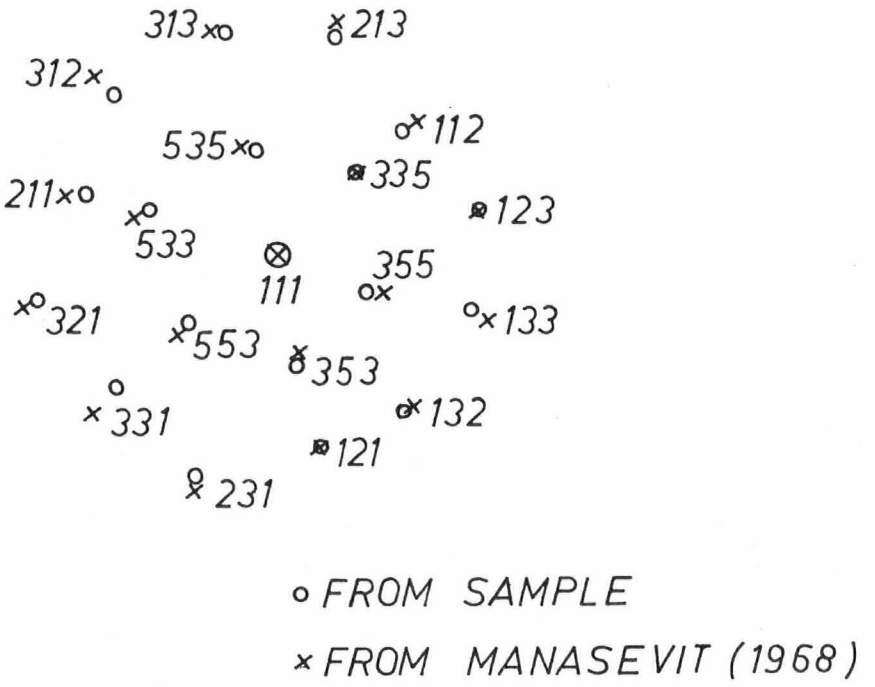

Fig. 3.12a Single-crystal Laue diffraction pattern of a 640°C film.

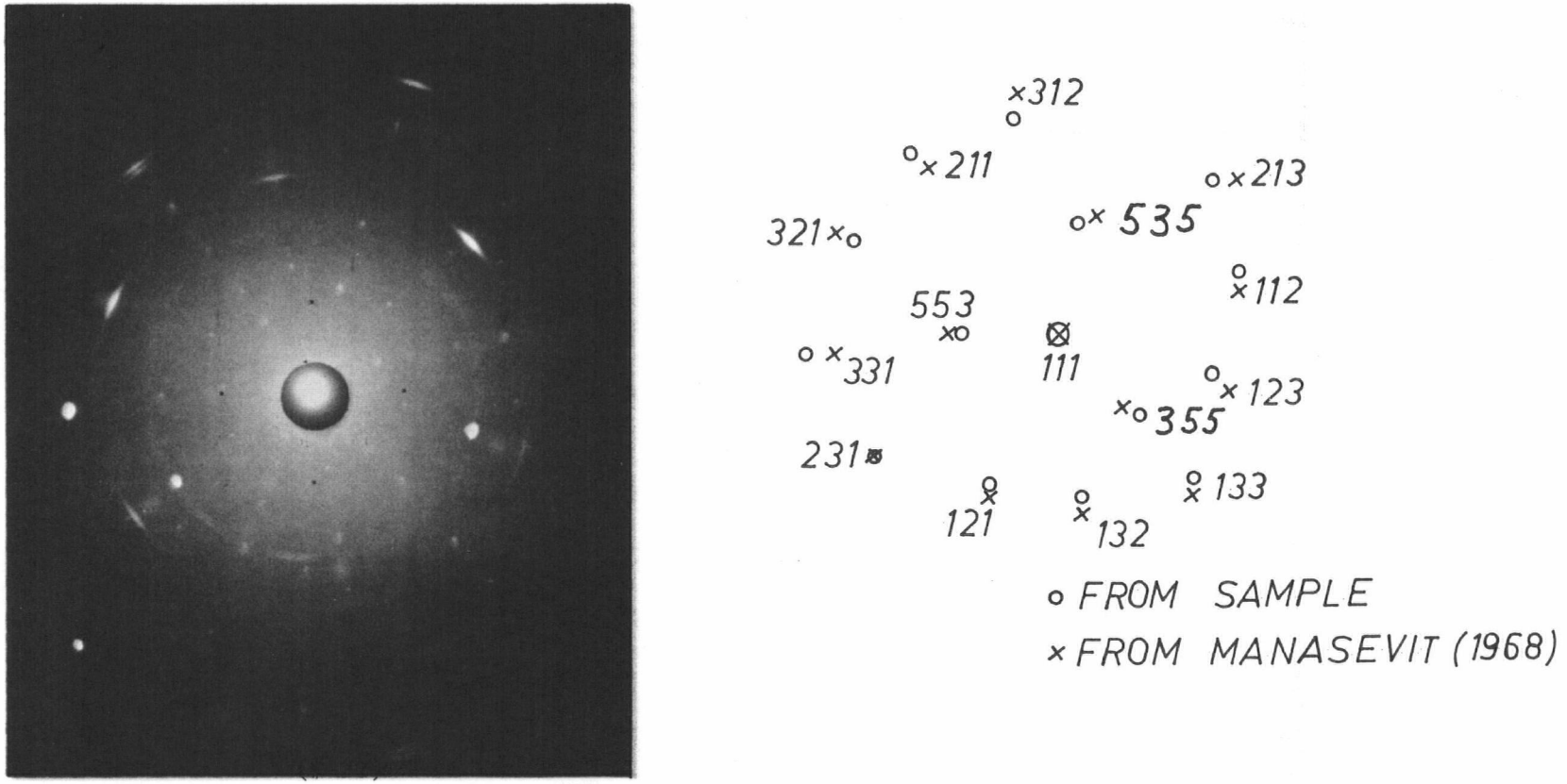

Fig. 3.12b Single-crystal diffraction pattern of a 630°C film.

Ga was not found when the source-to-substrate distance was less than about 0.7 mm. No excess Ga, due to re-evaporation of As from the deposit, was observed in all the CSS films. The highest substrate temperature used was 670°C. In comparison, Richards (1966) reported loss of As in flash-evaporated films at substrate temperatures above 535°C while Molnar, Flood and Francombe (1964) reported that As re-evaporated from sputtered films at substrate temperatures above 580°C.

The formation of the abnormal, metastable wurtzite structure has been observed in vacuum deposited GaAs films (Muller 1964, Davey and Pankey 1966, Farukhi and Charlson 1969). Nonstoichiometry, due to excess Ga, can cause the formation of the metastable wurtzite phase in GaAs (Davey and Pankey 1968, Chopra 1969). It would appear that the non-existence of the wurtzite phase and the undetected presence of excess Ga in the CSS films indicated that these films were stoichiometrically better than the films produced by other vacuum techniques.

4. ELECTRICAL PROPERTIES OF CSS GaAs FILMS

4.1 Introduction

In this chapter, a brief review is first given on the theory of carrier transport coefficients of bulk semiconductors based on the Boltzmann transport equation. The electrical properties and the effects of different scattering mechanisms on the carrier mobility in bulk GaAs are discussed. The electrical properties of CSS GaAs films are then discussed in terms of the important scattering mechanisms in GaAs, the films' polycrystalline structure, compensation of impurities, and of deviation from stoichiometry.

Thin-film insulated-gate field-effect transistors are fabricated on the as-grown films. Conversion of the as-grown p-type films to n-type is considered. Au-Schottky barrier diodes are made on a converted film.

The reasons for studying GaAs films on sapphire were given in Sec. 2.2. In order to find out the effects of using a different substrate, a CSS GaAs film on semi-insulating GaAs was grown and its electrical properties studied.

4.2 Carrier Transport Theory: A Brief Review

The Boltzmann Transport Equation (BTE) is solved for the case of n-type carriers in homogeneous semiconductors. Under certain restrictive assumptions, expressions for the one-dimensional isothermal electrical conductivity, isothermal Hall coefficient and Hall mobility are (see Appendix 4.1)

$$\sigma = \frac{4nq^2}{3\pi^{1/2}} \frac{\alpha(kT)^{\gamma}}{m^*} \int_0^{\infty} \eta^{\gamma+3/2} e^{-\eta} \, d\eta \tag{4.1}$$

$$R_H = -\frac{3\pi^{1/2}}{4} \frac{1}{nq} \frac{\Gamma(2\gamma + \frac{5}{2})}{\Gamma^2(\gamma + \frac{5}{2})} \tag{4.2}$$

$$\mu_H = \frac{q}{m^*} \alpha (kT)^{\gamma} \frac{\Gamma(2\gamma + \frac{5}{2})}{\Gamma(\gamma + \frac{5}{2})} \tag{4.3}$$

A major assumption is that the carriers are elastically scattered and the rate of change of the distribution function due to scattering is given by

$$\left(\frac{\partial f}{\partial t}\right)_{scat} = \frac{f-f_o}{\tau} \tag{4.4}$$

where the relaxation time, τ, has the form αE^{γ}. In the case where more than one scattering mechanism are operative, their effects may be taken into account by using an effective relaxation time given by

$$\frac{1}{\tau} = \sum_i \frac{1}{\tau_i} \tag{4.5}$$

The corresponding effective mobility is

$$\frac{1}{\mu} = \sum_i \frac{1}{\mu_i} \tag{4.6}$$

For the special case where a mean free path, ℓ, can be defined independent of energy

$$\ell \stackrel{d}{=} \tau v \tag{4.7}$$

$$\tau = \alpha E^{-1/2} \tag{4.8}$$

Equation 4.1 reduces to the same expression as obtained from the Drude-Lorentz theory and is

$$\sigma = nq \mu_{drift} \tag{4.9}$$

where

$$\mu_{drift} = \frac{4}{3} \frac{q\ell}{(2\pi m^* kT)^{1/2}}$$

The corresponding Hall coefficient and Hall mobility are given by

$$R_H = -\frac{3}{8} \frac{\pi}{nq} \stackrel{d}{=} -\frac{r}{nq} \tag{4.10}$$

$$\mu_H \stackrel{d}{=} |R_H|\sigma = \frac{3\pi}{8} \mu_{drift} \tag{4.11}$$

Equations 4.1, 4.2, 4.3 and 4.9, 4.10, 4.11 are also applicable to p-type semiconductors when the appropriate expressions of τ and m^* are used.

4.3 Electrical Properties of Bulk GaAs

The assumption $\tau = \alpha E^{\gamma}$ is valid only if the change in the energy of the scattered carrier is small compared to its initial energy. Howarth and Sondheimer (1953) showed that in the case of polar semiconductors such as GaAs, no relaxation time can be assumed if the energy absorbed or emitted by an electron is not small when compared with its initial energy. Since carriers in very pure (carrier concentration less than 10^{15} cm^{-3}) GaAs are strongly scattered by optical phonons, no relaxation time can be assumed for the optical phonon scattering process except at high fields and/or at temperatures higher than the Debye temperature Θ_D (Conwell 1967). The Debye temperature is defined by $\Theta_D \triangleq \frac{\hbar\omega_\ell}{k}$ where ω_ℓ is the longitudinal fundamental optical frequency of the lattice. Equation 4.5 is also not applicable. The mobility-limiting mechanism for both electron and holes in pure GaAs is polar optical scattering. At room temperature, the calculated electron and hole mobility are 10,400 and 520 cm^2/V-sec, respectively (Hilsum 1966).

For relatively pure n-type samples, ($n = 2.2 \times 10^{16}$ cm^{-3}), Ehrenreich (1960) showed that a combination of polar optical and ionized impurity scattering limits the mobility of electrons. The graph of electron mobility versus temperature is given in Fig. 4.1. The mobility can be approximated by

$$\mu \sim (m^*)^{-3/2} T^{1/2} \tag{4.12}$$

Rosi, Meyerhofer and Jensen (1960) analyzed the dependence of hole mobility on temperature in pure ($p \sim 4 \times 10^{16}$ cm^{-3}) GaAs. A good fit of their experimental data was obtained when the mobility due to optical phonons was

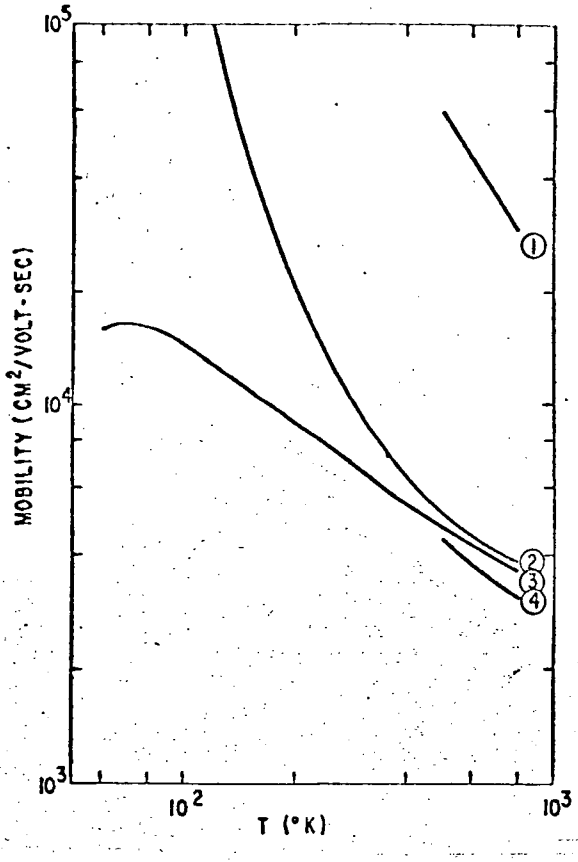

Calculated curves:

(1) deformation potential scattering;

(2) screened polar scattering;

(3) combined polar and charged impurity scattering ($n_I = 2.2 \times 10^{16}$ cm^{-3});

(4) combined polar, charged impurity, and deformation potential scattering, including effects of non-parabolic conduction band.

Fig. 4.1 Electron mobility in GaAs versus temperature (from Ehrenreich 1960).

given by

$$\mu_{opt} = 435\left(\frac{T}{295}\right)^{-2.3} \text{ cm}^2/\text{V-sec} \qquad (4.13)$$

Little information is available on p-type GaAs while extensive investigation on n-type GaAs has been and is being conducted. The main reason for focussing attention on n-type GaAs is that electrons are much more mobile than holes in GaAs. This makes n-type GaAs attractive as a starting material for devices.

For impure samples of either conductivity type, the dominant scattering mechanism is ionized impurity scattering. The mobility due to this process was given by Brooks (1955) as

$$\mu_i = \frac{2^{\frac{7}{2}} \pi^{-\frac{3}{2}} (kT)^{\frac{3}{2}} \varepsilon^2 q^{-3} (m^*)^{-\frac{1}{2}}}{n} \left[\ln\left\{\frac{6m^*(kT)^2\varepsilon}{\pi q^2 \hbar^2 n(2 - \frac{n}{N_D})}\right\}\right]^{-1} \qquad (4.14)$$

An equivalent expression of the mobility μ_i, which is more convenient for later use, was given by Hilsum and Rose-Innes (1961) as

$$\mu_i = \frac{3.2\times10^{15}(m_o/m^*)^{\frac{1}{2}}\varepsilon^2 T^{\frac{3}{2}}}{N_A + N_D} \left[\log\left\{\frac{1.3\times10^{14} T^2 \varepsilon (m^*/m_o)}{n}\right\}\right]^{-1} \qquad (4.15)$$

where n is the carrier concentration, ε the dielectric constant, N_D and N_A are the concentration of ionized donors and acceptors and m^* is the effective mass. The concentrations are per cm^3. The effective mass of electrons, light and heavy holes of GaAs at 300°K is 0.068 m_o, 0.12m_o and 0.5m_o, respectively (Sze 1969). The mass of an electron is m_o.

The resistivity and the Hall mobility of carriers in p-type and n-type single crystal GaAs as functions of impurity concentration at 300°K were given by Sze and Irvin (1968). They analyzed the most accurate and up-to-date experimental data using a least-square method. Their graphs are reproduced in Fig. 4.2. A $\pm$25% scatter in the Hall mobilities was quoted. It can be seen that the mobilities decrease with increasing impurity content in the semiconductor, as predicted in eqn. 4.15.

Acoustic mode intravalley scattering is relatively unimportant in GaAs. Other scattering mechanisms like electron-hole, electron-electron and neutral scattering usually can also be neglected (Conwell 1967). The dependence of the drift mobility on m* and T, the energy dependence of τ and the value of γ for the different scattering mechanisms which can be found in GaAs are shown in Table 4.1.

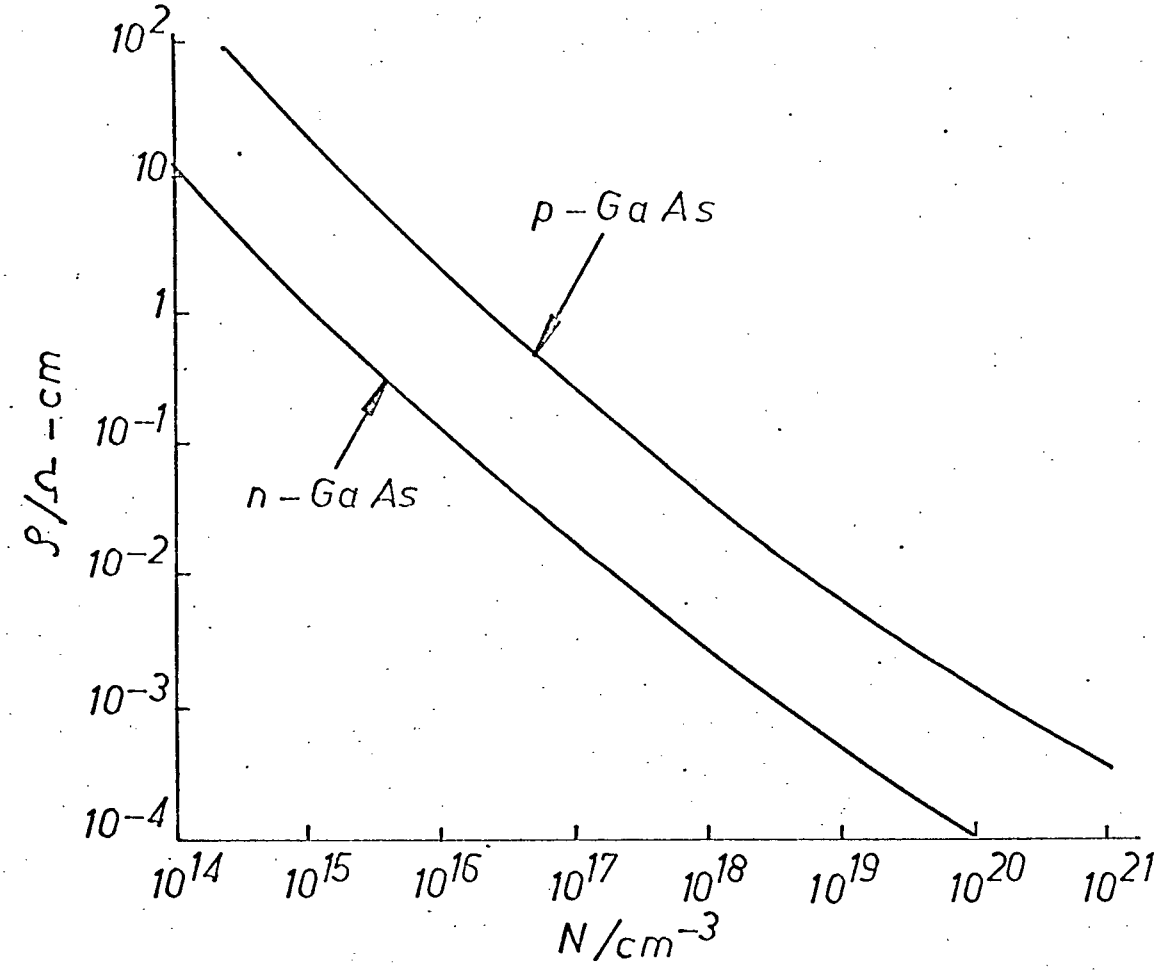

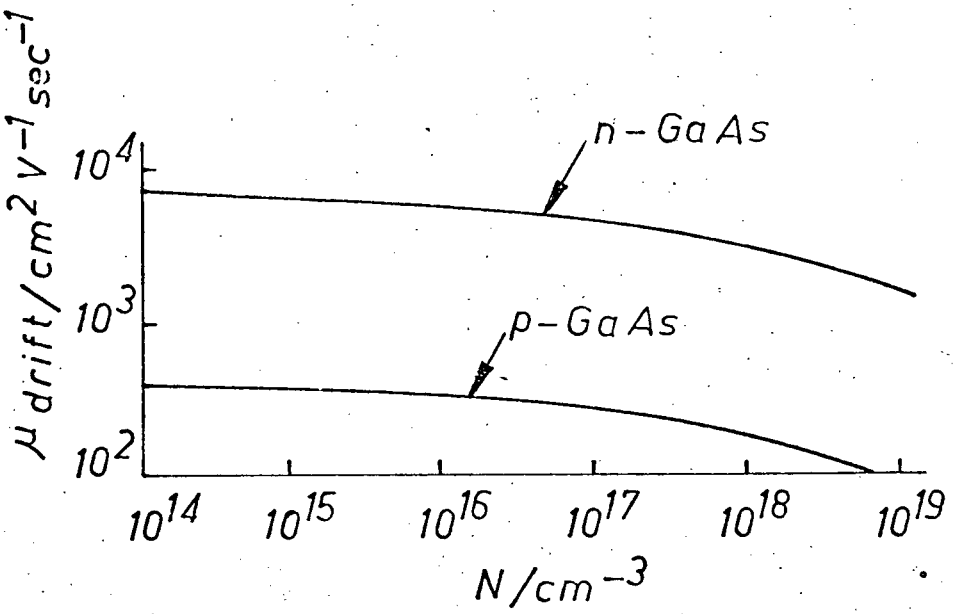

Fig. 4.2 Resistivity and Hall mobility of GaAs at 300°K versus impurity concentration (after Sze and Irvin 1968).

Scattering Mechanism	drift mobility $\mu \propto (m^*)^x T^y$		$\tau \propto E^\gamma$	$R_H = -r/nq$	Remarks	Reference
	x	y	γ	r		
optical phonon $T \leq \Theta_D$	$-\frac{3}{2}$	exponential	independent	1.00 to 1.14	r is temperature dependent $\Theta_D \equiv \frac{\hbar\omega_\ell}{k}$ = Debye temperature for GaAs, $\Theta_D = 418°K$	Hilsum and Rose-Innes (1961)
$T > \Theta_D$	$-\frac{3}{2}$	$-\frac{1}{2}$	$\frac{1}{2}$			Putley (1960)
ionized impurity	$-\frac{1}{2}$	$\frac{3}{2}$	$-\frac{3}{2}$	$\frac{315\pi}{512}$		Hilsum and Rose-Innes (1961)
combined polar and ionized impurity	$\sim(-\frac{3}{2})$	$\sim\frac{1}{2}$				Ehrenreich (1960) Sze (1969)
acoustic phonon	$-\frac{5}{2}$	$-\frac{3}{2}$	$-\frac{1}{2}$	$\frac{3\pi}{8}$	These scattering mechanisms are usually less important in GaAs.	Hilsum and Rose-Innes (1961)
neutral impurity	1	independent	independent	1		
electron-hole	$-\frac{1}{2}$	$\frac{3}{2}$	$-\frac{3}{2}$	$\frac{315\pi}{512}$		

Table 4.1 Scattering mechanisms in GaAs

4.4 Modification of Electrical Properties in Films

4.4.1 Effect of Sample Geometry

One of the assumptions used in the derivation of the transport coefficients is that the electrical contacts to the sample are sufficiently far away so that their effects on the fields in the region of interest are negligible. In practical systems, however, contact effects must be considered. For a standard Hall bar configuration, Isenberg, Russell and Greene (1948) calculated the effects of current electrode shorting on the Hall coefficient. It can be seen from Fig. 4.3 that in order to eliminate this shorting effect, the sample length-to-width ratio must be greater than 3.

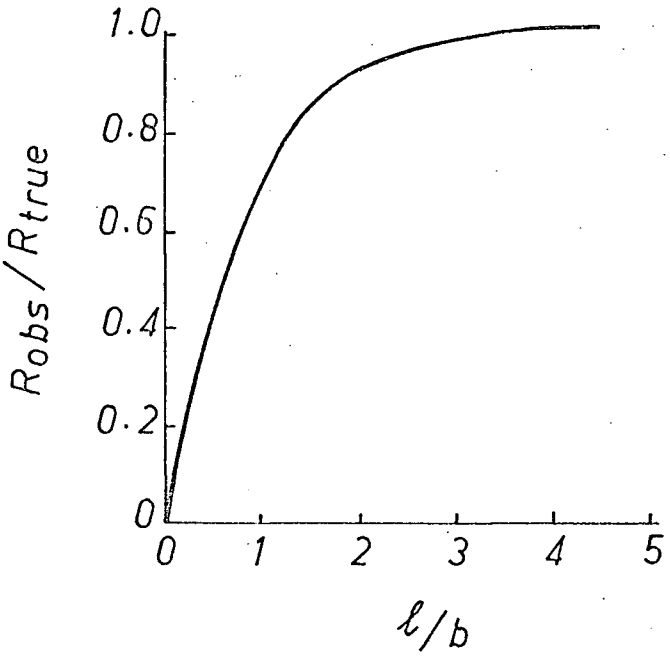

Fig. 4.3 Shorting effect of large-area current contacts on Hall coefficient (after Isenberg, Russell and Greene 1948).

For arbitrarily shaped flat samples whose surface is singly connected, van der Pauw (1958) showed that the sample electrical resistivity and Hall mobility are given by

$$\rho = \frac{\pi d}{\ell n 2} \frac{R_1+R_2}{2} \; f\left(\frac{R_1}{R_2}\right) \tag{4.16}$$

$$\mu_H = \frac{d}{B} \frac{\Delta R}{\rho} \tag{4.17}$$

provided that the electrical contacts are sufficiently small and are at the circumference of the sample. The resistance R_1 is the ratio of the voltage V_1 which appears across contacts 4 and 3 when a current I_1 is passed through contacts 1 and 2 (see Fig. 4.4). Similarly, the resistance R_2 is the ratio of the voltage V_2 across contacts 1 and 4 when a current I_2 is passed through contacts 2 and 3. The function $f(\frac{R_1}{R_2})$ was given in graphical form by van der Pauw. The change in resistance ΔR, is the ratio of ΔV to I. The extra voltage, ΔV, which appears across contact 2 and 4, is due to a magnetic field B perpendicular to the plane of the sample when a current I is passed between contacts 1 and 3.

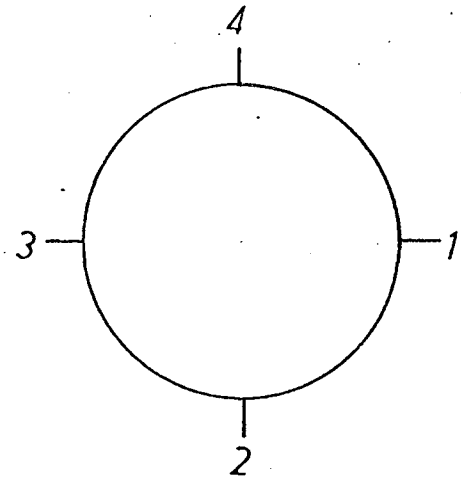

Fig. 4.4 Schematic diagram of a van der Pauw sample.

If the contacts are at the circumference of the sample but are of finite size with width w and if the diameter of the sample is D, then the relative errors introduced are given by van der Pauw as

$$\frac{\Delta\rho}{\rho} \simeq \frac{-w^2}{16\ D^2 \ell n_2} \tag{4.18}$$

$$\frac{\Delta\mu_H}{\mu_H} \simeq -\frac{2w}{\pi^2 D} \tag{4.19}$$

4.4.2 Effects of Surface Space Charge Layers and Surface Scattering

The BTE considered in Appendix 4.1 is for a medium of infinite extent. No boundary conditions are imposed on $f(\bar{k}, \bar{r})$. In the case of thin films, however, surface space charge layers can arise due to surface states. Tamm and Shockley states can act to trap or to repel free carriers; so do impurities adsorbed at the surface. Hence charge neutrality at the surface is destroyed. The space charge region is of the order of Debye length. The effective Debye length of a semiconductor is given by

$$L = \left[\frac{\varepsilon_r \varepsilon_o kT}{q^2 (n_b + p_b)}\right]^{\frac{1}{2}} \tag{4.20}$$

If eqn. 4.6 holds, then for the two cases (1) thick films in the flat band approximation and (2) sufficiently thin films such that $d/L \ll 1$, the average mobility is given by

$$\bar{\mu} = \frac{\mu_b}{1 + \frac{L}{d}} \tag{4.21}$$

where μ_b is the mobility of carriers in the bulk and d is the film thickness (Many, Goldstein and Grover 1965). In the more general cases where accumulation or depletion layers can exist, Greene, Frankl and Zemel (1960) gave a complete formulation of the effective carrier mobility in surface space charge layers within the framework of Schrieffer's (1955) assumptions that the carriers have constant effective mass, constant relaxation time and obey Maxwell-Boltzmann statistics.

Surface scattering reduces the mobility of carriers which are in a region less than one mean free path away from the boundary of a semiconductor. A perfect surface is expected to act as a specular scatterer. A surface is a specular scatterer if the magnitude and the parallel component of the momentum of the carrier which has collided with the surface remain unchanged; only the sign of the component of momentum perpendicular to the scattering

surface has changed. Increasing surface roughness tends to make the surface behave more like a diffuse scatterer. A diffuse scatterer causes the carrier momentum to become random after collision. If films are much thicker than the mean free path of the carriers in the bulk, then it is expected that the effect of surface scattering is negligible. The mean free path is given by Chopra (1969) as

$$\ell = \mu_b \frac{h}{q}\left(\frac{3}{8\pi} n_b\right)^{\frac{1}{3}} \tag{4.22}$$

where μ_b = mobility of carriers in the bulk,

n_b = carrier concentration in the bulk,

and h = Planck's constant.

A discussion on the effects of surface scattering was given by Many, Goldstein and Grover (1965).

4.4.3 Effects of Polycrystalline Structure

The carrier transport theory that was presented in the preceding sections is for single-crystal semiconductors. Results from Chapter 3 indicated that the CSS GaAs films were polycrystalline. The polycrystalline structure of the films must be taken into account in the analysis of the electrical properties of the films. In particular, the effects of grain boundaries must be considered. Associated with the grain boundaries are defects which may act as scatterers, thus reducing the mobility of the carriers at the boundaries. Defects can also act as dopants or trapping centres, which may result in a difference in carrier concentration between the interior of a crystallite (to be called region I) and its boundaries (to be called region II). Due to this difference, a potential barrier may exist between these regions. It is also possible, for example, that region I is n-type while region II is converted to p-type due to a preponderance of acceptors at the boundaries.

A representation of a polycrystalline film by a mosaic structure was proposed by Volger (1950). Based on a similar model, Slater (1956) considered the

effects of space charge regions in the crystallites on the electrical conductivity. Petritz (1956) and Waxman, Henrich, Shallcross, Borkan and Weimer (1965) considered the effects of grain boundaries on the mobility of the carriers. The concentration of grain boundaries and their potential barrier height are the parameters expected to limit the carrier mobility and to influence the temperature dependence of the electrical conductivity and carrier mobility.

Expressions for the electrical conductivity and the Hall mobility of carriers in a polycrystalline semiconducting film may be derived by considering the mosaic film model. Assume that the film is composed of crystallites of length ℓ_1, separated by grain boundaries of width ℓ_2. The carrier concentration in region I, p_1, is assumed to be larger than the carrier concentration in region II, p_2. Also, σ_1 is larger than σ_2, where σ_1 and σ_2 are the electrical conductivities of regions I and II, respectively. A schematic diagram of the model is shown in Fig. 4.5. For a p-type sample, the energy band diagram is as shown in Fig. 4.6.

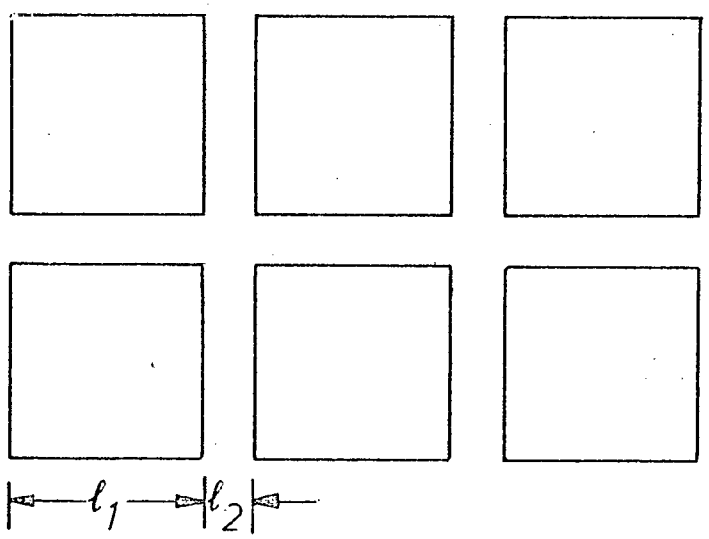

Fig. 4.5 Schematic diagram of a mosaic film.

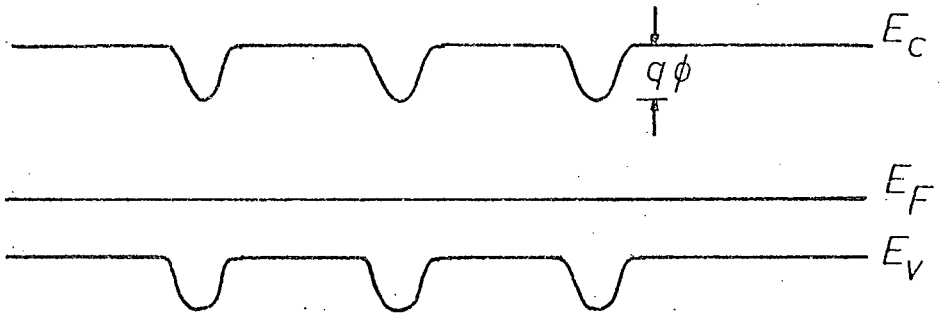

Fig. 4.6 Energy band diagram of a p-type mosaic film.

At thermal equilibirum, a potential barrier $q\phi$ exists between region I and region II. For a potential barrier of the type shown in Fig. 4.6, where it is assumed that the barrier width is thin compared with the mean free path of the carriers, Torrey and Whitmer (1948) showed that

$$J = \frac{1}{4} q \langle v \rangle p \, e^{-q\phi/kT}(e^{qV_b/kT} - 1) \tag{4.23}$$

where

$\langle v \rangle = 2(\frac{2kT}{\pi m^*})^{1/2}$ and is the average thermal velocity of the carriers (Shockley 1963)

$V_b = \frac{V_{app}}{n_1 L}$

n_1 = number of barriers per unit length

L = sample length between electrodes.

At low voltages, eqn. 4.23 may be linearized and a macroscopic conductivity defined as

$$\bar{\sigma} \triangleq \frac{J}{\bar{\mathcal{E}}} \tag{4.24}$$

where

$$\bar{\mathcal{E}} \triangleq \frac{V_{app}}{L} \tag{4.25}$$

$$\bar{\sigma} = pq \mu_o e^{-q\phi/kT} \tag{4.26}$$

$$\mu_o = \frac{q}{2n_1 kT} (\frac{2kT}{\pi m^*})^{1/2} \tag{4.27}$$

Equation 4.26 may be written as

$$\bar{\sigma} = pqu^* \quad ; \quad \mu^* = \mu_o e^{-q\phi/kT} \tag{4.28}$$

or

$$\bar{\sigma} = p^* q \mu_o \quad ; \quad p^* = p\, e^{-q\phi/kT} \tag{4.29}$$

In eqn. 4.28, it is implied that all of the holes in the crystallites take part in the conduction process but with a reduced mobility μ^*. On the other hand, eqn. 4.29 implies that the mobility of the carriers in the crystallites remain unchanged; the number of carriers taking part in the conduction process is p^*. Equation 4.28 is used when it is assumed that the measured Hall coefficient gives the total carrier concentration in the crystallites. Equation 4.29 is used when space charge regions, due to trapping of carriers, are present in region I.

4.4.4 Effects of Compensation of Impurities

Compensation in the CSS GaAs films may be expected to be large because of the increased number of defects and impurities which were incorporated during growth. Free carrier concentration will be smaller than the total impurity concentration. In p-type semiconductors, the concentration of acceptors, N_A, is more than the concentration of donors, N_D. An estimate of N_A and N_D may be made from the following considerations. Assume that, at T = 0°K, the N centres contain $N = N_A - N_D$ holes. At T greater than 0°K, the total number of holes available is

$$N = \frac{N_A}{1 + \frac{1}{g} e^{-(E_A - E_F)/kT}} + p \tag{4.30}$$

where

$$p = N_V e^{-E_F/kT}$$

$$N_V \triangleq 2\left(\frac{2\pi m^*_{dh} kT}{h^2}\right)^{3/2} \tag{4.31}$$

The energy levels E_A and E_F are measured from the valence band edge, g is the degeneracy factor, N_V is the effective density of states in the valence band and m^*_{dh} is the density-of-state effective mass of holes. The energy band diagram is shown in Fig. 4.7. If it is assumed that $p \ll N_A$, then

$$\frac{N_A - N_D}{N_D} = \frac{4p}{N_V} e^{E_A/kT} \tag{4.32}$$

The energy level or activation energy E_A may be obtained from the slope of a log p versus 1/T plot.

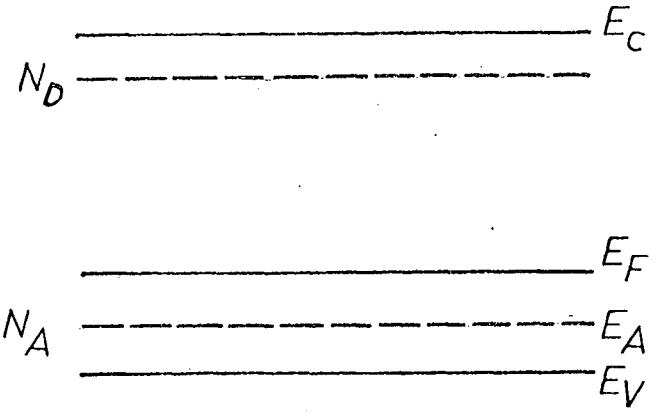

Fig. 4.7 Energy band diagram of a compensated p-type semiconductor

In the case of carriers in GaAs with a mobility μ_i, the corresponding total impurity concentration may be obtained either from Fig. 4.2 or from eqn. 4.15. Thus N_A and N_D may be obtained.

For a semiconductor with a given $N_A + N_D$, eqn. 4.15 shows that the carrier mobility would still depend upon the ratio N_A/N_D. The semiconductor is more compensated the closer N_A/N_D approaches unity. The carrier mobility of a compensated semiconductor will be smallest when the free carrier concentration is at a minimum.

4.5 Experimental Procedures

In this section, the methods of putting electrical contacts on GaAs films are described. The sample holders, the Hall apparatus and the thermal-probe method used in measuring the films' electrical properties are also described.

4.5.1 Preparation of Electrical Contacts

Electrical contacts to the p-type GaAs films were made by the following methods. The sample was first cleaned following the standard cleaning procedure,

flash-etched in $7H_2SO_4$ (95%):H_2O_2(30%):H_2O by volume, rinsed thoroughly in doubly-distilled water and then with isopropanol. An 80 Ag : 10 In : 10 Zn (wt %) alloy (Cox and Strack 1967) was evaporated from a Ta boat through photo-etched beryllium-copper mask onto the GaAs film. Evaporation was done in a Veeco 400 vacuum system. This system is pumped by a conventional 4-inch oil diffusion pump backed by a mechanical rotary pump. A liquid nitrogen cold trap was used to minimize backstreaming of the diffusion pump oil. Typical background pressure was 5×10^{-6} Torr rising to about 1×10^{-5} Torr during deposition. Film thickness was monitored using a quartz crystal controlled oscillator. Films about 0.1 to 0.2μ thick were used. A special specimen-and-mask holder was used (see Sec. 4.5.2). The eutectic was alloyed in a H_2 ambient at about 600°C for about 1.5 min. The eutectic temperature is 540°C. The alloying temperature was monitored using a chromel-alumel thermocouple. Melting of the evaporated contact lands was observed by using a Bausch and Lomb zoom microscope (x30 magnification). Gold contact wires were attached to the lands either by using silver paint or soldered by using In. For high resistance samples, silver paint gave erratic contacts. High purity (99.99%) indium which had been degreased by ultrasonic agitation in trichlorethylene was used for these cases.

For p-type samples fresh out of the CSS chamber, the whole cleaning procedure was by-passed. The rest of the procedure, however, was the same.

For n-type samples, a Au-Ge alloy (12 wt % Ge, eutectic temperature = 356°C) was used (Braslau, Gunn and Staples 1967).

A photograph showing a GaAs film with 4 contact lands is shown in Fig. 4.8.

4.5.2 Sample Holders

Figure 4.9 shows the beryllium-copper mask and the sample-and-mask holder used in the deposition of electrical contacts. The sapphire substrate

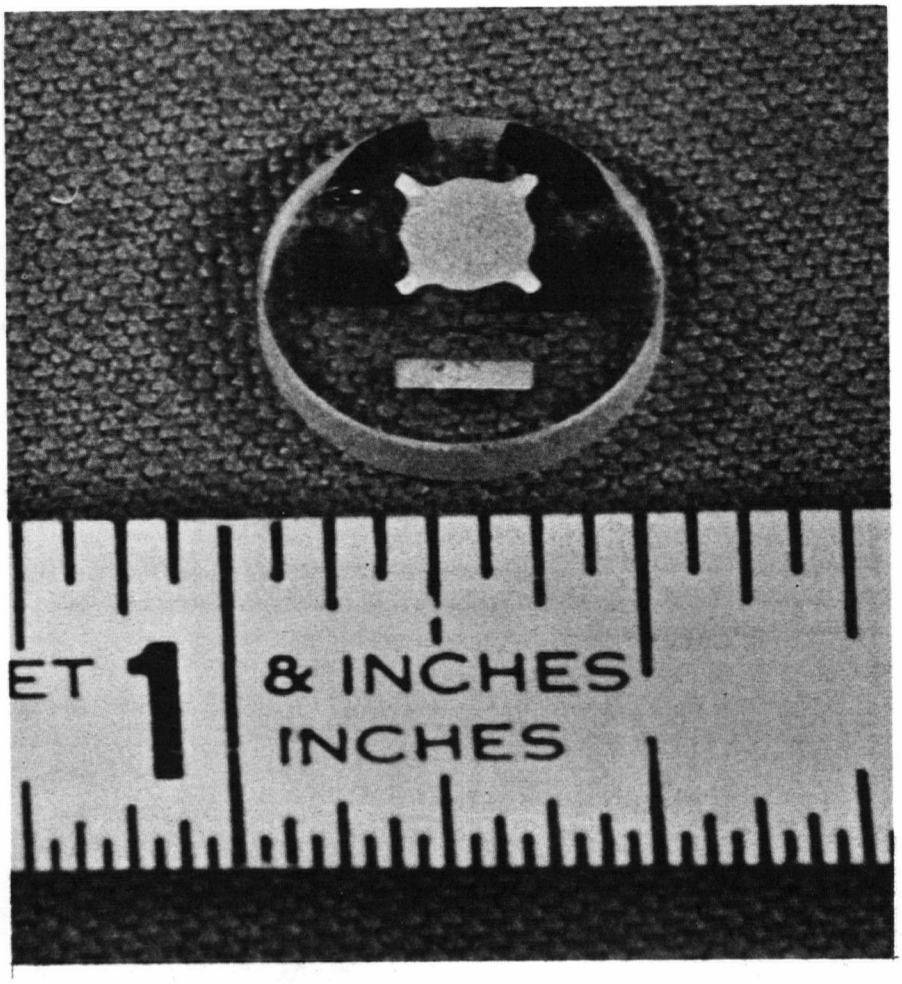

Fig. 4.8 Photograph of a metallized CSS GaAs film.

is located on a stage which has independent x-y movements. Photoetched beryllium-copper masks can be clamped between two stainless steel plates, which make up the mask-mount assembly. The mask-mount assembly can be moved in the z-direction. Alignment between sample and mask is achieved by suitably manipulating the x-y positioners. After alignment, the mask-mount assembly is lowered until the mask touches the GaAs film surface. This feature provides for ease in alignment while avoiding scratches on the GaAs film surface due to relative motions between film and mask. Because the mask is touching the film surface, penumbra effects are reduced.

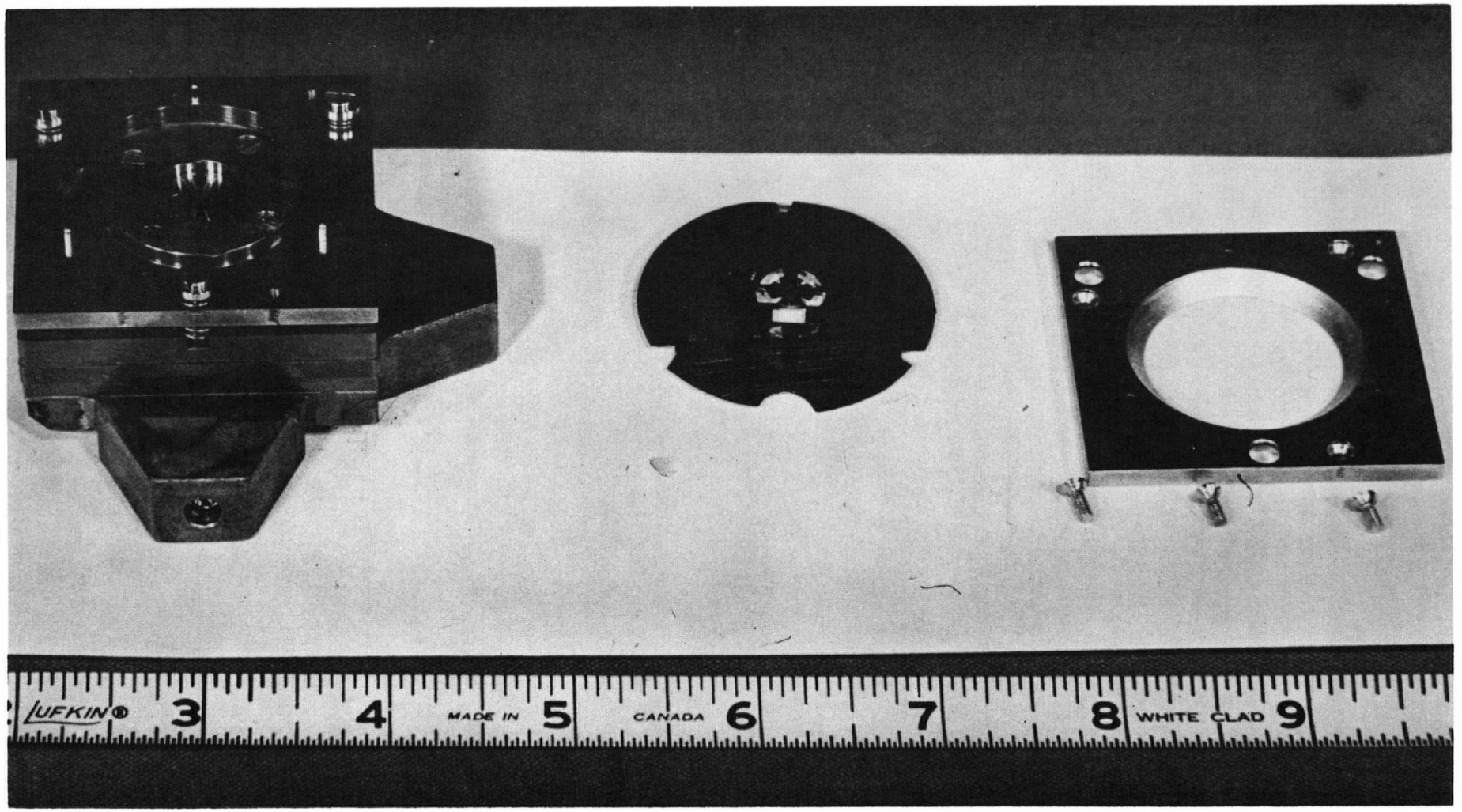

Fig. 4.9 Photograph of the sample-and-mask holder and the beryllium-copper mask used in the deposition of electrical contacts.

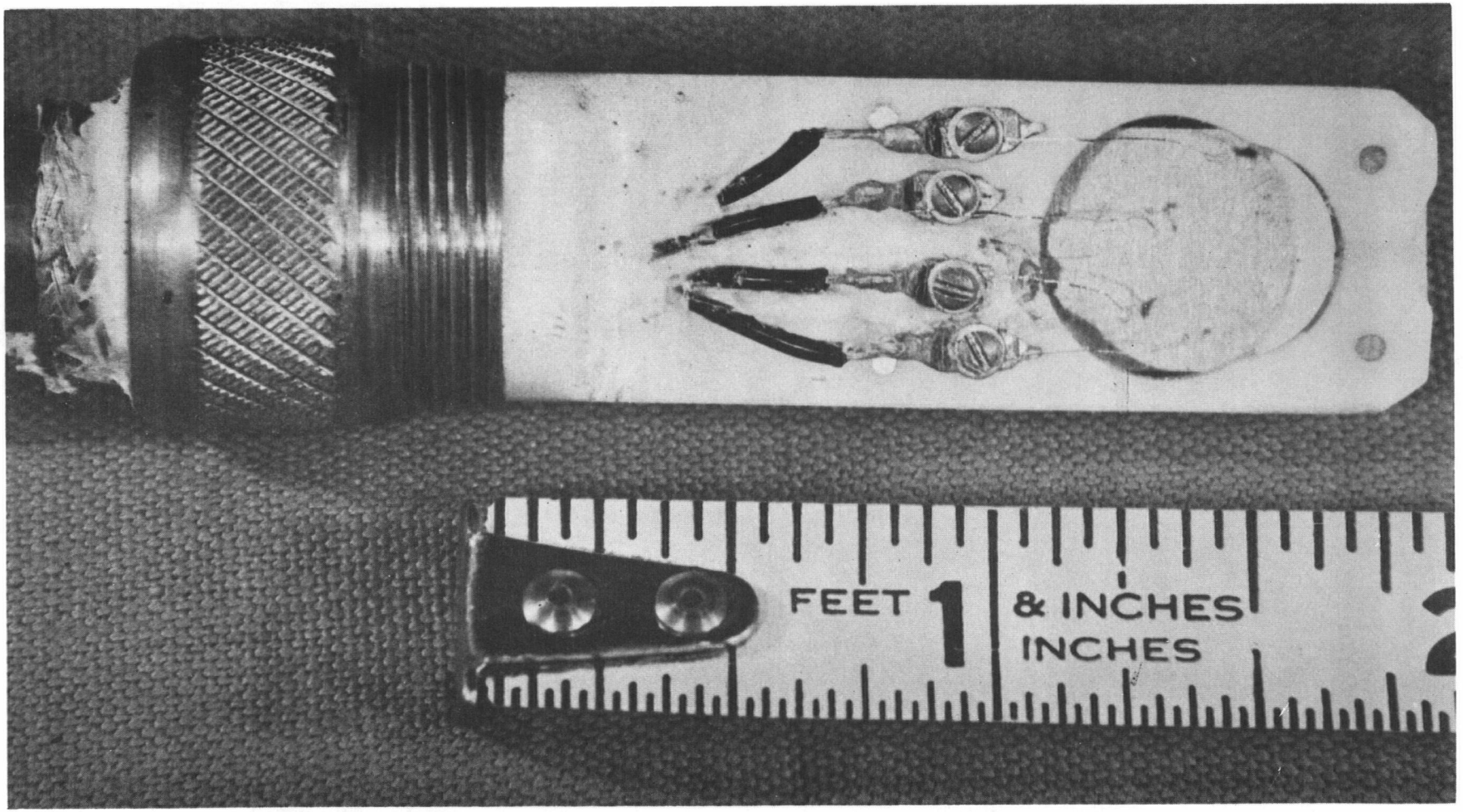

Fig. 4.10 Photograph of the sample holder (less protective cap).

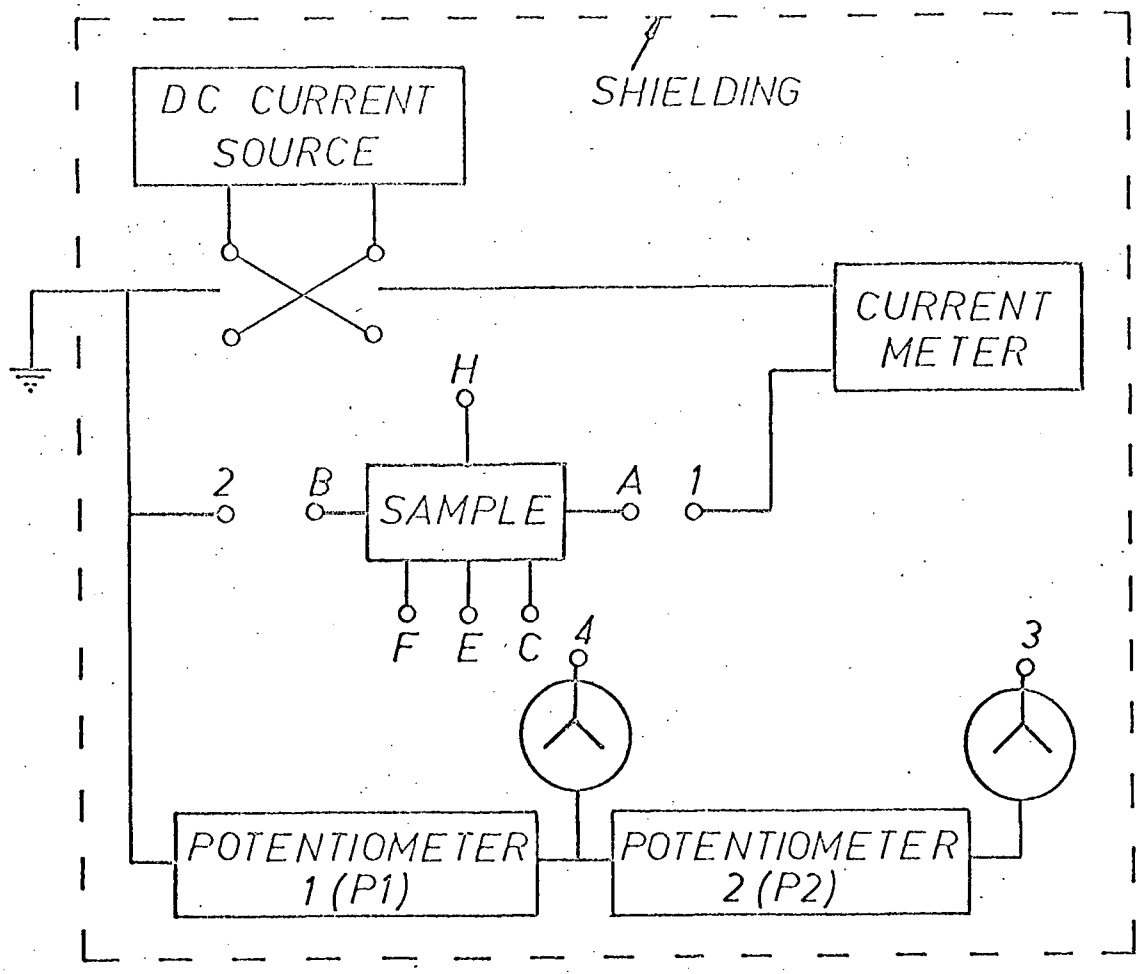

Function	Switch connections (sample terminals to measurement circuit terminals)
Meas. of sample conductivity by 4-probe method	A-1, B-2, F-4, C-3
Meas. of Hall voltage in a standard Hall bar or in a van der Pauw sample	A-1, B-2, E-4, H-3
Meas. of R_1 in a van der Pauw sample	A-1, H-2, B-4, E-3 Set P2 = 0
Meas. of R_2 in a van der Pauw sample	H-1, B-2, E-4, A-3 Set P2 = 0

Fig. 4.11 Block diagram of the Hall apparatus and a table of switch connections for the different measurement modes.

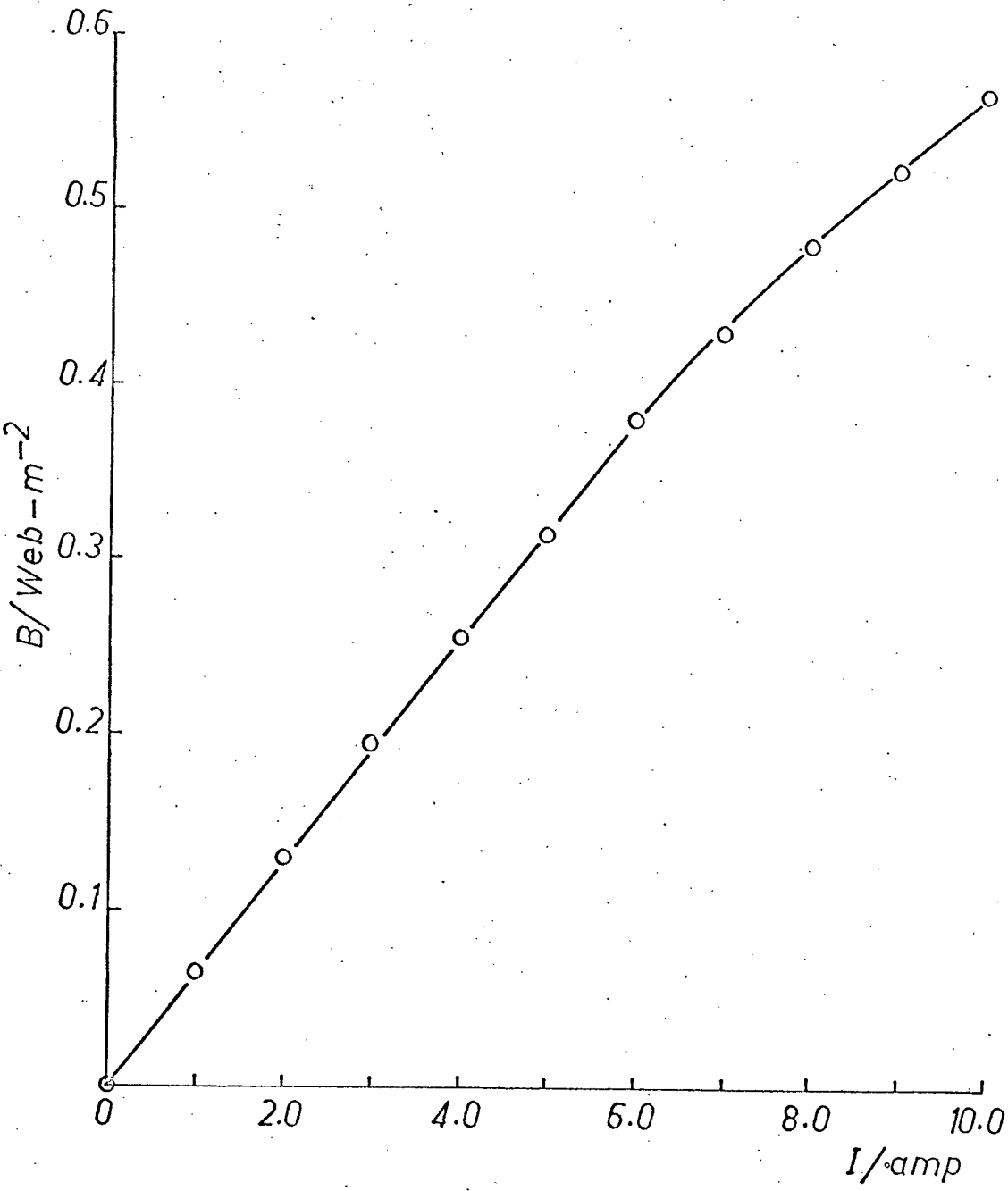

Fig. 4.12 Magnetic field versus d.c. current of the Alpha 8500 electromagnet

The specimen holder (less protective cap) shown in Fig. 4.10 was used when electrical measurements on the films were taken. Contacting of the films was described in Sec. 4.5.1. A strip heater and a chromel-alumel thermocouple were provided. The thermocouple was arranged so that its tip pushed against the sapphire substrate that was mounted in the holder.

4.5.3 Hall Apparatus

A block diagram of the Hall apparatus, together with the switch connections for the different measurement modes, are shown in Fig. 4.11. This apparatus is a modified version of the apparatus of Fischer, Greig and Mooser (1961). Vibron model 33B, Keithley models 600-A and 602 electrometers were used as null detector. A Fluke d.c. differential voltmeter (model 881 AB) shunted by a resistor was used to measure the current. Leakage paths to ground were minimal as teflon insulation was used in areas indicated. Double-shielding and common-mode suppression were used to reduce noise pick-up. Kelvin-Varley potentiometers, in conjunction with dry cells, were used to null out offset voltages.

The magnetic field was supplied by an Alpha 8500 electromagnet powered by an Alpha P8500 power supply. The field at the centre of the region between the pole pieces was measured using a Radio Frequency Laboratories (RFL) model 1890 Hall Probe Gaussmeter. The measured magnetic field as a function of d.c. current is shown in Fig. 4.12.

The specimen was cooled by immersing the entire tip of the specimen holder into a Dewar containing liquid nitrogen. Temperatures between room temperature and liquid nitrogen temperature were maintained by heating the specimen with a strip heater. The heating power, hence the temperature T, was controlled by an amplified signal of the difference between the thermocouple voltage and a predetermined voltage, set equivalent to the desired temperature T as obtained from a chromel-alumel thermocouple calibration chart. The temperature was maintained at T $\pm$2°C during the time it took to complete one voltage

and one current measurement.

Polarity of the Hall voltage for p and n-type samples, for the present circuit and geometrical arrangement, was checked by testing with known samples of Ge and GaAs.

4.5.4 Accuracy of Measurements

The accuracy of measurements of the 4-probe sample resistances was limited by the accuracy of the Keithley electrometers. This was ±2% full scale on all ranges exclusive of drift. To reduce errors due to drift, the meters were usually left on for several hours prior to use and their zero settings were checked before every reading. Accuracy of the calculated resistivities was limited by the accuracy of the measured film thickness. The resultant accuracy of the resistivity was estimated to be about ±5%.

Measurements of Hall voltages of high resistance (10^6 to $10^{10}\Omega$) and low mobility (~ 1 to 5 cm^2/V-sec) films were the least accurate. The magnitudesof the Hall voltages were typically about 1 mV. The peak-to-peak low-frequency noise superimposed on the Hall voltage was found to be within this range. The accuracy of the measured Hall voltages of lower resistance films was estimated to be about ±15%. Errors due to existence of temperature gradients across the sample were checked by averaging the following four sets of readings: current in "normal" direction with magnetic field in "normal" and "reverse" direction, and current in "reverse" direction with magnetic field in "normal" and "reverse" direction (Putley 1960).

From eqns. 4.18 and 4.19, the relative errors in electrical conductivity and Hall mobility of the CSS films due to the finite size of the contacts were $\frac{\Delta\rho}{\rho} \simeq -1.84 \times 10^{-3}$ and $\frac{\Delta\mu_H}{\mu_H} \simeq -0.058$, respectively.

4.5.5 Thermal-Probe Method

The thermal-probe circuit is shown in Fig. 4.13. If a temperature difference between two probes placed in contact with the sample is maintained,

a potential difference will exist between them. The polarity of the hotter probe is positive for an n-type and negative for a p-type material (Hunter 1962). The thermal probe circuit was checked by testing with known samples of Si, Ge and GaAs.

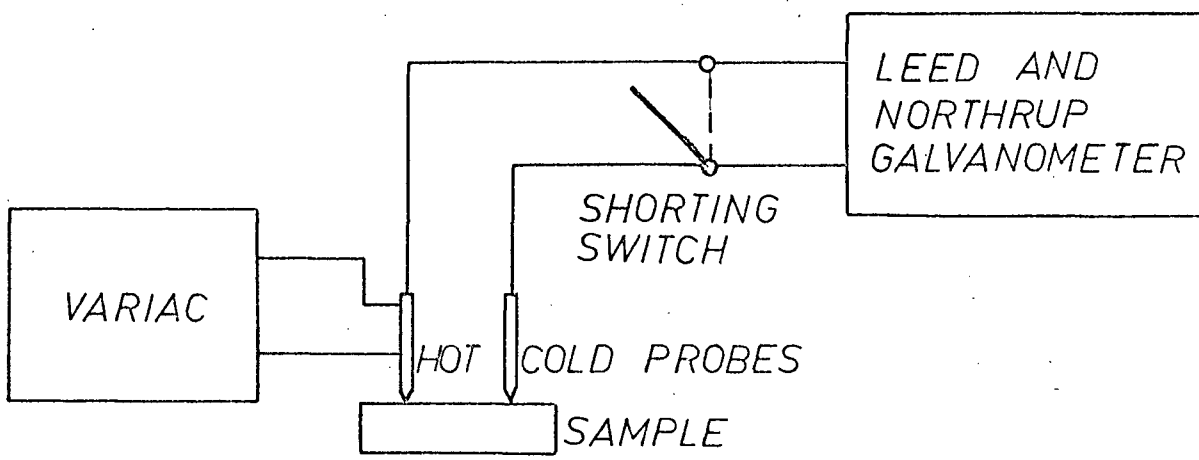

Fig. 4.13 Thermal-probe circuit.

4.6 Results and Discussion: CSS GaAs Films on Sapphire

In this section, experimental results obtained from Sec. 4.5 are discussed in terms of the theoretical considerations given in Secs. 4.2, 4.3 and 4.4.

4.6.1 Conductivity Type Determination by Thermal-Probe Method

The determination of the conductivity type of every CSS film was attempted. Knowledge of the conductivity type of a film is necessary before an appropriate alloy can be chosen and evaporated on to the film as contact lands for electrical measurements. Most of the as-grown "shiny" GaAs films on sapphire were p-type. The conductivity type of some of the "shiny" and all of

the "dull" films could not be determined by using the thermal-probe method.

4.6.2 Effects of Film Thickness and Surface Scattering

The thicknesses of the CSS GaAs films ranged from 16 to 95μ. The effects of surface space charge layers will have to be considered if film thicknesses were in the order of a Debye length. With the exception of the 650 and 670°C films at T < 220°K, it was calculated that $d/L \geq 20$ for the rest. From eqn. 4.17

$$\mu = \frac{\mu_b}{1+0.05} \simeq 0.95\mu_b$$

Surface scattering is expected to be negligible since the thinnest sample (16μ) is much larger than the mean free path of carriers in bulk GaAs ($\ell_e \sim 600$ Å, $\ell_h \sim 40$ Å).

4.6.3 Effects of Substrate Temperature and Impurities

In Chapter 3, it was shown that the structural properties of films were largely determined by the substrate temperature. It is expected that the electrical properties of the films are affected by the films' structure, and thus by the substrate temperature. In general, lower substrate temperature films, which appeared "dull", had very low carrier mobilities (< 1 cm^2/V-sec). Higher substrate temperature films, which appeared "shiny", had higher carrier mobilities. Because the electrical properties of "dull" films were less interesting, their study was not pursued. Two types of films were observed among the "shiny" films; these were the "high ρ" and the "low ρ" films. At room temperature, their resistivities were in the range 4×10^2 to 10^5Ω-cm, and 0.6 to 86Ω-cm, respectively.

Films deposited above 650°C had lower mobilities and higher resistivities than most of the films deposited at 630 to 640°C. Since, as shown in Fig. 2.2.1 that As is much more volatile than Ga, it is expected that at higher temperatures, more As was reevaporated from the films, resulting in a larger

amount of As vacancies. Due to the increased number of As vacancies, the concentration of acceptor-like impurities may have increased, with a resultant rise in impurity scattering and hence, lower mobility. Harris, Nannichi, Pearson and Day (1969) found that As vacancies themselves can act as acceptors, they can also form acceptor complexes with impurity atoms, or there may be amphoteric dopants such as Si which can move into the As vacancies and act as acceptors. The As loss in the CSS films could still be less than what would be detected by the methods used in Chapter 3.

The three source materials were all n-type. Their room temperature resistivity, carrier concentration and carrier mobility are given in Table 4.2.

Source	ρ/Ω-cm	$\mu_H/cm^2V^{-1}sec^{-1}$	Dopant	n/cm^{-3}	Supplier
1	0.063	6,820	"undoped"	$1.48x10^{14}$	Monsanto
2	0.07	1,800	Te	$5x10^{16}$	Monsanto
3	0.0038	3,300	Te	$5x10^{17}$	ASARCO

Table 4.2 Electrical properties of the source material at room temperature.

From thermal-probe and Hall measurements, the as-grown films were found to be p-type. There was also a big difference between the resistivity of the films and their corresponding source material. These can be due to one or a combination of the following reasons. Partial pressures of the source dopants may differ with the partial pressures of Ga and As. Hence, the concentration of source dopants at the films has changed. Impurities like Si and Cu may have been introduced during growth. Under As deficient conditions, Si can behave in an acceptor-like fashion since it is a Group IV element and is a known amphoteric dopant of GaAs (Sze and Irvin 1968). Even at moderate

(600°C) temperatures, Cu is known to convert n-GaAs to p-type (Weisberg, Rosi and Herkart 1960). Cu may also act to activate lattice defects resulting in the occurrence of donor-acceptor pairs. According to Blanc, Bube and Weisberg (1962, 1964), the possible donor-acceptor pairs are Ga (interstitial) - As (vacancy) pairs or As (interstitial) - Ga (vancancy) pairs which can exist in the crystal as microprecipitates, or Ga (vacancy) - As (vacancy) pairs, which are built in as microvoids. Defects associated with grain boundaries can further increase the concentration of acceptors and donors. If the concentration of acceptors dominate, then the film would become p-type.

For convenience, the electrical properties of "low ρ" and "high ρ" films will be discussed separately.

4.6.4 Electrical Properties of "Low ρ" Films

The temperature dependence of the resistivity of three "low ρ" films which were studied in detail is shown in Fig. 4.14. At room temperature the resistivity of the films was 1 to 2 orders of magnitude higher than that of the sources. The resistivity of the films increased slowly with decreasing temperature. This would be expected of semiconductors wherein most of the dopants are shallow. As already stated, thermal-probe and Hall measurements indicated that these films were p-type. The temperature dependence of the Hall mobility of holes in these films is given in Fig. 4.15. The magnetic field dependence of Hall voltage for sample 21 is shown in Fig. 4.15a. The hole concentration which was calculated from the Hall constant R_H, was plotted against temperature and is shown in Fig. 4.16. The room temperature resistivity, Hall mobility and hole concentration of four films, together with their corresponding source material are given in Table 4.3.

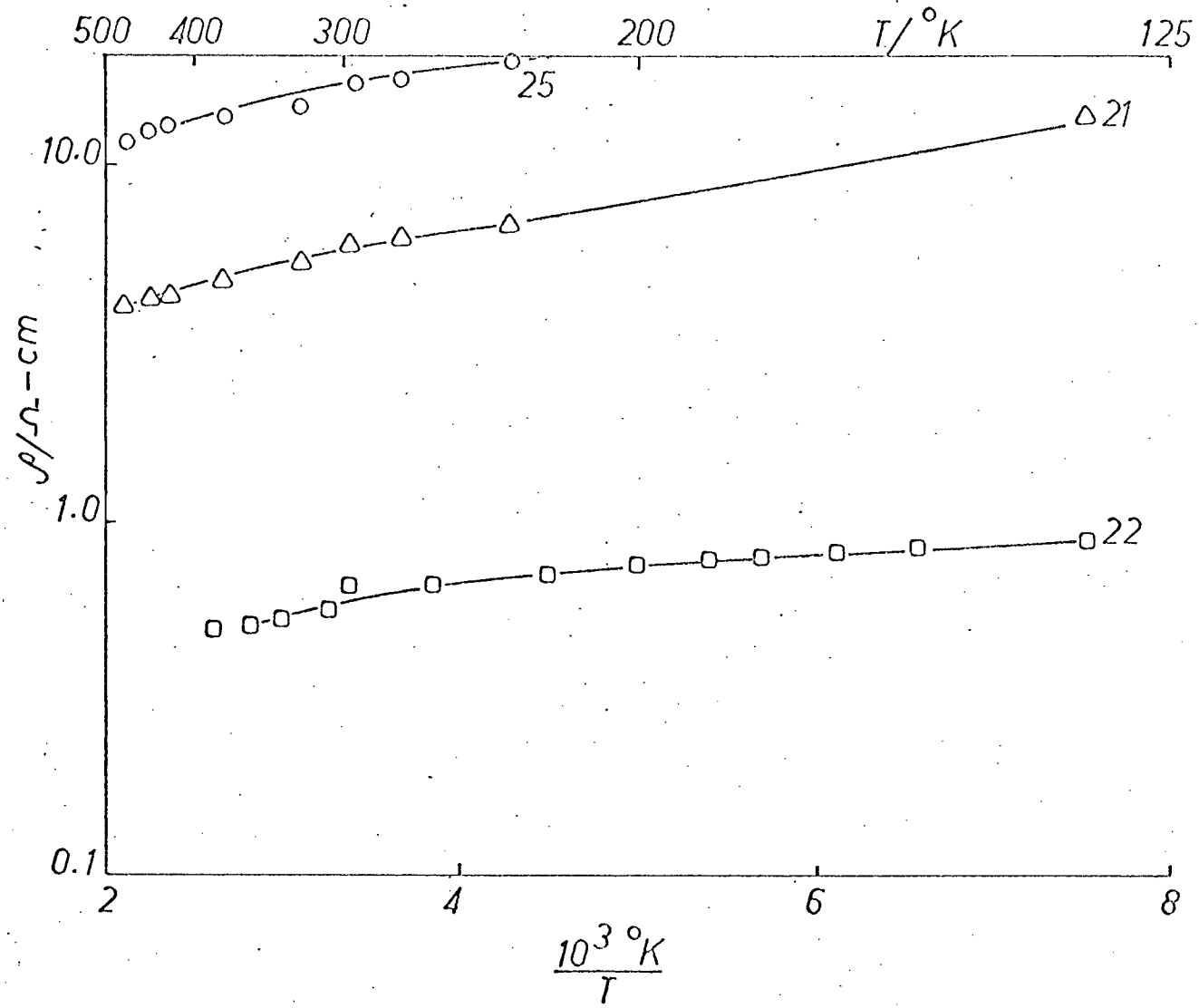

Fig. 4.14 Resistivity of "low ρ" films versus temperature.

Sample	Substrate Temperature (°C)	Source	electrical properties of films at room temperature			
			ρ/Ω-cm	conductivity type	$\mu_H/cm^2V^{-1}-sec^{-1}$	p/cm^{-3}
12	630	3	86	p	19	4.6×10^{15}
21	640	2	6	p	42	2.5×10^{16}
22	630	2	0.6	p	26	4.1×10^{17}
25	630	1	14	p	12	4×10^{16}

Table 4.3 Electrical properties of "low ρ" films of room temperature.

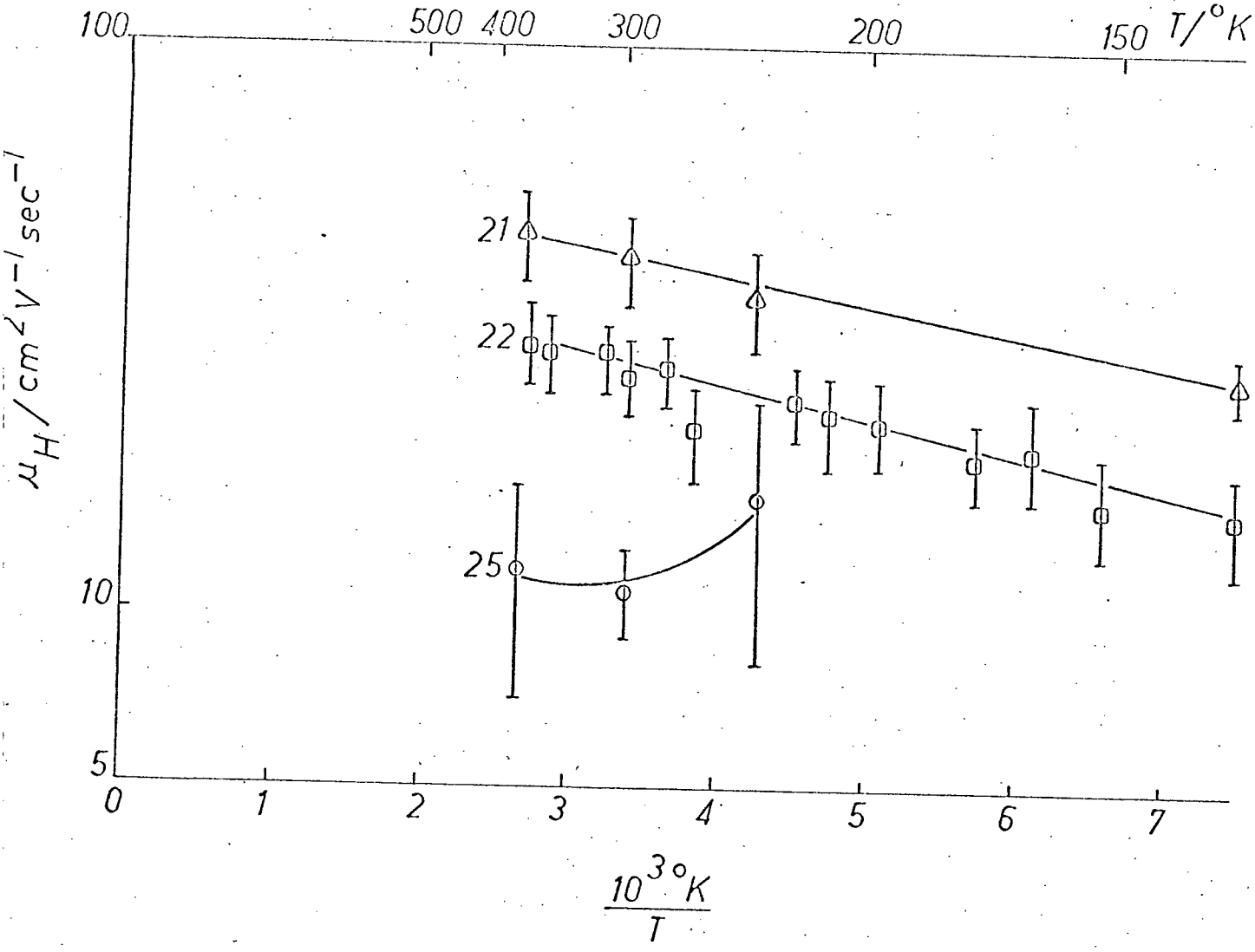

Fig. 4.15 Hall mobility of holes in "low ρ" films versus temperature.

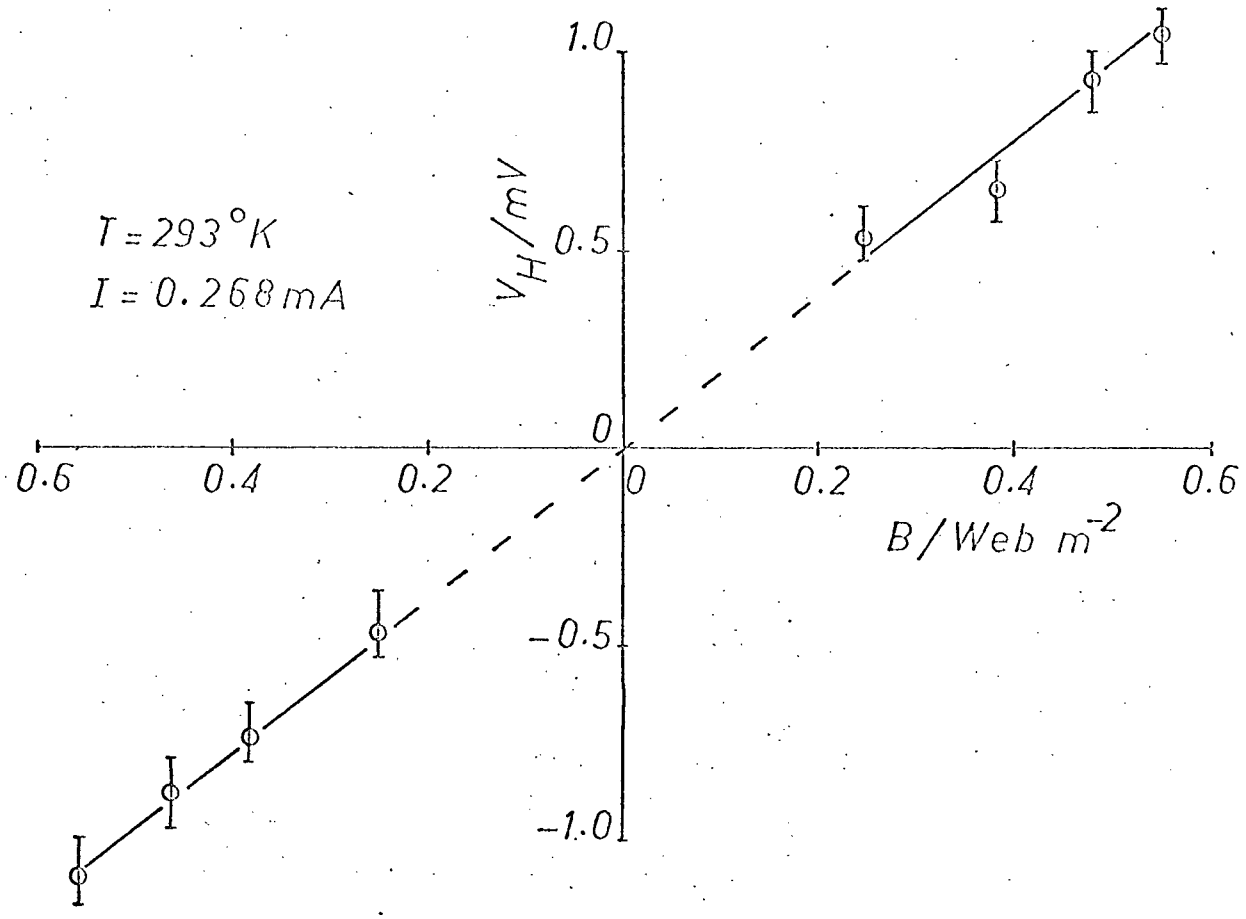

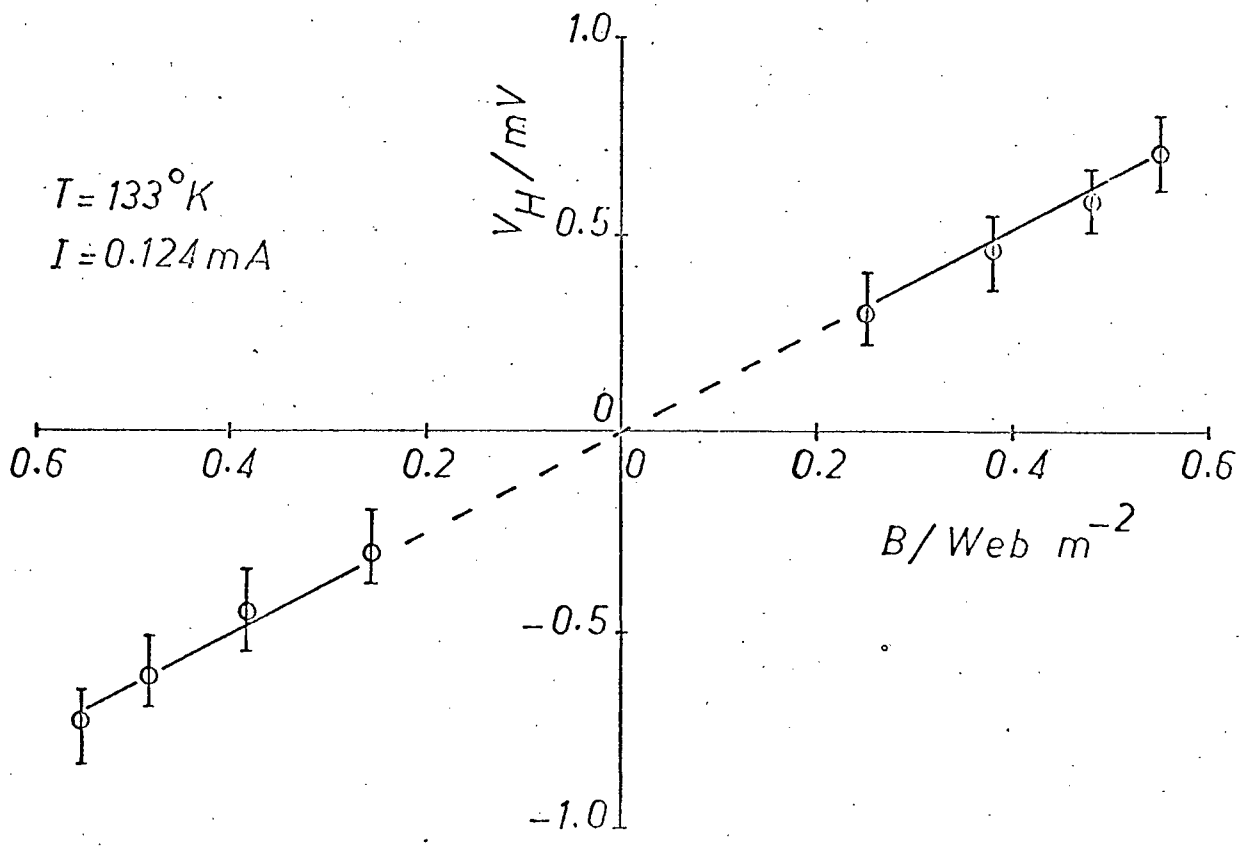

Fig. 4.15a Hall voltage versus magnetic field for sample 21.

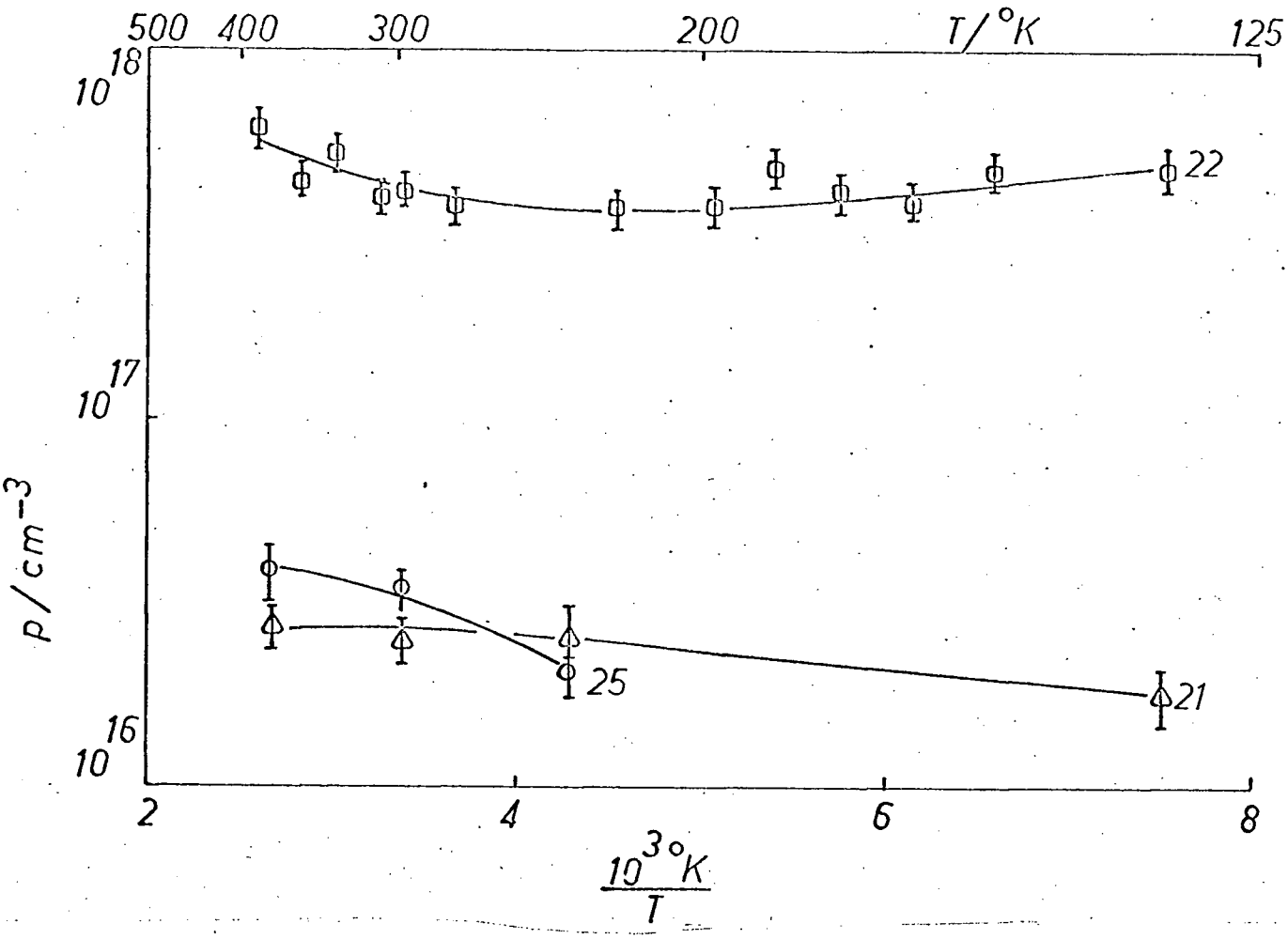

Fig. 4.16 Hole concentration in "low ρ" films versus temperature.

The temperature dependence of the hole mobility in samples 22 and 21 were fitted by straight lines satisfying the equations $\mu_H = 44e^{-120/T}$ and $\mu_H = 64e^{-144/T}$ cm^2/V-sec, respectively. These equations have the same form as eqn. 4.28. Because these films are polycrystalline, it is likely that one of the scattering mechanism is due to the potential barrier at the grain boundaries. If this scattering mechanism is the dominant one then the experimentally determined μ_o should agree with that calculated by using eqn. 4.27.

Samples 21 and 22 were composed of crystallites about 10μ wide (Chapter 3). Hence the number of boundaries per unit length, n_1, is about 10^5 m^{-1}. At room temperature the mass of light holes is 0.12 m_o. Substituting these values into eqn. 4.27 gives

$$\mu_o = \frac{q}{2n_1 kT}\left(\frac{2kT}{m^*}\right)^{\frac{1}{2}}$$

$$= \frac{3\times10^6}{n_1}\ \frac{m^2}{V\text{-sec.}} = 30 \times 10^4\ cm^2/V\text{-sec},$$

a value that is unlikely to be observed in GaAs films. A converse calculation could be made. If the hole mobility were limited by grain boundary scattering alone, then n_1 for samples 21 and 22 is 4.7×10^9 and $6.8\times10^9 m^{-1}$, respectively. The corresponding grain size is 2.1×10^{-10} and 1.5×10^{-10} m, respectively, These results do not agree with the findings of Chapter 3. In order to explain the low mobility of these films, other scattering mechanisms must be taken into account. Of the important scattering mechanisms in GaAs, ionized impurity scattering is the one most likely to limit the hole mobility. Due to compensation, the measured hole concentration was less than the concentration of acceptors. Estimates of $\frac{N_A-N_D}{N_D}$ and N_A+N_D were done by using the method described in Sec. 4.4.4. These quantities, together with E_A, p and μ_H, are given in Table 4.4.

Sample	E_A/eV	p/cm^{-3}	$\frac{N_A-N_D}{2N_D}$	μ_H/cm^2V^{-1}-sec^{-1}	N_A+N_D/cm^{-3}
12	-	4.6×10^{15}	-	19	8.7×10^{19}
21	0.97×10^{-2}	2.5×10^{16}	0.0104	42	5.0×10^{19}
22	2.32×10^{-2}	4.1×10^{17}	0.285	26	1.4×10^{20}
25	2.49×10^{-2}	4×10^{16}	0.297	12	1.9×10^{20}

Table 4.4 Concentration of impurities in "low ρ" films.

4.6.5 Electrical Properties of "High ρ" Films

Figure 4.17 shows the temperature dependence of the conductivity of 4 "high ρ" films. For convenience, either the electrical conductivity or resistivity will be discussed, whichever is more applicable. These films differed markedly with the "low ρ" films in two respects. Firstly, the room temperature resistivity was 4 to 10 orders of magnitude larger than the source resistivity. In comparison, the resistivity of the "low ρ" films was 1 to 2 orders of magnitude larger.* Secondly, the resistivity of these films was strongly temperature dependent, but leveling off at temperatures less than 200°K. The mobility of the "high ρ" films, however, was lower than the "low ρ" ones by a factor varying from 20 to 40, at room temperature. The room temperature electrical properties of 5 "high ρ" films and their corresponding source material are given in Table 4.5. The temperature dependence of μ_H and p are given in Fig. 4.18 and 4.19, respectively.

Sample	Substrate temperature (°C)	Source	Electrical properties of films at room temperature			
			ρ/Ω-cm	conductivity type	$\mu_H/cm^2V^{-1}-sec^{-1}$	p/cm^{-3}
14	640	3	9.2×10^4	p	-	-
23	636	2	7.9×10^3	p	13	6.1×10^{14}
24	660	1	3.9×10^2	p	3	5.3×10^{15}
38	660	1	7.2×10^4	p	2	4.3×10^{13}
39	650	1	1.6×10^5	p	3	1.3×10^{13}
42	670	2	6.4×10^2	p	3	3.3×10^{15}

Table 4.5 Electrical properties of "high ρ" films.

From Fig. 4.17, it can be seen that for all the samples, the curves of

* The photovoltaic effect was observed in the "high ρ" films. Photovoltages in the "low ρ" films may have been shorted out by low resistance paths in the films.

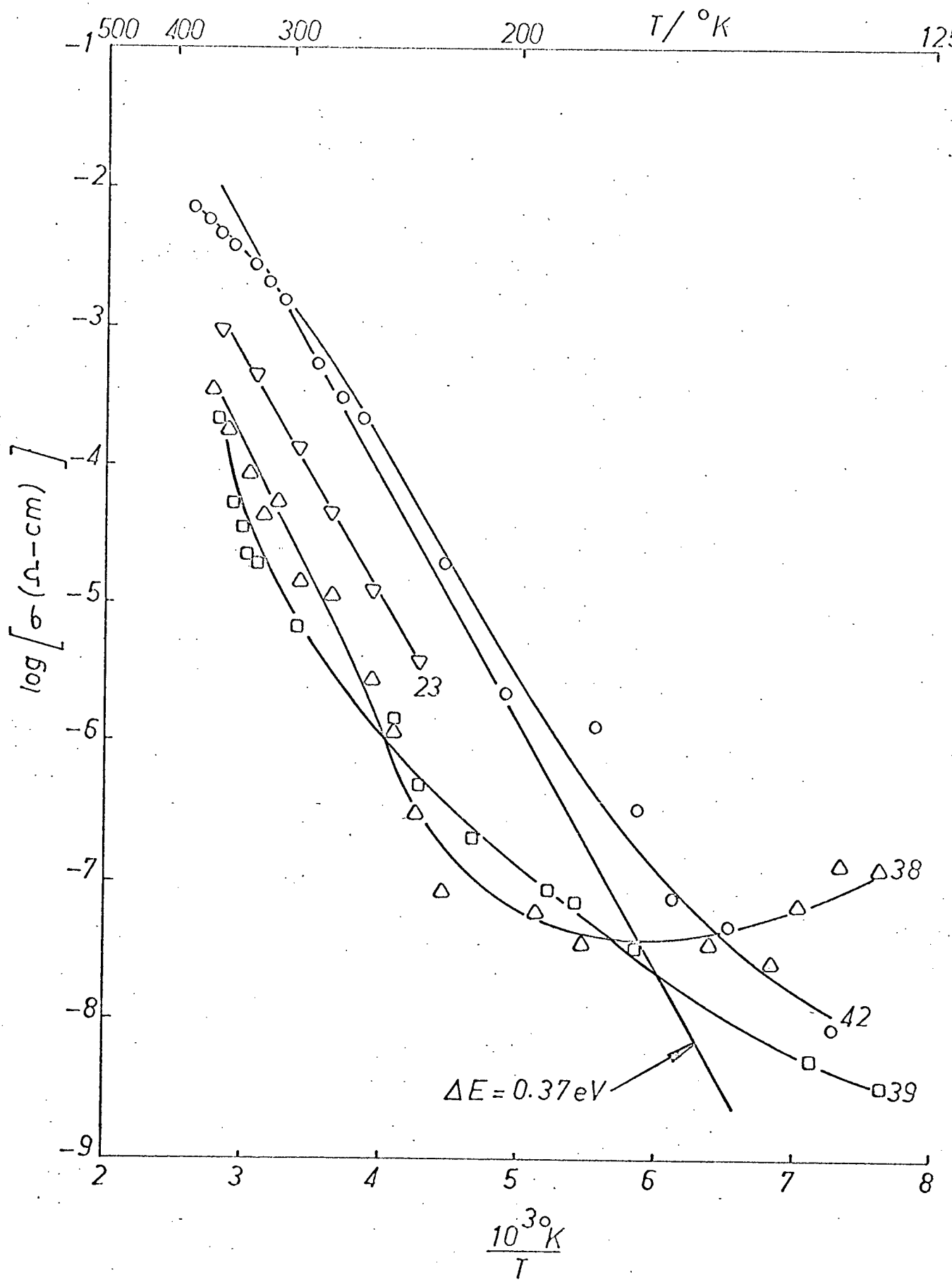

Fig. 4.17 Conductivity of "high ρ" films versus temperature.

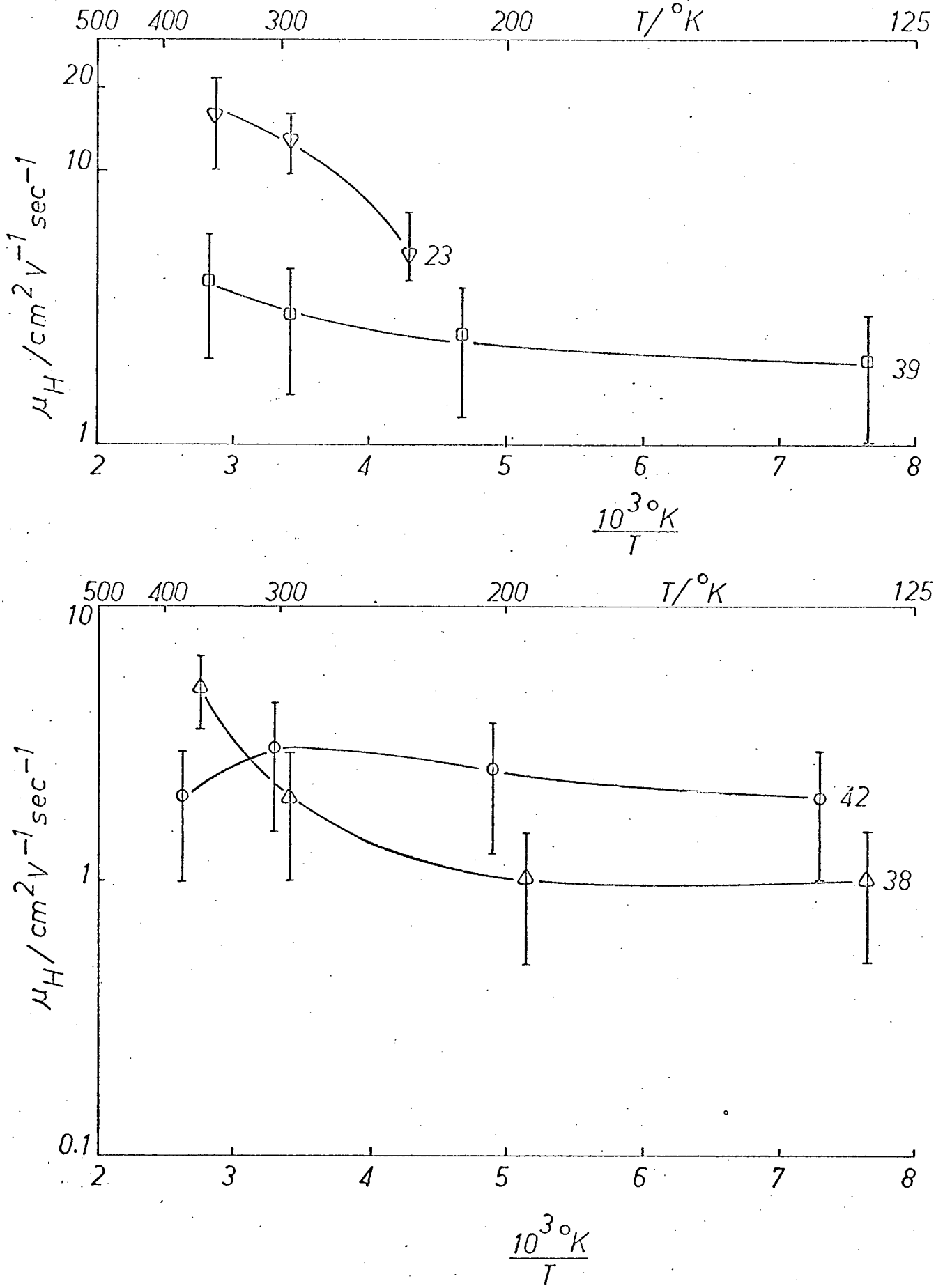

Fig. 4.18 Hall mobility of holes in "high ρ" films versus temperature.

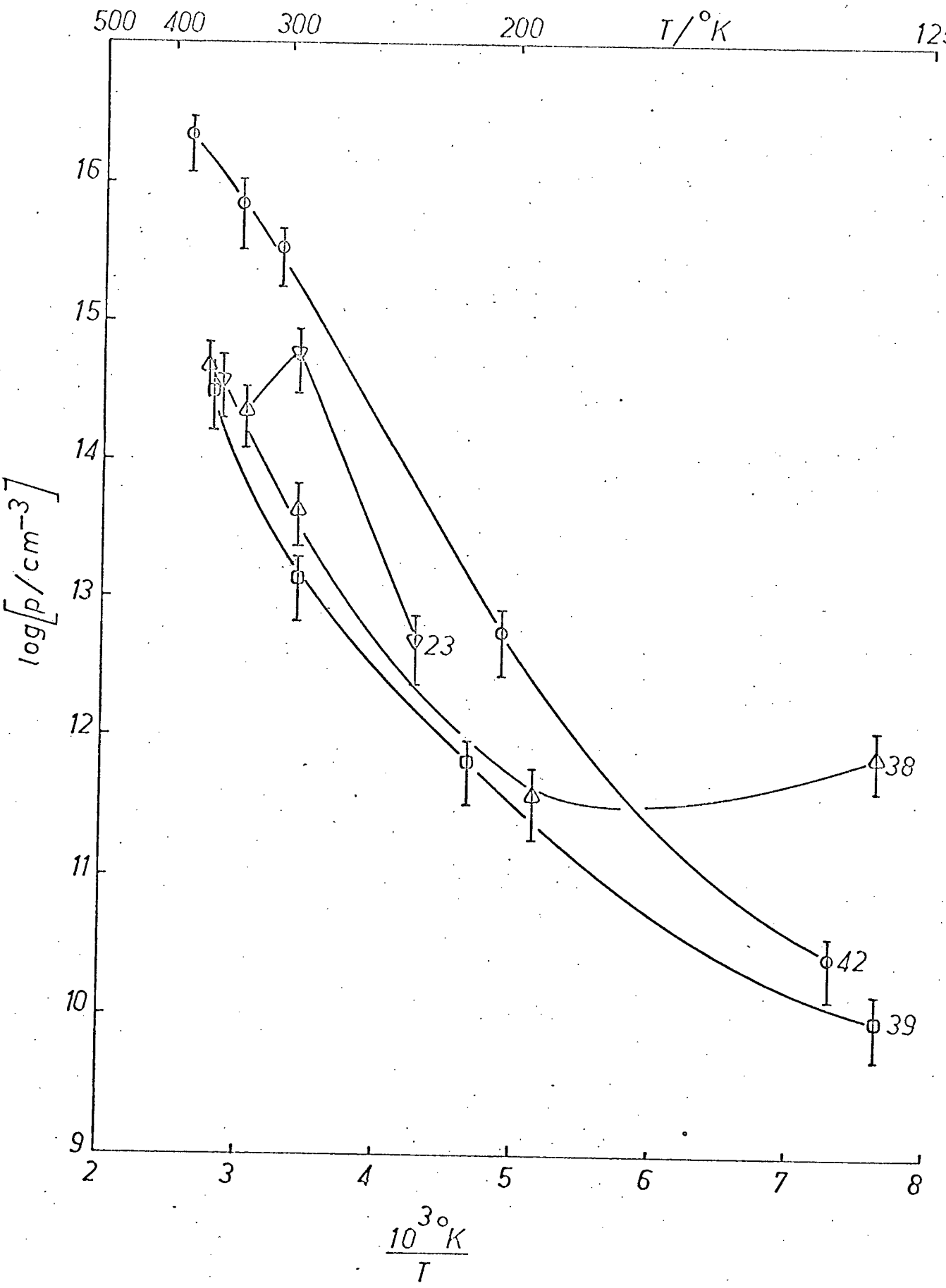

Fig. 4.19 Hole concentration in "high ρ" films versus temperature.

σ versus $\frac{10^3}{T}$ are nearly straight lines over several powers of 10. However, at low temperatures, they all tend to saturate. A possible explanation for this is as follows. Volger (1950) had shown that if the crystallites were assumed to be squares and if $\ell_1 >> \ell_2$ and $\rho_2 >> \rho_1$ then

$$\rho \simeq \rho_1 + \frac{\ell_2}{\ell_1} \rho_2 \tag{4.34}$$

However, it is conceivable that the grain boundaries have a lower resistivity than the crystallites. Tucker (1966) showed that if $\rho_1 >> \rho_2$, then

$$\rho \simeq \rho_2 \frac{\ell_1+\ell_2}{\ell_2} \tag{4.35}$$

Both Volger and Tucker did not consider the temperature dependence of ρ_1 and ρ_2. At higher temperatures, the assumptions of Volger may hold and the macroscopic resistivity is then given by eqn. 4.34. Furthermore, the temperature dependence of ρ_1 may be strong. Thus, the effects of the grain boundaries are completely swamped by the main conductivity through the bulk of the material. At lower temperatures the conductivity of the crystallites decreases due to a decrease in free carrier concentration. The shunting effect of the boundaries will now dominate. Since the defect density at the boundaries is expected to be higher than at the crystallites, greater compensation may have taken place. This could result in a resistivity varying slowly with temperature and would result in the flattening out of the resistivity versus temperature plots at low temperatures. A similar effect in PbS films was observed by Mahlman (1956) and was discussed by Slater (1956).

It can be seen from Fig. 4.17 and 4.18 that while σ of the films changed by 6 orders of magnitude in the temperature range under consideration, the corresponding μ_H remained nearly the same. This observation is considered in the following discussion, which follows from Slater's barrier theory (1956). The conductivity of the "high ρ" films may be represented by eqn. 4.29 or

$$\bar{\sigma} = \sigma_o e^{-\Delta E/kT} \qquad (4.36)$$

$$\sigma_o = pq\mu$$

where ΔE is the barrier height of the grain boundaries measured from the Fermi level. The carriers in the crystallites must overcome this barrier in order to participate in the conduction process. It is assumed that the mobility of the carriers was not changed significantly by these barriers and that their value is limited by ionized impurity scattering. The barrier height may range from zero, for no grain boundaries, to a value equal to the bandgap, i.e. the barriers are fully developed. The barrier height in the films may be estimated from the following considerations.

The energy band diagram that is used in conjunction with the following discussion is shown in Fig. 4.20. Assume that the net impurity concentration in both the n-type and p-type regions are equal and is N_o. The dotted lines

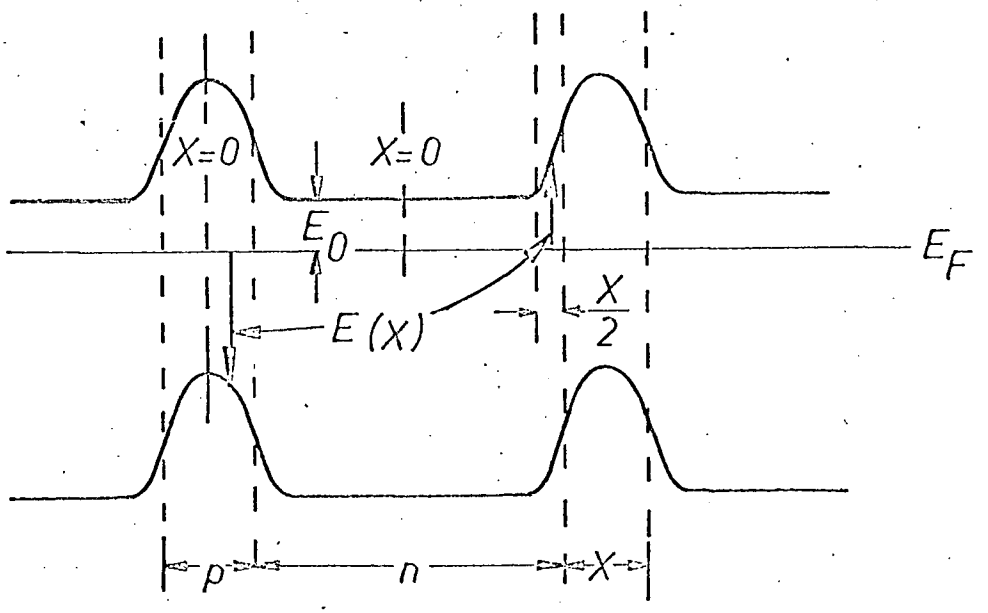

Fig. 4.20 Energy band diagram of a mosaic film with partially developed barriers (from Slater 1956).

separate the two regions. The energy E(x) is measured from the Fermi level. It is measured upwards to the conduction band edge in the n-region and downwards to the valence band edge in the p-region. Thus, E(x) is positive in both cases. With these assumptions, Slater (1956) showed that the barrier height, ΔE, is given by

$$\Delta E \simeq \left(\frac{N_o e^2}{4\varepsilon_r \varepsilon_o}\right) X^2 \qquad (4.37)$$

The thickness of the barrier is X. In the case of CSS GaAs films, ε_r=11, $N_o \simeq 10^{15}$ cm^{-3} and X ≃ 1μ. With these values,

$$\Delta E \simeq 0.37 \text{ eV}$$

A plot of logσ versus $\frac{10^3}{T}$ with ΔE = 0.37 eV was included in Fig. 4.17, for comparison. The room temperature conductivity was assumed equal to the 670°C film. It can be seen that the activation energies of the experimental curves agreed reasonably well with that calculated by using Slater's simple model.

The total impurity concentration (N_A+N_D) of 5 "high ρ" films were estimated using the method described in Sec. 4.4.4. These quantities together with the corresponding p and μ_H of the films are given in Table 4.6.

Sample	E_A/eV	p/cm^{-3}	$\frac{N_A-N_D}{2N_D}$	μ_H/cm^{2}V^{-1}-sec^{-1}	N_A+N_D/cm^{-3}
23	0.331	6.1×10^{14}	57	13	1.1×10^{20}
24	-	5.3×10^{15}	-	3	5.6×10^{20}
38	0.398	4.3×10^{13}	56	2	5.2×10^{20}
39	0.398	1.3×10^{13}	15.8	3	3.2×10^{20}
42	0.303	3.3×10^{15}	126	3	5.9×10^{20}

Table 4.6 Concentration of impurities in "high ρ" films

4.7 Postdeposition Doping of CSS GaAs Films on Sapphire

The surface layer of sample 22 was converted into n-type by doping with Ge. The sample was cleaned following the standard procedure and then flash-etched in $7H_2SO_4$(95%):H_2O_2(30%):H_2O (by volume) at about 80°C. A layer of Ge, about 700 Å thick, was deposited on the CSS film. The deposition was carried out in the Veeco 400 vacuum system at a background pressure of 5×10^{-6} Torr. A wafer of polycrystalline GaAs was placed on top of the CSS film and the "sandwich" was then placed inside a quartz furnace. The "sandwich" arrangement was used in order to avoid excessive As loss from the film surface. The temperature inside the furnace was measured by using a chromel-alumel thermocouple whose tip touched the sapphire substrate. Diffusion of the deposited Ge was carried out at 700°C in a vacuum of 10^{-4} Torr for about 8 hours. The sample was then contacted using a Au-Ge alloy and mounted in a manner as described in Sec. 4.5.

Thermal probe and Hall measurements indicated that the film was n-type. The electrical properties of the converted film is tabulated in Table 4.7.

temperature (°K)	ρ/Ω-cm	$\mu_H/cm^2V^{-1}sec^{-1}$	n/cm^{-3}
293	0.183	77	4.44×10^{17}
273	0.201	58	5.37×10^{17}
133	0.214	56	5.22×10^{17}

Table 4.7 Electrical properties of a converted film

Unsuccessful attempts to convert the CSS films into n-type by Ge or Sn diffusion were made on 3 other samples. Since Ge and Sn are amphoteric dopants of GaAs, they can occupy vacant As sites and become acceptor-like

impurities. The amphoteric dopants will act as donors when they occupy Ga vacancies. In order to convert a p-type sample into n-type, the concentration of donors must be made larger than the concentration of acceptors. For the CSS films, this would mean that the concentration of the intentionally added dopant must be greater than 10^{20} cm^{-3}. The mobility of carriers in the converted layers would be small due to ionized impurity scattering. The group IV elements were used for, so far, they are the best n-type dopants to be used in the solid-to-solid diffussion of impurities into GaAs layers. The more common group VI dopants react with Ga and corrode the GaAs surface (Goldstein 1962, Muench 1966).

4.8 Device Fabrication Using CSS GaAs Films on Sapphire

Thin-film insulated-gate field-effect transistors and Au-Schottky barrier diodes were fabricated using the CSS films.

The transistor structure used was similar to the ones used by Weimer (1964) and by Salama (1966). The source-drain gap was about 70μ. The as-grown GaAs films were about 1000 to 3000 Å thick. Evaporated SiO_x served as the insulator. Thicknesses of about 1500 to 2000 Å were used. Two out of 12 transistors fabricated had transconductances of 0.1μ-℧. The effective mobility was 4 cm^2/V-sec. These devices operated in the p-type depletion mode. Source-drain current modulation by gate voltage was not observed in the rest of the devices. This may be due to a high density of surface states at the SiO_x/GaAs interface.

Five Au-Schottky barrier diodes were fabricated on an n-type layer converted by Ge doping. The diodes all had "soft" characteristics. The d.c. rectification ratio and the voltage |V| for diodes 1, 2 and 3 were 40 (1.2 V), 12 (1.2 V) and 42 (0.6 V), respectively.

4.9 Results and Discussion: CSS GaAs film on Semi-Insulating GaAs

A homoepitaxial layer of GaAs was deposited on semi-insulating GaAs using the CSS method. The GaAs was supplied by Monsanto and according to the manufacturer's specifications was Cr doped with a room temperature resistivity of 5.32 to 5.5 x 10^8 Ω-cm. The wafer surface was oriented in the [111] direction and was cut from a Czochralski single crystal.

The substrate was mechanically polished to 0.3μ finish and then cleaned following the standard cleaning procedure. Just prior to introduction into the Ultek vacuum chamber, the substrate was chemically polished for about 30 sec, at room temperature, in a solution of 40 HCl(38%): 4 H_2O_2(30%):H_2O_2 (by volume) (Shaw 1968). The substrate was then thoroughly rinsed in doubly-distilled water and in propanol. The substrate surface was examined with an optical microscope. The polished surface was shiny and smooth and appeared to be uniformly etched by the chemical polish.

The source material was n-type GaAs with the following room temperature electrical properties: ρ = 0.07Ω-cm, n = 5 x 10^{16} cm^{-3}, and μ_H = 1,800 cm^2/V-sec.

During deposition, the source and substrate temperatures were maintained at 666 and 585°C, respectively. The background pressure was 9.5 x 10^{-9} Torr rising to 1.4 x 10^{-8} Torr during deposition. The nominal deposition time was 1 hour.

Thermal-probe measurements indicated that the film was n-type. Thus, the film was contacted by evaporating Au-Ge alloy lands. The deposition, alloying and sample mounting procedures were described in Sec. 4.5.1. A plot of Hall voltage versus magnetic field for current in the "normal" and in the "reverse" directions is given in Fig. 4.21. The temperature dependence of μ_H is given in Fig. 4.22. It can be seen that the electron mobility followed a $T^{3/2}$ law, which is predicted in eqn. 4.15 for ionized impurity scattering. At higher temperatures, the measured mobility tended to saturate. As the temperature

increases, the electrons are scattered more by optical phonons. There will be a temperature range where electrons are scattered by a combination of ionized impurities and optical phonons. Ehrenreich (1960) showed that the mobility, due to a combination of these mechanisms, varies as $T^{1/2}$. At even higher temperatures, polar optical scattering dominates and this gives a mobility varying as $T^{-1/2}$ (Sec. 4.3).

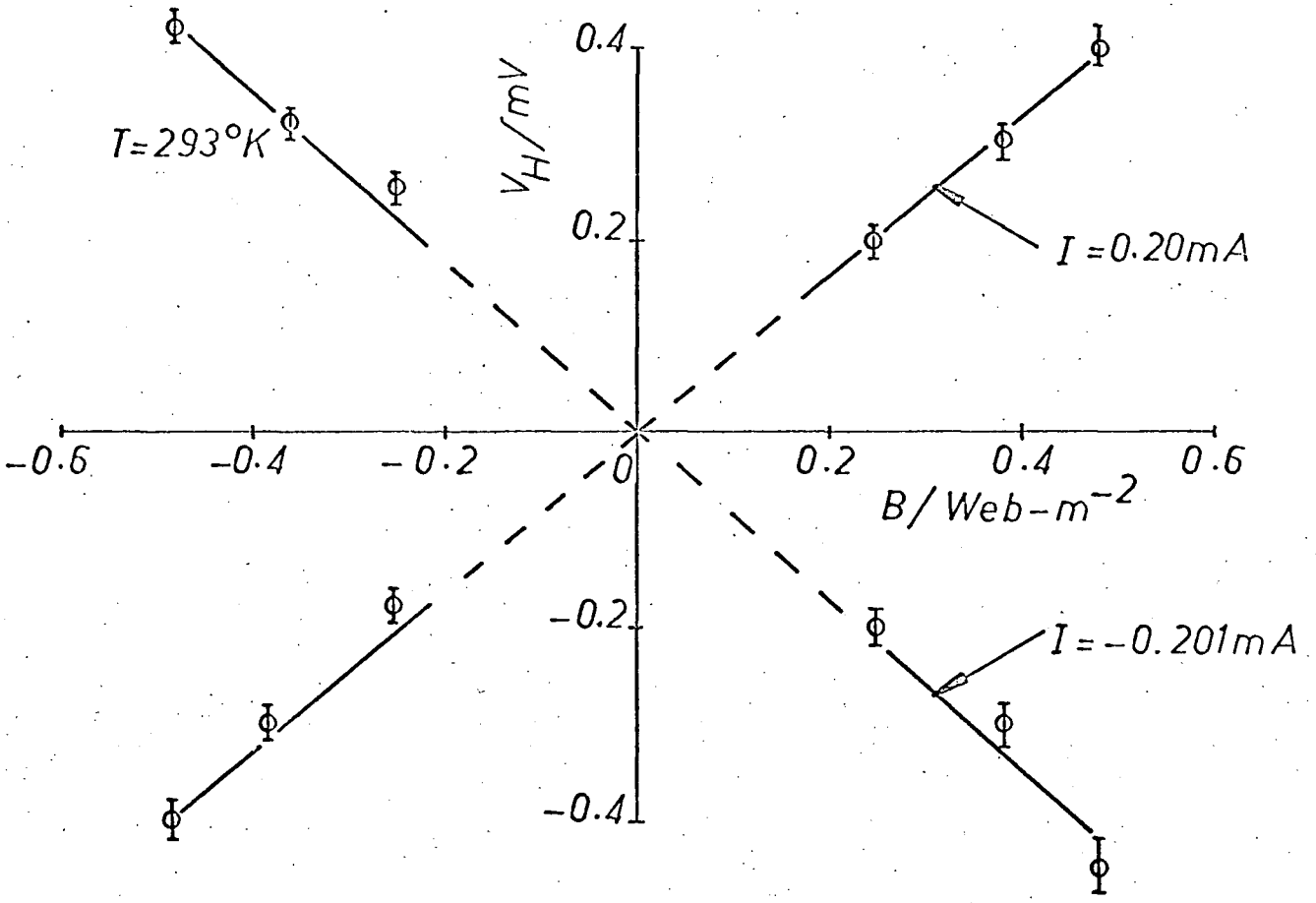

Fig. 4.21 Hall voltage versus magnetic field for current in the "normal" and in the "reverse" direction.

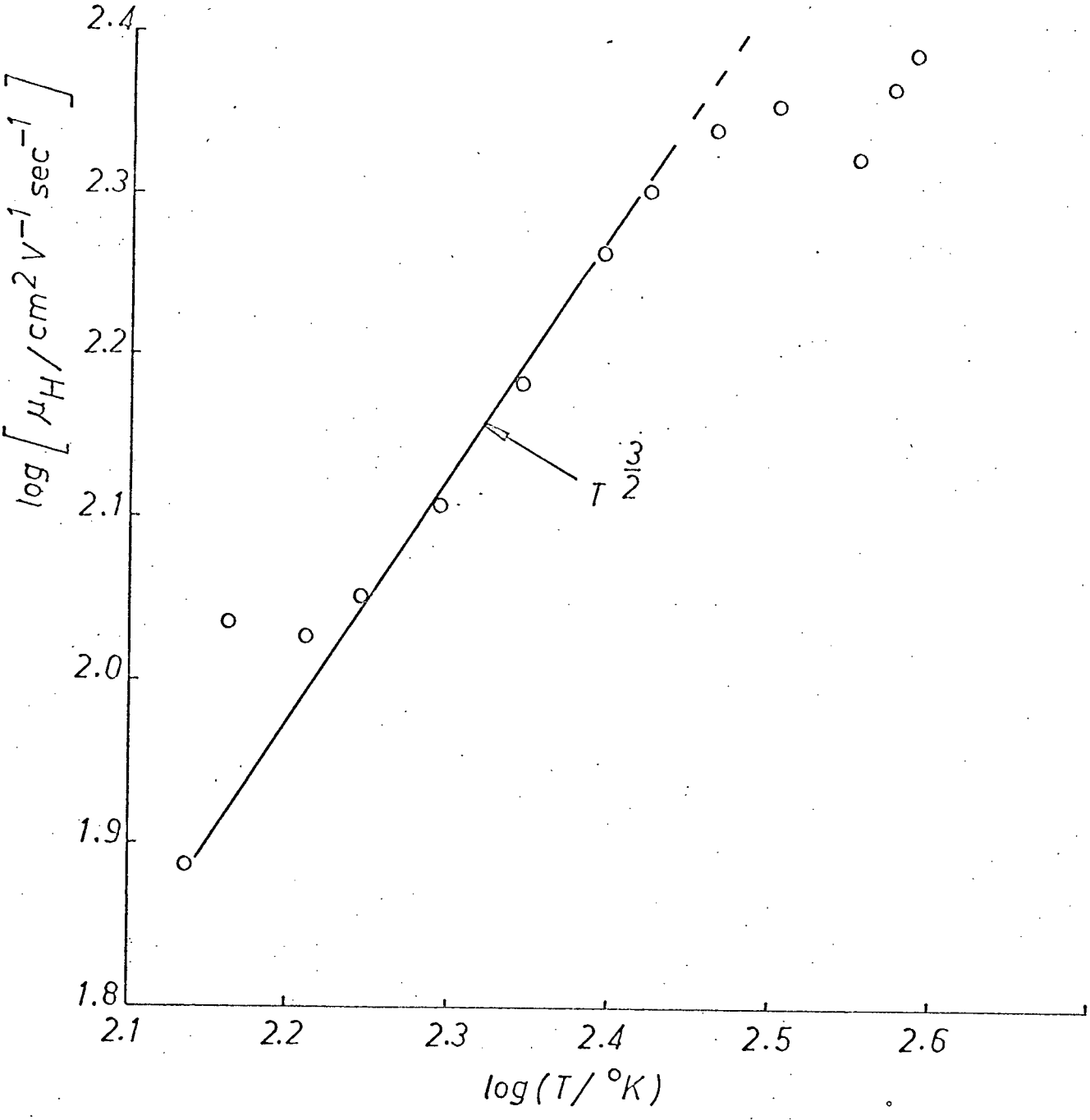

Fig. 4.22 Temperature dependence of the Hall mobility of electrons in a homoepitaxial GaAs film.

5. DIELECTRIC PROPERTIES OF ANODIC Al_2O_3 FILMS

5.1 Introduction

The most commonly used and most extensively studied insulator in semiconductor, particularly Si, device technology is SiO_2 produced either by thermal oxidation of Si (Atalla 1960) or by pyrolytic deposition, e.g. ethyl triethoxy-silane [C_2H_5 Si $(C_2H_5)_3$] deposited at 650 to 750°C (Klerer 1961). The other commonly used insulator in semiconductor device technology is Si_3N_4 (Chu, Lee and Gruber 1967). Other insulators which are being investigated for use in semiconductor devices are CaF_2 (Haering and O'Hanlon 1967), evaporated SiO_x (Johansen 1965), pyrolytic Al_2O_3 (Aboaf 1967), reactively evaporated Al_2O_3 (Ferrieu and Pruniaux 1969), wet (Mier and Buvinger 1969) and plasma (Waxman 1968) anodized Al.

This study is concerned primarily with the dielectric properties of evaporated Al films anodized in ammonium pentaborate dissolved in ethylene glycol. The objectives of this study are to develop a procedure of fabricating Al_2O_3 films and to investigate their properties which will be used later in the study of metal-insulator-semiconductor (MIS) systems. A.c. bridge, step response and d.c. conduction measurements were done to determine the dielectric constant as a function of frequency and d.c. resistivity of the films.

In comparison with SiO_2, anodic Al_2O_3 may offer several advantages when used as the insulator in semiconductor devices. Anodic Al_2O_3 can be formed at room temperature while thermal SiO_2 is formed at 1000 to 1300°C and pyrolytic SiO_2 is deposited at 650 to 750°C. High temperature treatment, which may degrade device performance, is avoided if anodic Al_2O_3 is used. Waxman and Zaininger (1968, 1969) found that devices made with plasma anodized Al as the insulator were stable and resistant to radiation damage. They also found that Al_2O_3 is less susceptible to impurity ion migration resulting in less drift in the device characteristics. On the other hand, ease with which ions, particularly

Na ions, migrate across SiO_2 is well known (Yon, Ko and Kuper 1966). The dielectric constant of SiO_2 and Al_2O_3 are 3.9 and 7 to 9, respectively. More flexibility in the design of insulated-gate devices is available when Al_2O_3 instead of SiO_2 is used. For example, a higher gate-voltage device can be designed by using an Al_2O_3 film twice as thick as a SiO_2 film. The amount of induced charges would still be about the same for both cases. As another example, because a change in conductivity of the surface space charge layer is proportional to a change in the free carrier concentration, an insulated-gate device with a higher transconductance may be fabricated if Al_2O_3 rather than SiO_2 is used.

The two major disadvantages of using wet anodized Al_2O_3 are as follows. The anodization of Al is sensitive to Cl ions (Harkness and Young 1966). Extreme care must be used to avoid Cl ion contamination. The entire device is exposed to the electrolyte during anodization. This may be an added source of contamination. Viscous electrolyte, however, may be used only on areas where desired.

5.2 Dielectric Properties of Amorphous Films

The complex permittivity $\varepsilon(\omega,T)$ is used to describe the dielectric properties of amorphous films.

$$\varepsilon(\omega,T) = \varepsilon_o[\varepsilon'(\omega,T) - j\,\varepsilon''(\omega,T)] \tag{5.1}$$

$$\stackrel{d}{=} \varepsilon_o\,\varepsilon_r$$

Conventionally, ε'' is defined by the magnitude of the inphase current flowing through a capacitor when a sinusoidal voltage is applied across the capacitor. In terms of the phase angle, δ, between the total current, i, and the out-of-phase current, i_q

$$\tan\delta = \frac{[i^2 - i_q^2]^{1/2}}{i_q} = \varepsilon''/\varepsilon' \qquad (5.2)$$

The dielectric properties of amorphous films have been the subject of many papers. (See, for example, Cherki and Coelko 1967; Argall and Jonscher 1968; Pulfrey, Wilcox and Young 1969). It has been determined that, for most amorphous insulators, ε'' and $\tan\delta$ are relatively independent of frequency in the audio range and that ε''/T is constant for certain temperatures.* The ionic relaxation model with a fairly flat distribution of activation energies, W, was used by Gevers and Dupre (1946) to describe the near independence of ε'' on ω. They showed that

$$\varepsilon' = \varepsilon_\infty + (\varepsilon_s - \varepsilon_\infty) \int_o^{W_o} G(W)dW \qquad (5.3)$$

$$\varepsilon'' = (\varepsilon_s - \varepsilon_\infty) \frac{\pi}{2} kT\, G(W_o) \qquad (5.4)$$

where

$$\frac{2\pi}{\omega} = \frac{\tau_o}{2} e^{W_o/kT} \qquad (5.4a)$$

$\varepsilon_s = \varepsilon_r(\omega=0)$

$\varepsilon_\infty = \varepsilon_r(\omega=\infty)$

τ_o = a constant, inverse of jump frequency.

Eqn. 5.3 implies that only those processes with activation energies less than W_o respond to an applied frequency ω. Equation 5.4 implies that losses occur only for those processes with the characteristic frequency ω. The angular frequency ω is related to the activation W_o by equation 5.4a.

5.2.1 A.c. Bridge Method

The relative permittivity of insulators in the frequency range 10^2 to 10^7 Hz can be easily measured using one of the many conventional a.c. bridges.

---

* Argall and Jonscher (1968) found that for their Al_2O_3 films constancy in ε'' and ε''/T was a special case at room temperature.

The losses measured by the capacitance bridge must be corrected for losses due to the series resistance R_L, which can be due to contact and lead resistances. Once R_L is known, the loss tangent due to ε'' alone can be calculated. Consider the parallel R-C equivalent circuit model of a capacitor.

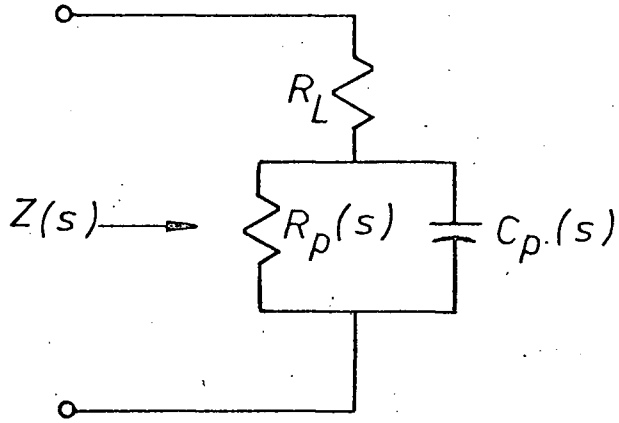

The loss tangent is

$$\tan\delta = \frac{R}{X} = \frac{R_L(1 + \omega^2 R_p^2 C_p^2) + R_p}{\omega R_p^2 C_o}$$

or

$$\frac{\tan\delta}{\omega C_p} = R_L + \frac{R_L + R_p}{\omega^2 R_p^2 C_p^2} \tag{5.5}$$

As ω approaches ∞, $\frac{\tan\delta}{\omega C_p}$ approaches R_L. Thus R_L can be calculated once the intercept of a $\frac{\tan\delta}{\omega C_p}$ versus $\frac{1}{\omega}$ plot is known. The loss tangent due to ε'' is

$$\tan\delta_c = \tan\delta - \tan\delta_L \tag{5.6}$$

The frequency dependence of ε'' can be calculated immediately from

$$C(\omega) = C_o \varepsilon'(\omega)$$

$$\tan\delta_c = \frac{\varepsilon''(\omega)}{\varepsilon'(\omega)}$$

therefore,

$$C_o\, \varepsilon''(\omega) = C(\omega)\, \tan\delta_c(\omega) \tag{5.7}$$

where C_o is the capacitance of the capacitor when the dielectric is replaced by air or vacuum and C is the measured capacitance.

5.2.2 Step Response Method

At low frequencies (10^{-2} to 10^{-4} Hz), losses in the dielectric can be calculated by measuring the polarization current as a function of time upon the application or removal of a step voltage across the dielectric. Hamon (1952) and later, Baird (1968) analyzed measurements of this type by assuming a time dependence of the form $A\ t^{-n}$ for the polarization current i(t). For n=1, this assumption is equivalent to saying that the distribution of activation energies is flat.

If linear response theory holds, then ε' and ε'' are given by

$$\varepsilon'(\omega) = \frac{1}{C_o}\left[C_\infty + \int_o^\infty A\ t^{-n} \cos \omega t\ dt\right] \tag{5.8}$$

$$\varepsilon''(\omega) = \frac{1}{C_o}\left[\frac{G}{\omega} + \int_o^\infty A\ t^{-n} \sin \omega t\ dt\right] \tag{5.9}$$

where G is the d.c. conductance, C_∞ is the capacitance of the sample at very high frequencies, C_o is the corresponding value of capacitance with vacuum or air between the electrodes and ω is the angular frequency. By a simple substitution, it can be shown that

$$\varepsilon'(\omega) = \frac{1}{C_o}\left[C_\infty + A\ \omega^{n-1}\ \Gamma(1-n)\ \cos(1-n)\frac{\pi}{2}\right] \tag{5.10}$$

$$\varepsilon''(\omega) = \frac{1}{C_o}\left[\frac{G}{\omega} + A\ \omega^{n-1}\ \Gamma(1-n)\ \cos\frac{n\pi}{2}\right] \tag{5.11}$$

where $\Gamma(1-n)$ is the gamma function. Usually, discharge currents are considered, then G = 0 and the effect of leakage current can be eliminated.

Two methods may be used in calculating ε''. In the first one, A is obtained from the intercept of a $\frac{i(t)t^n}{V}$ versus V plot. By extrapolating to zero V, the non-linear effects, which may be due to space charge, are minimized.

$C_o \varepsilon''(\omega)$ can be obtained immediately from eqn. 5.11. In the second one, Hamon (1952) showed that for $0.3 < n < 1.2$, ε'' is given by

$$\varepsilon'' \simeq \frac{i(t_i)}{C_o V} \tag{5.12}$$

where $i(t_i)$ is the value of the discharge current at t_i and the corresponding angular frequency is

$$\omega_i = 0.63/t_i \tag{5.13}$$

5.3 Growth of Oxide Films

The properties of anodic films, the physical mechanisms involved in their growth and their kinetics have been studied extensively (see, for example, Young 1961; Goruk, Young and Zobel 1966; Dell'Oca 1969). Only the results relevant to the preparative techniques will be quoted here.

5.3.1 Constant Current Formation

An oxide may be grown to a predetermined thickness by applying a constant current until an amount of charge corresponding to the desired thickness has been passed through the oxide/electrolyte interface. The thickness of an oxide with formula $M_x O_y$ and density ρ is given by

$$D = (QM\eta)/(2AyF\rho) \tag{5.14}$$

where

$Q = \int_o^t i(\tau)d\tau$ = total charge passed

M = molecular weight of metal

A = area of oxide

F = the Faraday (96500 coulombs)

η = current efficiency = the proportion of charge not used in other reactions.

At a fixed temperature and current density, the rate of change of voltage is

$$\left(\frac{dV}{dt}\right)_{J,T} = \left(\frac{dV}{dD}\right)_{J,T} \left(\frac{dD}{dt}\right)_{J,T}$$

$$= \mathcal{E}\, J\, \eta\, \chi \qquad (5.15)$$

$$\chi \triangleq M/(2yF\rho)$$

To a first approximation

$$J = J_o\, e^{\beta \mathcal{E}} \qquad (5.16)$$

therefore $$\left(\frac{dV}{dt}\right)_{J,T} = \frac{1}{\beta}\, \ell n\left(\frac{J}{J_o}\right) J\, \eta\, \chi \qquad (5.17)$$

The rate of change of V is almost proportional to the current density.

5.3.2 Constant Voltage Formation

During formation at constant voltage, the rate of change of current density may be given by (Dreiner 1964)

$$\left(\frac{dJ}{dt}\right)_V = \frac{d}{dt}\left[J_o\, e^{\beta V/D}\right]$$

$$= -\frac{\beta V}{D^2}\, J\, \frac{dD}{dt} = -\frac{\beta V}{D^2}\, J^2\, \alpha \qquad (5.18)$$

If D is assumed constant,

$$-\int \frac{dJ}{J^2} = \int \frac{\beta V}{D^2}\, \alpha\, dt$$

therefore $$\frac{1}{J} = \text{const} + \frac{\beta V \alpha}{D^2}\, t \qquad (5.19)$$

$$\alpha \triangleq \frac{M\eta}{2yF\rho}$$

Plots of $\frac{1}{J}$ versus t will be linear until such time that the leakage current dominates the formation current. Thus, a $\frac{1}{J}$ versus t plot can be used as a simple and useful check that the oxide formation is proceeding properly.

5.4 Experimental Procedures

5.4.1 Substrate Preparation

Precleaned microscope slide (Fisher 12-550) were ultrasonically

agitated in reagent grade acetone for about 3 min. Then they were vapour degreased first in a Soxhlet extractor containing acetone and then in another one containing propanol. Next, they were boiled in doubly-distilled water for about 5 min , dried in a stream of N_2 gas and immediately placed inside the Veeco vacuum chamber for Al deposition.

5.4.2 Al Source Preparation

High purity (99.999%) Al wires, cut in about 1 cm lengths, were first degreased by dipping in technical grade trichlorethylene, in reagent grade acetone ultrasonically agitated in a KOH solution (1 gram in about 15 ml of doubly-distilled water) for about 2 min., and then thoroughly rinsed in doubly-distilled water. A piece of W wire, about 7 cm long, was cleaned in a similar manner. The Al wires were clipped onto the W wire heater and excess water was blown dry by a stream of N_2 gas. The Al source was then mounted inside the vacuum chamber.

5.4.3 Vacuum Deposition of Al

Typically, the background pressure inside the vacuum belljar was about 5×10^{-6} Torr and rising to about 0.5 to 1×10^{-4} Torr during deposition. The Veeco vacuum system has been described elsewhere in the thesis (see Sec. 4.5). As a further precaution against contamination, a shutter was used during the initial outgassing of the Al source. A quartz crystal controlled oscillator was used to monitor the thickness of the deposited films. The oscillator was first calibrated by measuring the change in frequencies for a series of films deposited on different glass substrates. The thicknesses of these films were measured using a Sloan M-100 Angstrometer (see Sec. 2.3.4). Typically, films of about 1000 Å thick were deposited at a rate of about 7 Å/sec.

5.4.4 Anodization of Al Films

Al films were anodized by using the experimental set-up as shown

schematically in Fig. 5.1. A piece of Pt wire was used as the cathode and the electrolyte was ammonium pentaborate dissolved in ethylene glycol (33.4 gm/lit). The glass beaker and Pt wire were boiled in doubly-distilled water for at least 10 min and subsequently dried in an oven. Extreme care was taken during the entire anodization procedure to avoid Cl ion contamination.

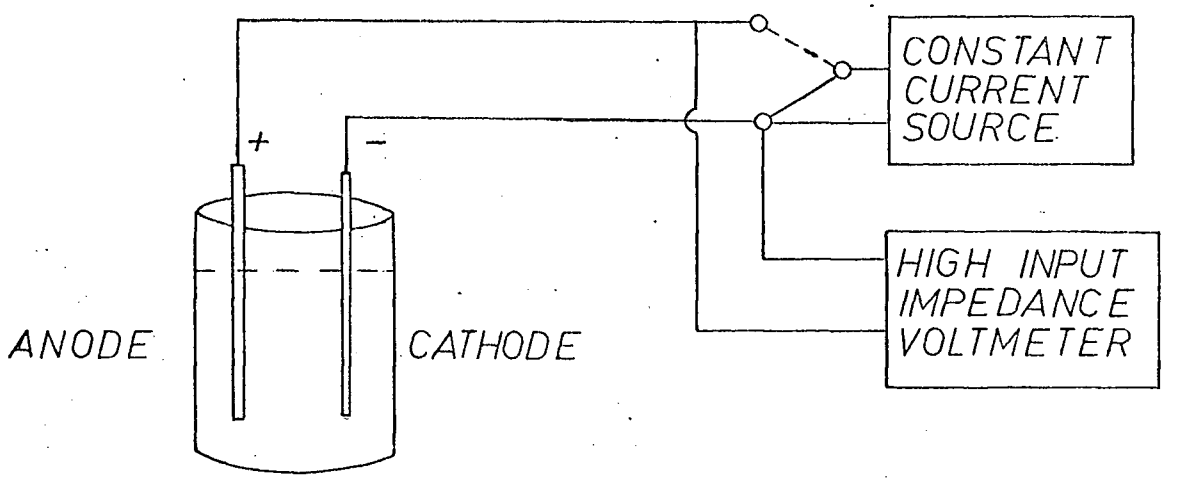

Fig. 5.1 Schematic diagram of the anodization set-up.

A method of estimating the oxide thickness is as follows. Assume that, under constant current conditions, an Al film is completely anodized in t_f sec. The oxide thickness, D_f, is measured using a Sloan Angstrometer. From eqn. 5.14, oxide thickness is proportional to time. By applying the same current density, the oxide thickness of another Al film which has been anodized to t_1 is given by

$$D_1 = (t_1/t_f)\, D_f \tag{5.20}$$

A second method of estimating the oxide thickness is from capacitance measurements. The area, A, of the counterelectrode is calculated. By assuming

that $\varepsilon' = 8.4 \pm 0.2$ (Bernard and Cook 1959), the thickness is simply given by

$$D = A \varepsilon_o \varepsilon' / C \tag{5.21}$$

The thicknesses determined by the two methods agreed to within 15%. This discrepancy may be due to errors in obtaining D_f and A. Accuracy in Angstrometer readings are limited by the resolution of the fringe linewidths. This was estimated to be about $\pm$ 150 Å. Accuracy in A depends upon the accuracy in measuring the diameter of the counterelectrode. This is dealt with in Sec. 5.4.5. The relative permittivity ε' was measured by Bernard and Cook at 120 Hz. The electrolyte they used was ammonium pentaborate dissolved in ethylene glycol (30% by weight of salt). It was assumed here that ε' is independent of the electrolyte concentration and that it is also fairly independent of frequency at room temperature (see Sec. 5.5.1).

5.4.5 Deposition of Counterelectrodes

Counterelectrodes of Al or Au dots were evaporated. Their shapes were defined by using photoetched beryllium-copper masks. The dots ranged from 0.1 to 0.7 mm in diameter. Diameters of the dots were measured by using a travelling microscope. Several sources of errors can arise in the determination of counterelectrode area. Due to imperfections in the beryllium-copper masks or to distortions in the mask during deposition from being heated by the source, the evaporated counterelectrodes deviated from the circular shape. Several readings with the travelling microscope were taken and an average value of the diameter of each particular dot was determined. A penumbra effect was also observed. If the Al_2O_3 film was not situated parallel and close to the mask, the boundary of the dots will appear smeared, rendering the determination of the diameters of the dots difficult. The counterelectrode areas were estimated to be accurate to $\pm$5%.

5.4.6 A.c. Bridge, Step Response and d.c. Conduction Measurements

Capacitances and dissipation factors were measured using either a GR 1615A (frequency range: 50 Hz to 100 kHz) or a Boonton 75C (frequency range: 5 to 500 kHz) capacitance bridge, depending on the frequency used. The GR 1615A is a transformer arm ratio bridge with the following rated accuracies: $C_{meas} = C \pm 2 \times 10^{-5}$ f/kHz% + 2×10^{-3}(C/μF)(f^2/kHz^2)%, $D_{meas} = D \pm 0.1 \times (D_{meas})\%$ + 0.001. The Boonton 75C is essentially a modified transformer arm ratio bridge and is equipped with its own signal generator, d.c. supply and null dector. Its rated accuracies depend upon the range used. For the multiplier range C = 1, G = 10 kΩ,

$$C_{meas} = C \pm (0.25\% + \frac{1000}{R_p/\Omega} \text{ pF} + 0.2 \text{ pF})$$

$$G_{meas} = G \pm (10\% + \frac{Q}{500}\ \% + 0.001\mu\Omega)$$

$$\frac{1}{D} = Q = \frac{(2\pi f/mHz)(C/pF)}{G_{meas}/\mu\Omega}$$

The a.c. signal frequency was calibrated using a Beckman 6146 frequency counter. Stray and lead capacitances were minimized by using the three terminal configuration for all bridge measurements. The sample was placed inside a grounded, light-tight metal box. Electrical contacts to be electrodes were made by using Au plated beryllium-copper springs mounted on Kulicke and Soffa micromanipulators.

Step response and d.c. conduction currents were measured by using a Keithley 417 high-speed Picoammeter (accuracy: ±3% full scale for all ranges except the lowest, which is ±5%). The circuit used is shown in Fig. 5.2. Co-axial go and return leads were used and other usual precautions for measurement of low currents were also taken. The d.c. voltage supply was calibrated using a Fluke d.c. Differential Voltmeter model 881 AB. A fixed voltage of 10.000 ± 0.002 V in conjunction with a high precision GR voltage divider was used. Drift in the d.c. supply was found to be negligible during an 8-hour period. The circuit was checked by measuring the current flowing through a

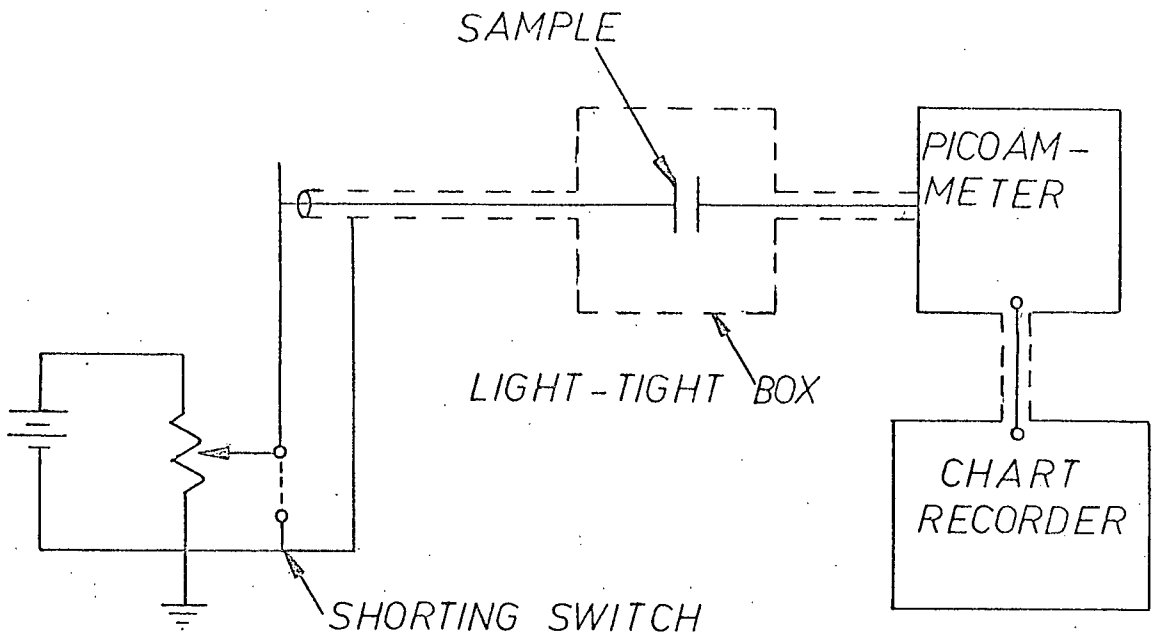

Fig. 5.2 Schematic diagram of the d.c. conduction measurement set-up.

standard $10^{10}\Omega$ resistor. Under open circuit conditions (sample absent), no measurable leakage current was recorded even when a voltage about 5 volts higher than the highest used in the actual experiments was applied. Charging and discharging currents were recorded using a Moseley 7100 BM strip chart recorder connected to the recorder output of the Picoammeter. Steady-state conduction currents were estimated by extrapolating the measured charging currents to long periods of time. The sample was mounted in a manner similar to that during bridge measurements and was left on overnight with the terminals shorted before taking any d.c. conduction measurements. All capacitance and d.c. measurements were done in an air ambient and at room temperature.

5.5 Analysis of Results

5.5.1 A.c. Bridge

The following discussions refer particularly to sample #9C43. Similar

results were obtained from Al_2O_3 films that were made in conjunction with the metal/Al_2O_3/GaAs MIS experiments (Sec. 6.6). Following the procedure detailed in Secs. 5.4.1 to 5.4.3, an Al film 900 Å thick was deposited onto a glass substrate. The oxide was formed at a constant current density of 1 mA/cm^2 to 15V (t_1 = 15.5 sec) and left at constant voltage for almost 24 hr. The oxide thickness was estimated to be 280 $\pm$ 40 Å. Counterelectrodes of Al, about 600 Å thick, were deposited. The electrode area of sample #9C43 was $3.91 \times 10^{-3} \pm 0.2 \times 10^{-3}$ cm^2.

Measured values of the loss tangent were corrected for series resistance using the procedure outlined in Sec. 5.2.1. A plot of $\frac{\tan\delta}{fC_p}$ versus 1/f is given in Fig. 5.3. At 1/f = 0, the intercept gives $2\pi R_L$; $\tan\delta_c$ was calculated using eqn. 5.6. Figs. 5.4 and 5.5 show plots of $C_o\varepsilon'$ and $\tan\delta_c$ versus frequency, respectively. It can be seen that ε' varied less than 3% in the frequency range 0.5 to 100 kHz, rising at lower frequencies. $\tan\delta_c$ was found to be a slow function of frequency with higher values at lower frequencies.

5.5.2 Step Response

The current density, neglecting diffusion current, flowing through a capacitor is given by

$$J_T = \frac{\partial D}{\partial t} + J(\mathcal{E}) \tag{5.22}$$

In the case of an applied step field $\mathcal{E} = \mathcal{E}_o\, u(t)$,

$$J_T = \varepsilon_o \mathcal{E}_o\, \delta(t) + \frac{\partial P}{\partial t} + J[\mathcal{E}_o u(t)] \tag{5.23}$$

If it is assumed that the polarization processes in the dielectric can be represented by a superposition of Debye -type processes involving ion hopping with a $1/\tau$ distribution of relaxation times,

$$J_p = \frac{\partial P}{\partial t} = A_1 \frac{\mathcal{E}}{t} \tag{5.24}$$

Equation 5.24 is derived in Appendix 5.1.

The input resistance of the PicoAmmeter increases from $10^2\,\Omega$ at the 10^{-5} A range to $10^{10}\,\Omega$ at the 10^{-13} A range in decade steps. If the capacitance

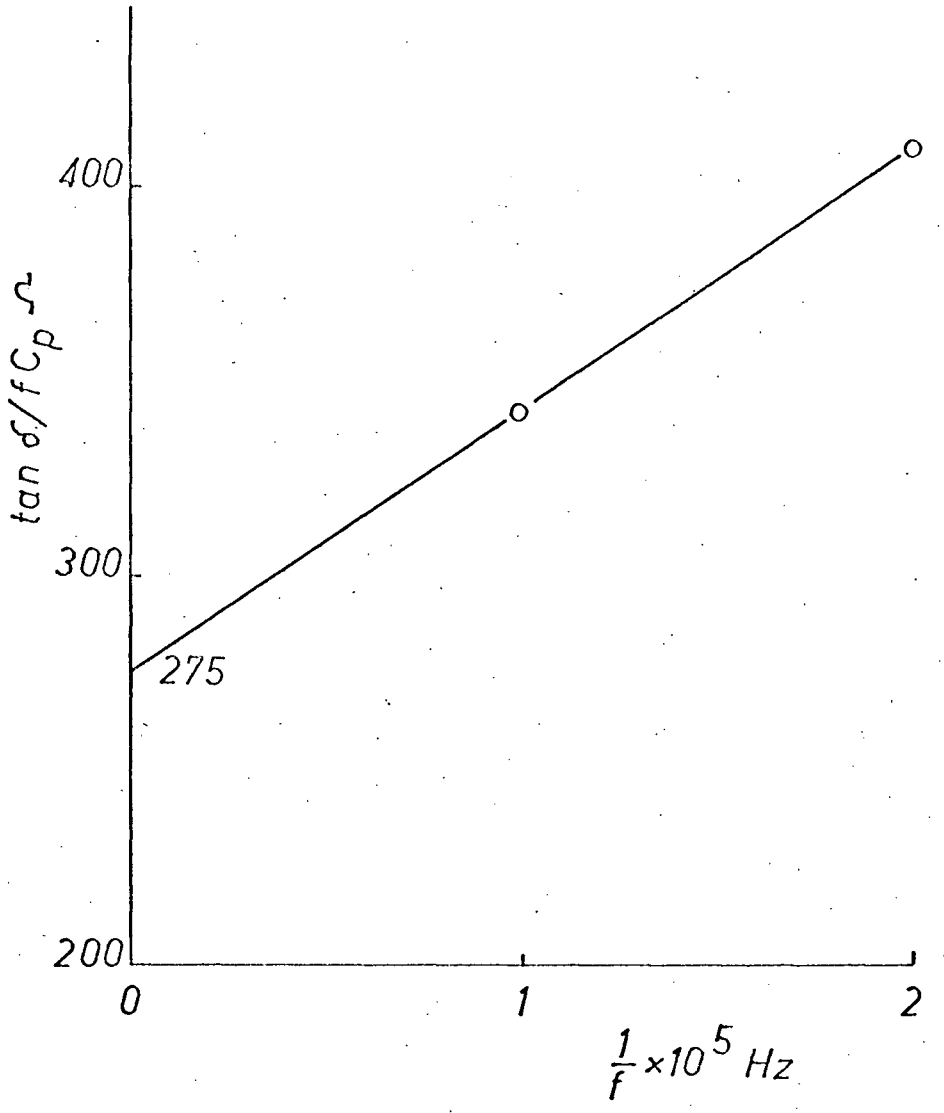

Fig. 5.3 Plot of tan δ/fC_p versus 1/f.

of the sample is 1000 pF, the transient currents may be neglected provided that $t > 10^{-7}$ sec to t > 1.0 sec spanning the extreme current ranges in decade steps. From Fig. 5.4, C ≃ 1000 pF, and at the highest applied voltage (5V), the current range used was 10^{-10} A. Since RC = 0.1 sec, $\varepsilon_o \mathcal{E}_o \delta(t)$ may be neglected for t > 1 sec and

$$J_T = A_1 \frac{\mathcal{E}}{t} + J[\mathcal{E}_o u(t)]$$

Figs. 5.6 and 5.7 show the charging and discharging currents as functions of time with the applied or removed voltages as parameters, respectively. The charging currents tended to saturate at large t and their slopes were less than

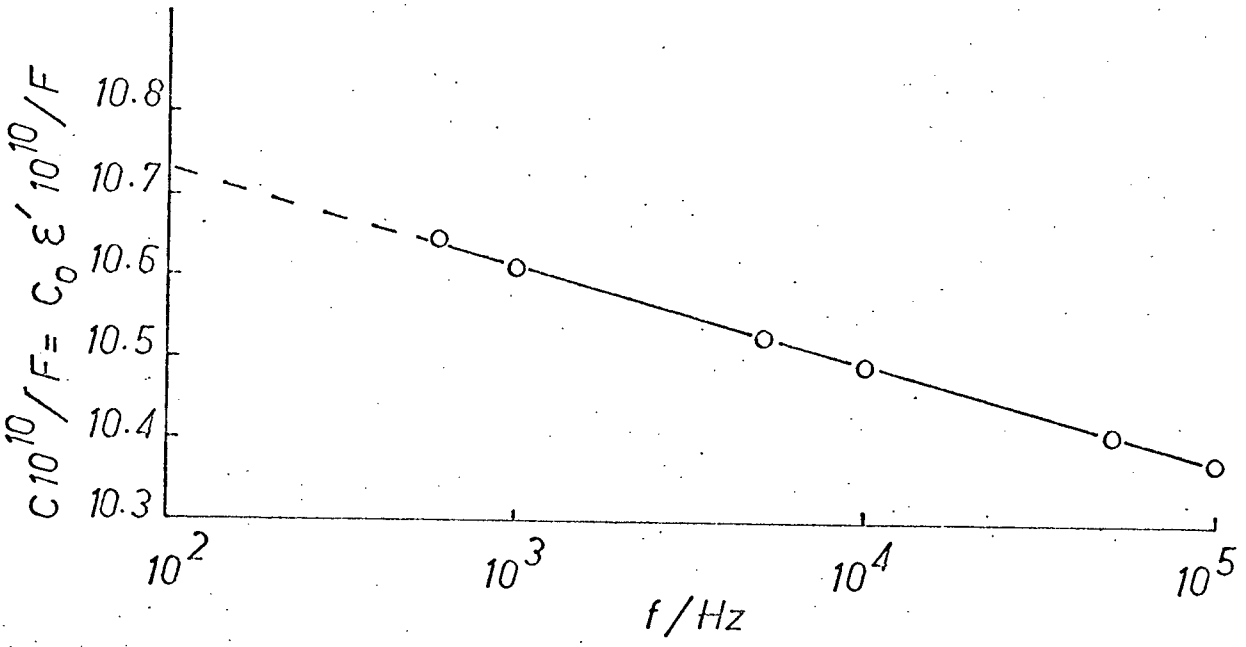

Fig. 5.4 Plot of $C_o \varepsilon'$ versus f.

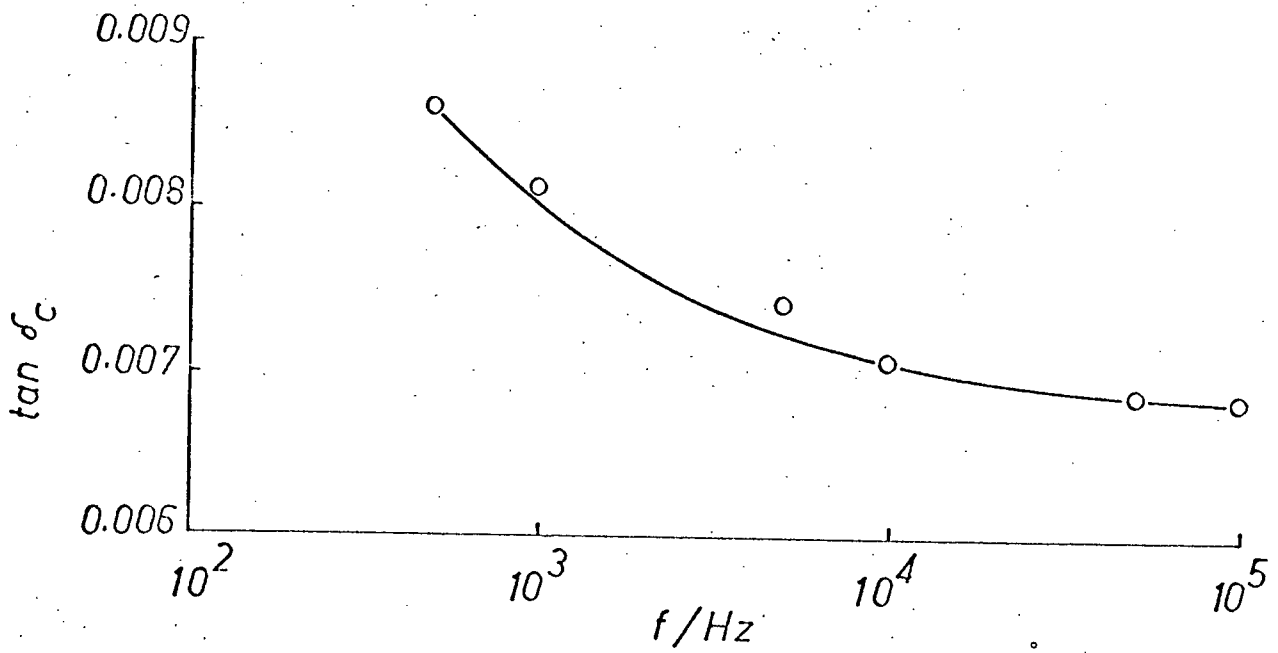

Fig. 5.5 Plot of tan δ_c versus f.

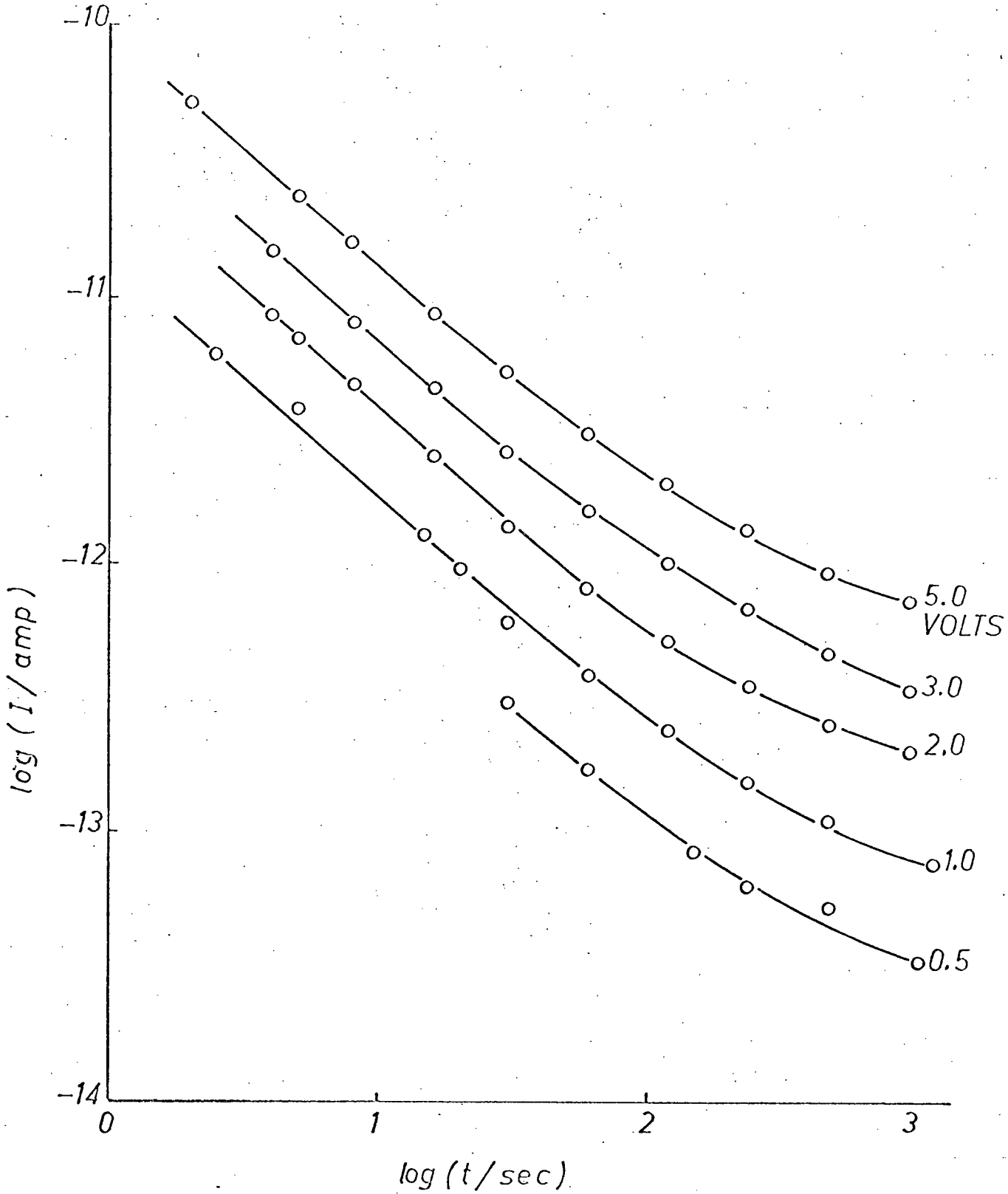

Fig. 5.6 Charging currents versus time as a function of applied d.c. voltage.

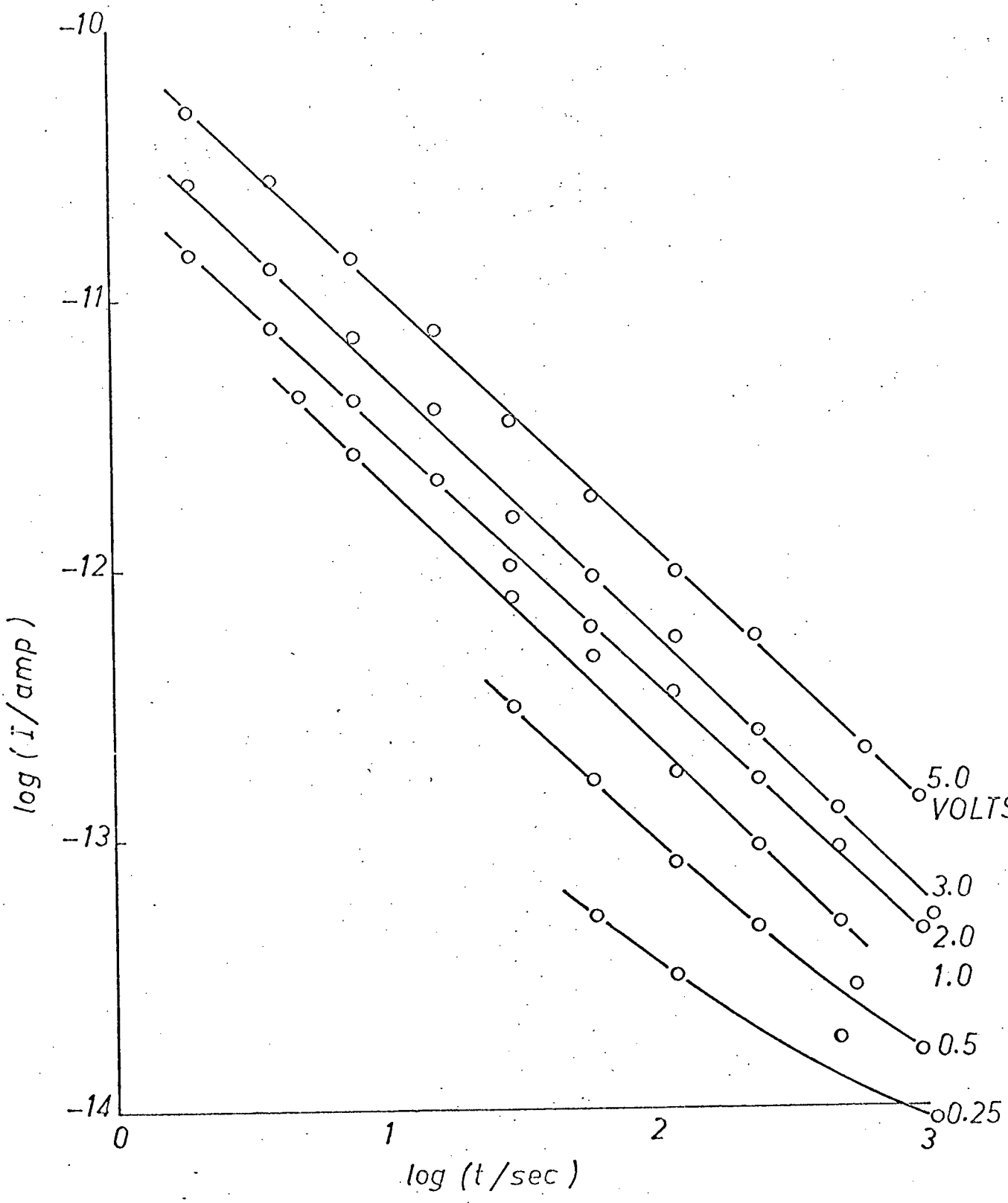

Fig. 5.7 Discharging currents versus time as a function of preapplied d.c. voltage.

that for the discharging currents (-0.70 as compared to -0.95). This may be due to the leakage current J becoming more dominant because J_p approaches 0 as t approaches ∞. On the other hand, for discharging currents, J = 0 and $J_T = J_P$.

The frequency dependence of ε'' at low frequencies was determined using the two methods discussed in Sec. 5.2.2 and is shown in Fig. 5.8. The equation of the heavy line (eqn. 5.25) was calculated from eqn. 5.11, with G = 0 and n = 0.95.

$$\log[C_o\varepsilon''/pF] = 1.40 - 0.05 \log(f/Hz) \tag{5.25}$$

The points represented by open circles were calculated using Hamon's method. This method may be used for n was 0.95 which lies within the limits of n imposed by Hamon. In the same plot were points (represented by filled circles) calculated using eqn. 5.7 to determine the frequency dependence of ε'' in the audio range. As shown in Fig. 5.8, ε'' increased with decreasing frequency. This may be due to increased losses at low frequencies arising from flaws.

D.c. conduction currents were obtained from charging currents by extrapolating to long periods of time. Fig. 5.9 shows a Log (J) versus $\mathcal{E}^{1/2}$ plot. The straight line was drawn by assuming a Schottky law with $\varepsilon_r = 4$. The theoretical Schottky slope is given by

$$\frac{\alpha}{KT} = \frac{1}{KT}\sqrt{\frac{q^3}{4\pi\varepsilon_r\varepsilon_o}} \tag{5.26}$$

The d.c. resistivity for low fields was about $10^{13}\Omega$-cm. The breakdown field was about 5×10^6 V/cm.

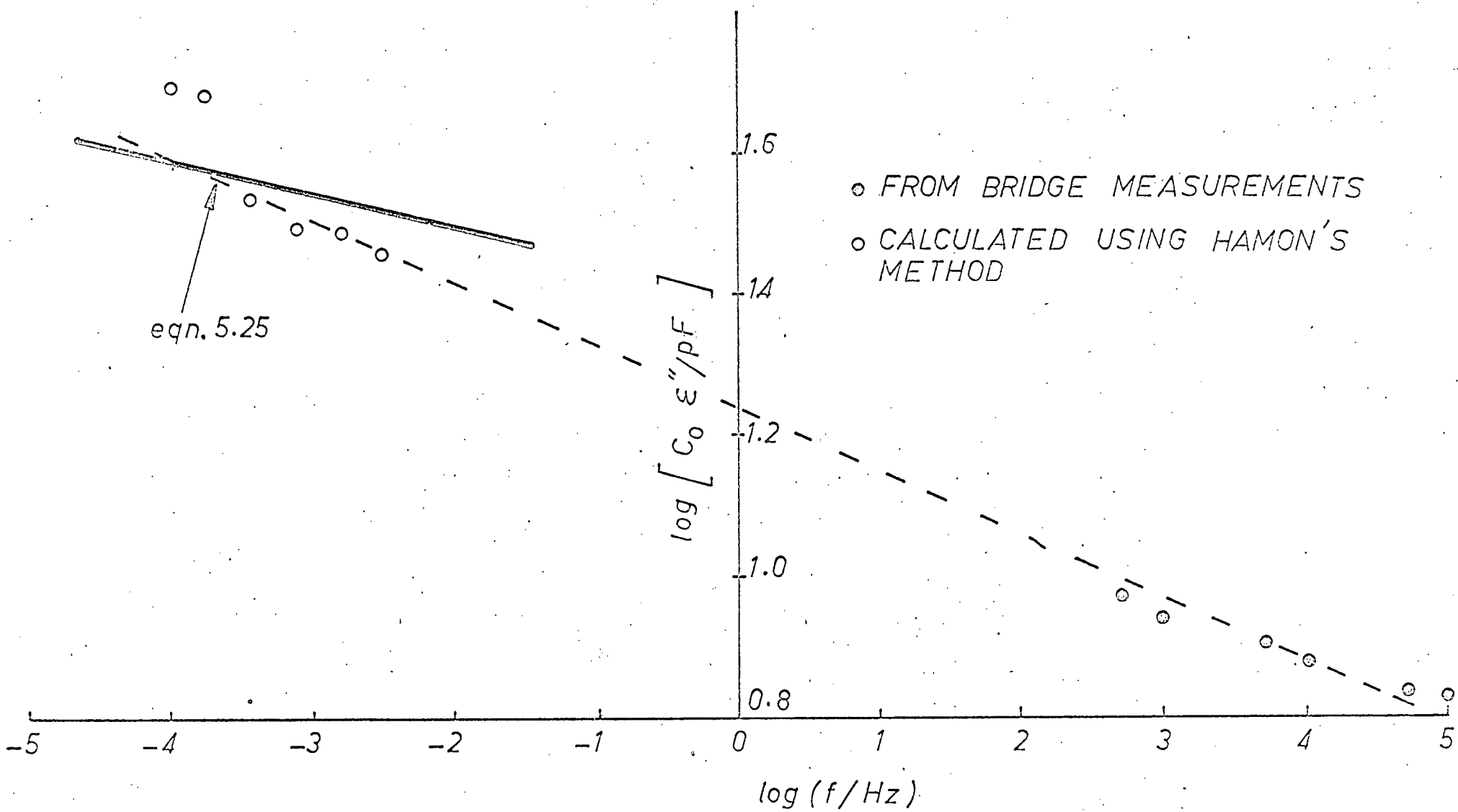

Fig. 5.8 Frequency dependence of ε" as determined by a.c. bridge and step response methods.

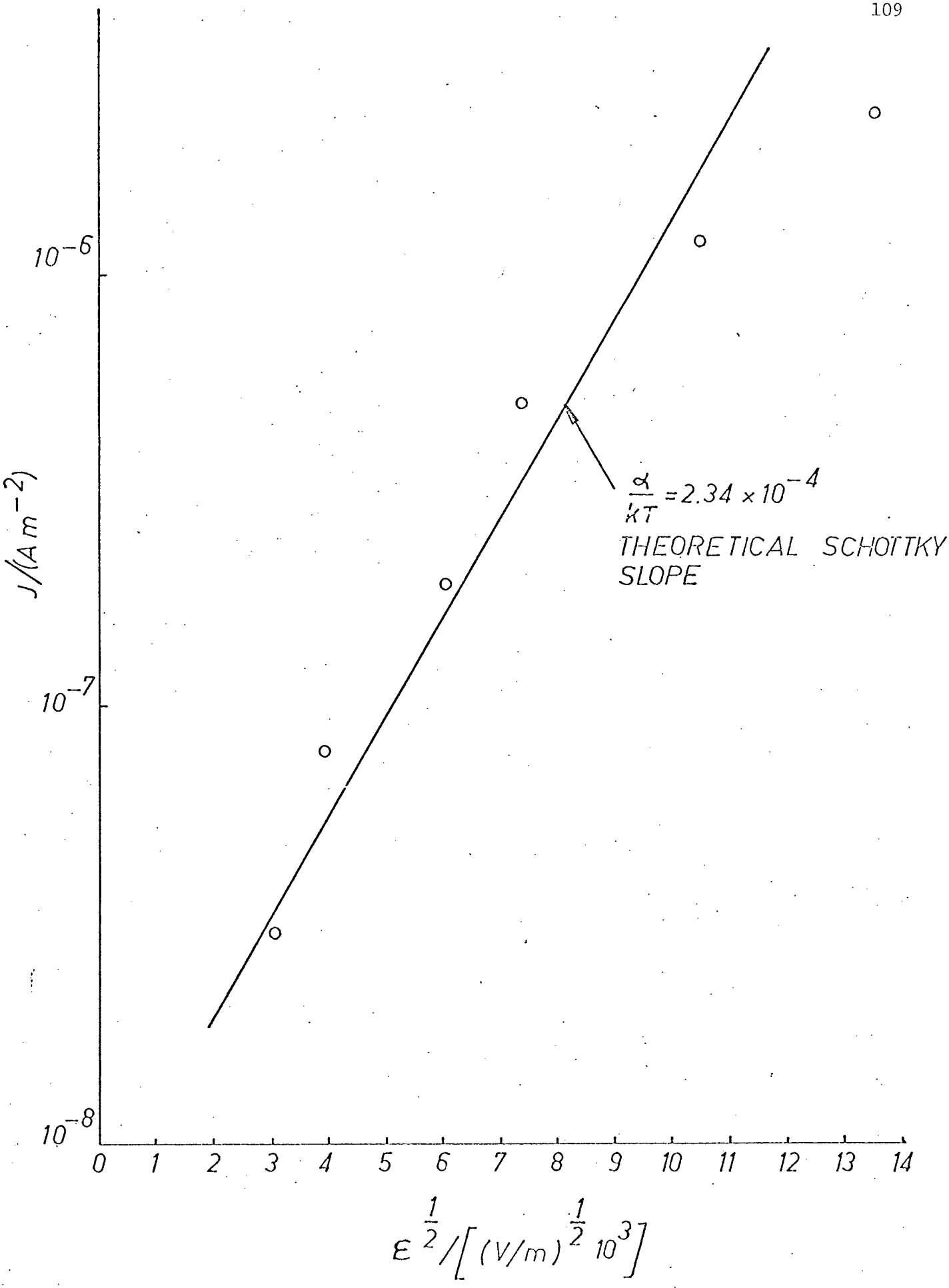

Fig. 5.9 D.c. conduction current versus applied field.

6. CHARACTERISTICS OF THE Al_2O_3/GaAs INTERFACE

6.1 Introduction

The properties of semiconductor surfaces and insulator-semiconductor interfaces have been extensively studied. (See, for example, Many, Goldstein and Grover 1965; Frankl 1967). The two principal methods used are field-effect conductance and metal-insulator-semiconductor (MIS) capacitance measurements. An advantage of the MIS capacitance method is that a knowledge of the surface mobility* is not required.

The MIS technique consists of measuring the capacitance of a metal-insulator-semiconductor sandwich as a function of an applied d.c. voltage and a small a.c. signal. Conclusions on the characteristics of the insulator/semiconductor interface are arrived at by interpreting the deviations of the experimental C-V curve from a theoretical C-V curve based on an idealized model of the MIS capacitor.

The most extensively studied system to date is the SiO_2/Si interface system. A recent review was published by Revesz and Zaininger (1968). Very little

---

* The surface mobility, μ_{ns}, is defined by

$$\mu_{ns} \triangleq \frac{\Delta I_{nx}}{q\ \Delta N\ \mathcal{E}_x}$$

where ΔI_{ns} = increase in electron current over the flatband value for one unit width of a surface

$\Delta N \triangleq \int_o^\infty (n-n_b)dz$ = excess surface carrier density with respect to the conditions at flatband.

$\mathcal{E}_x$ = electric field

See Many, Goldstein and Grover (1965) for further discussion.

work had been published on the insulator/GaAs system. Hall and White (1965) reported some results on the pyrolytically deposited SiO_2/GaAs system. Since Al_2O_3 appears to have certain advantages over SiO_2 (Sec. 5.1), the characteristics of the Al_2O_3/GaAs interface system would be of interest from the field-effect devices fabrication viewpoint.* The reasons for studying GaAs were mentioned in chapter 1.

6.2 The Ideal MIS Capacitor

The capacitance of the MIS structure is defined by

$$C \triangleq \frac{\partial Q_p}{\partial V_g} \tag{6.1}$$

where Q_p = surface charge density induced on the metal electrode by an applied voltage V_g.

For the moment, neglect metal-semiconductor contact potential differences, space charge in the insulator and ohmic drop across the semiconductor bulk. Their effect will be discussed in Sec. 6.3.4. The applied voltage V_g is

$$V_g = V_{ox} + V_s \tag{6.2}$$

where

V_{ox} = voltage drop across the insulator

V_s = voltage drop across the space charge layer near the insulator/semiconductor interface.

The applied voltage V_g is defined to be positive when the metal plate is positively biased with respect to the semiconductor. From Gauss' theorem, and the following definitions

$$C_{sc} \triangleq \left|\frac{\partial Q_{sc}}{\partial V_s}\right| = \text{differential capacitance of space charge layer.} \tag{6.3a}$$

* Some preliminary work was done on a plasma anodized Al_2O_3/GaAs system.

$$C_{ss} \triangleq \left| \frac{\partial Q_{ss}}{\partial V_s} \right| = \text{differential capacitance due to surface states.} \qquad (6.3b)$$

and the fact that $Q_p = -(Q_{ss} + Q_{sc})$ the normalized MIS capacitance c/c_i can be written as

$$\frac{c}{c_i} = \frac{c_{ss} + c_{sc}}{c_{ss} + c_{sc} + c_i} \qquad (6.4)$$

The quantities Q_{ss}, Q_{sc} are the total surface state and surface space charge densities, respectively. The capacitance per unit area of the insulator alone is given by c_i. For an ideal MIS capacitor, Q_{ss} is equal to zero. Hence

$$\frac{c}{c_i} = \frac{1}{1 + \frac{c_i}{c_{sc}}} \qquad (6.5)$$

The capacitance c_i is assumed to be independent of temperature and the magnitude and frequency of the applied voltages. It can be calculated once the dielectric constant and the thickness of the insulator are known. Depending upon the approximations used, an expression for c_{sc} can be calculated. Thus, using eqns. 6.2, 6.5 and the appropriate expression for c_{sc}, theoretical C-V curves may be obtained and used in the analysis of the experimentally measured C-V curves.

6.3 Capacitance-Voltage Characteristics of an Ideal MIS Capacitor

Many physical models and equivalent circuits have been proposed as attempts in explaining the characteristics of a real MIS capacitor. The MIS structure, as a voltage variable capacitor, was analyzed by Lindner (1962). Lehovec and Slobdskoy (1964) analyzed the a.c. behaviour of the MIS capacitor as a function of the frequency of the applied a.c. signal and of the d.c. bias. Terman (1962) was the first to use the MIS capacitor in the study of thermally oxidized Si surfaces. Later, Grove, Deal, Snow and Sah (1965) presented, in a

unified form, simple physical models of a MIS structure and used these models to explain the characteristics of thermally oxidized Si surfaces. The models of the MIS capacitor discussed in this section follow from Lindner and from Grove, Deal, Snow and Sah.

6.3.1 The Depletion Approximation

Assume for this, and for all subsequent discussions, that the semiconductor is p-type, that classical statistics hold and that all impurity atoms are ionized.

From the energy band diagram (Fig. 6.1), it can be seen that holes are depleted from the insulator/semiconductor interface if $V_g > 0$. The total space charge per unit area is given by

$$Q_{sc} = -q N_A x_d \tag{6.6}$$

where N_A = density of impurity ions

x_d = width of the depletion layer

Implicit in eqn. 6.6 are the assumptions that N_A is uniform throughout the space charge regions in the semiconductor and that the minority carriers are totally absent even in the bias range where E_i becomes smaller than E_F. This situation can arise if the insulator is leaky or if the capacitance is measured under transient conditions. That is, the d.c. bias is switched rapidly and the capacitance measured before minority carriers can accumulate at the interface.

For impurity concentrations of less than 10^{14} cm^{-3}, the depletion layer is in the order of 1μ thick. Typically, the metal counterelectrodes used are about 0.3 to 0.7 mm in diameter. Hence, to a good approximation, the one-dimensional Poission's equation may be used.

$$\frac{\partial^2 V}{\partial x^2} = -\frac{\rho}{\varepsilon} = \frac{q}{\varepsilon} N_A \tag{6.7}$$

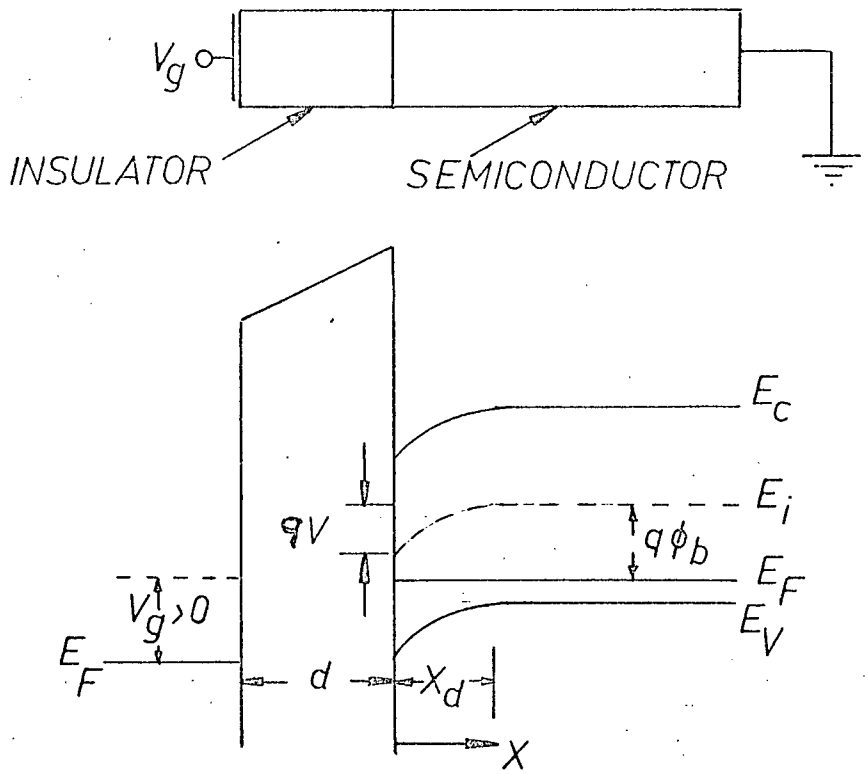

Fig. 6.1 Energy band diagram of an ideal metal/insulator/p-type semiconductor MIS capacitor.

with the boundary conditions

$$V(0) = V_s$$

$$V(x_d) = 0$$

Thus

$$V = V_s \left[1 - \frac{x}{x_d}\right]^2 \tag{6.8}$$

where

$$V_s = \frac{q\, N_A\, x_d^2}{2\, \varepsilon}$$

From equations 6.2, 6.3, 6.5 and 6.8, it can be shown that

$$\frac{c}{c_i} = \frac{1}{\left[1 + \frac{2\, c_i^2}{q\, N_A\, \varepsilon_r \varepsilon_o}\, V_g\right]^{1/2}} \tag{6.9}$$

which predicts that the normalized capacitance varies inversely as the square root of the applied voltage while the semiconductor surface is being depleted of majority carriers. For non-positive gate voltages, no depletion region exists and eqn. 6.9 does not apply.

6.3.2 The Low Frequency Approximation

For this case, it is assumed that the space charge region and the semiconductor bulk are in thermal equilibrium. This means that the a.c. signal must have a frequency low enough so that the minority carriers can follow its variation.

The charge density ρ is given by

$$\rho = q[N_D - N_A + p - n] \tag{6.10}$$

From the condition that charge neutrality holds in the bulk and that classical statistics is applicable,

$$\rho = q[n_b - p_b + p_b e^{-q/kT} - n_b e^{qV/kT}] \tag{6.11}$$

In terms of the normalized potential, $v \overset{d}{=} qV/kT$, Poission's equation becomes

$$\frac{\partial^2 v}{\partial x^2} = -\frac{q^2}{\varepsilon kT}[n_b - p_b + p_b e^{-v} - n_b e^{v}] \tag{6.12}$$

subject to the boundary conditions

$$\begin{aligned} \frac{\partial v}{\partial x}(\infty) &= 0 \\ v(\infty) &= 0 \end{aligned} \tag{6.13}$$

In practice, the boundary conditions stated in eqn. 6.13 are valid provided that $x >> L$, the effective Debye length which is defined as

$$L \overset{d}{=} \sqrt{\frac{\varepsilon kT}{q^2(n_b+p_b)}} \; . \tag{6.14}$$

Since

$$Q_{sc} = \int_o^\infty \rho(x)\, dx \tag{6.15}$$

It can be shown that

$$Q_{sc} = -\frac{v_s}{|v_s|} q(n_b+p_b) L F_s \tag{6.16}$$

where

$$F_s \overset{d}{=} \sqrt{2}\left[\frac{\cosh(u_b+v_s)}{\cosh u_b} - v_s \tanh u_b - 1\right]^{1/2} \tag{6.17}$$

and $u_b \overset{d}{=} \frac{q\phi_b}{kT}$ where $q\phi_b = E_F - E_i$ in the bulk. In terms of the intrinsic concentration,

$$Q_{sc} = -2\frac{v_s}{|v_s|} qn_i L_D\{2[\cosh(v_s+u_b) - \cosh u_b - v_s \sinh u_b]\}^{1/2} \tag{6.18}$$

$$L_D \overset{d}{=} \left[\frac{\varepsilon kT}{2q^2 n_i}\right]^{\frac{1}{2}}, \text{ the intrinsic Debye length.} \tag{6.19}$$

The total minority carriers in the inversion layer, Q_n, is given by

$$Q_n = -q\int_o^{x_i} n(x)dx = -q\int_{v_s}^{-u_b} \frac{n(v)}{\frac{\partial v}{\partial x}} dx$$

$$= -\frac{v_s}{|v_s|} q\, n_i L_D \int_{-u_b}^{v_s} \frac{e^{v+u_b}\, dv}{\{2[\cosh(v+u_b) - \cosh u_b - v\sinh u_b]\}^{1/2}} \tag{6.20}$$

where $E_i = E_F$ at the point x_i, and is the point at which the semiconductor is intrinsic.

Since $c_{sc} \overset{d}{=} \left|\frac{\partial Q_{sc}}{\partial v_s}\right|$

$$c_{sc} = \frac{\varepsilon q}{Q_{sc}}[n_i e^{-(v_s+u_b)} - n_i e^{v_s+u_b} + N_D - N_A] \tag{6.21}$$

for p-type semiconductor, $N_A >> N_D$, and

$$c_{sc} = \frac{\varepsilon q}{Q_{sc}}[p_s - n_s - N_A] \tag{6.22}$$

where $N_A = n_i e^{-u_b}$ and $p_s - n_s = n_i[e^{-(v_s+u_b)} - e^{v_s+u_b}]$. In terms of the space

charge density, eqn. 6.2 can be written as

$$V_g = V_s - \frac{Q_{sc}}{c_i} \tag{6.23}$$

since

$$Q_p + Q_{sc} = 0.$$

When the surface potential is zero, the corresponding "flat-band" space charge capacitance, c_{sco}, may be obtained from eqn. 6.22, by expanding p_s, n_s and Q_{sc} in their power series and neglecting higher order terms

$$c_{sco} \simeq [\frac{q^2}{kT} \varepsilon p_b]^{1/2} \tag{6.24}$$

If the impurities are completely ionized

$$c_{sco} \simeq [\frac{q^2}{kT} \varepsilon N_A]^{1/2} \tag{6.25}$$

The minimum space charge capacitance, c_{scm}, is not necessarily equal to c_{sco}. The former is found by setting the differential of eqn. 6.22 equal to zero. For $v_s > 0.3V$, c_{scm} was given by Hall and White (1965) as

$$c_{scm} \simeq \frac{q N_A}{2|v_s|} \tag{6.26}$$

The minimum space charge capacitance occurs when the space charge layer is strongly inverted. Strong inversion begins at $V_s \geq 2\phi_b$.

6.3.3 The High Frequency Approximation

At sufficiently high frequencies, the minority carriers cannot follow the applied a.c. signal and thermal equilibrium cannot be maintained in the space charge layer. When a gate bias which corresponds to the depletion to inversion range is applied, the space charge density is given by

$$Q_{sc} = Q_n + q[N_D - N_A]x_d \tag{6.27}$$

For $v_s >> 1$,

$$Q_{sc} \simeq -2 \frac{v_s}{|v_s|} q n_i L_D e^{(v_s+u_b)/2}$$

$$Q_n \simeq -2 \frac{V_s}{|V_s|} q\, n_i\, L_D\, e^{(V_s+u_b)/2}$$

The ratio Q_{sc}/Q_n approaches 1 and x_d tends towards a saturation value given by

$$x_{d_{max}} = \left[\frac{4\,\varepsilon\,\ell n(N_A/n_i)}{qN_A}\right]^{1/2} \tag{6.28}$$

The criterion used for determining the onset of strong inversion is that the minority carrier concentration in the space charge layer is greater than or equal to the impurity ion concentration. This means that $V_s = 2\phi_b$, which when substituted into eqn. 6.8 gives eqn. 6.28.

The space charge capacitance is now given by

$$c_{sc} = \frac{\varepsilon}{x_d} \tag{6.29}$$

For applied voltages which give rise to accumulation layers, the high frequency approximation becomes invalid. For p-type semiconductors, this approximation can be used only if $V_g \geq 0$.

The C-V characteristics may now be calculated from

$$\frac{c}{c_i} = \frac{1}{1 + c_i/c_{sc}} \tag{6.5}$$

and

$$V_g = -\frac{Q_{sc}}{c_i} + V_s \tag{6.23}$$

where c_{sc} is given by eqn. 6.29. When $V_g >> 1$, c/c_i reaches a minimum and is given by

$$\left(\frac{c}{c_i}\right)_{min} = \frac{1}{1 + \frac{c_i}{\varepsilon} x_{d_{max}}} \tag{6.30}$$

6.3.4 The Effect of Metal/Semiconductor Work Function Difference, Slow Surface States and Charges in the Insulator

The effect of the metal/semiconductor work function difference, slow surface states and charges in the oxide on the C-V characteristics of the MIS capacitor can be conveniently taken into account by simply replacing V_g by

$V_g - V_{fb}$ in the equations derived in Sec. 6.3.1 to 6.3.3. The voltage V_{fb} is defined as the "flat-band" potential and is given by

$$V_{fb} \triangleq \phi_{ms} - \frac{Q_{sl}}{c_i} - \frac{1}{c_i} \int_o^d \frac{x}{d} \rho_i(x)\, dx \qquad (6.31)$$

where $\phi_{ms} = \phi_m - \phi_s$ = metal/semiconductor work function difference

Q_{sl} = density of slow surface states, i.e. states that cannot follow the applied a.c. signal.

$\rho_i(x)$ = density of fixed space charge in the insulator

d = insulator thickness

The term "flat-band" was derived from the fact that when $V_g = V_{fb}$, $V_s = 0$. That is the energy bands in the semiconductor are flat right up to the insulator/semiconductor interface and no space charge layer exists.

6.4 Capacitance-Voltage Characteristics of a MIS Capacitor with Frequency Dependent Traps

As opposed to the "slow" surface states considered in Sec. 6.3.4, the insulator/semiconductor interface may have traps that can follow the applied a.c. signal. These are known as "fast" surface states. Hall and White's (1965) treatment of the effect of "fast" surface states on the C-V characteristics of an MIS capacitor will now be considered.

Assume that P(E) is the surface state density per electron volt, with the energy E measured from the intrinsic Fermi level at the surface of the semiconductor. (See Fig. 6.2) If the traps are filled in the energy range from E_1 to E_2 then

$$Q_{s2} = q \int_{E_1}^{E_2} P(E)dE \qquad (6.31)$$

The energy E_2 is assumed to be independent of V_s, while $E_1 = e(\phi_b - V_s)$. The quantity "e" in this case is taken to mean "one electron" and has a magnitude

of one. To avoid confusion, the symbol "e" is used as opposed to the magnitude of the charge of an electron which is $|q| = 1.6 \times 10^{-19}$ couloumbs.

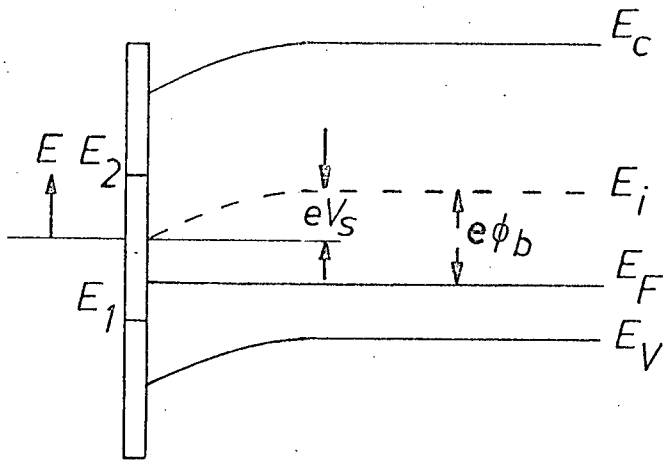

Fig. 6.2 Energy band diagram of p-type semiconductor with surface traps (after Hall and White 1965).

From eqn. 6.3 and by applying Leibniz' rule for differentiation of integrals to eqn. 6.31,

$$c_{ss} = |q\ e\ P(E_1)| \tag{6.32}$$

Implicit in eqn. 6.32 is the assumption that all the fast surface states are able to follow the applied a.c. signal. In general, this is not true. The frequency dependence of c_{ss} can be accounted for by assuming a dimensionless frequency dependent factor, $f(\omega)$, where

$$0 \leq f(\omega) \leq 1 \tag{6.32a}$$

$$\lim_{\omega \to 0} f(\omega) = 1 \tag{6.32b}$$

$$\lim_{\omega \to \infty} f(\omega) = 0 \tag{6.32c}$$

and eqn. 6.32 becomes

$$c_{ss} = |q\ e\ f(\omega)\ P(E_1)| \tag{6.33}$$

In order to proceed further, the form of $P(E)$ must be known. There are no a priori reasons why $P(E)$ should be constant across the energy gap

of the semiconductor. In fact, for SiO_2/Si, Nicollian and Goetzberger (1967) found that P(E) varied from about 1.5 to 4 x 10^{11} cm^{-2} eV^{-1} near midgap. However, by assuming that P(E) is constant equal to N_{ss}, the mathematics is simplified and quantitative results can be obtained which may give some indication as to the nature of the insulator/semiconductor interface. Equations 6.31 and 6.33 become

$$Q_{s2} = q[E_2-E_1]N_{ss} = |e| N_{ss} q [\phi_b - V_s - V_2] \tag{6.34}$$

$$C_{ss} = |q e f(\omega) N_{ss}| \tag{6.35}$$

The normalized MIS capacitance and applied voltage (eqns. 6.4, 6.2 and 6.31) become

$$\frac{c}{c_i} = \frac{qfN + c_{sc}}{qfN + c_{sc} + c_i} \tag{6.36}$$

or

$$qfN = \frac{c_i c_n}{1 - c_n} - c_{sc} \tag{6.37}$$

where

$$N \stackrel{d}{=} e N_{ss}$$

$$c_n \stackrel{d}{=} \frac{c}{c_i}$$

and

$$V_g = -[\frac{Q_{sc}+Q_{ss}}{c_i}] + V_s + \phi_{ms} - \frac{1}{c_i} \int_o^d \frac{x}{d} \rho_i(x)dx$$

or

$$V_g - V_{fb} = - \frac{Q_{sc}}{c_i} + q\frac{(V_2-\phi_b+V_s)}{c_i} N + V_s \tag{6.38}$$

where

$$V_{fb} = - \frac{Q_{s1}}{c_i} + \phi_{ms} - \frac{1}{c_i} \int_o^d \frac{x}{d} \rho_i(x)dx - V_{so} \tag{6.39}$$

and

$$Q_{ss} = Q_{s1} + Q_{s2} \tag{6.39a}$$

The C-V characteristics can be obtained from eqn. 6.36 and 6.38. The voltage V_{so} is the surface potential when V_g and $[- \frac{Q_{s1}}{c_i} + \phi_{ms} - \frac{1}{c_i} \int_o^d \frac{x}{d} \rho_i(x)\, dx]$ are both equal to zero.

6.5 Computations

Theoretical C-V characteristics were calculated with the aid of an IBM 360 computer and plotted using a Calcomp plotter. The following calculations and plots were done specifically for the Al_2O_3/p-type GaAs system. For n-type GaAs, simply replace V_g by $-V_g$. The dielectric constants used were 8.4 (Bernard and Cook 1959) for Al_2O_3 and 12 (Grove 1967) for GaAs. The intrinsic carrier concentration at 300°K for GaAs was assumed to be 9×10^{12} m^{-3} (Grove 1967). Unless otherwise stated, the MKS system of units was used. The computer programmes and plot subroutines were first tested and checked for errors by plotting C-V curves for known values of SiO_2 and Si and comparing them with published results (Goetzberger 1966).

The following sets of curves were plotted.

(1) The normalized capacitance versus applied d.c. voltage with the insulator thickness and dopant concentration as parameters in the depletion, low frequency and high frequency approximations.

(2) The flat-band and the minimum capacitances as functions of dopant concentration in the low frequency approximation.

(3) The normalized capacitance versus applied d.c. voltage with the frequency factor, surface state density, insulator thickness and dopant concentration as parameters.

(4) The minimum surface potential as a function of dopant concentration.

(5) The minimum surface space charge density as a function of dopant concentration.

These curves are given in the next pages. More C-V curves as functions of dopant concentration and insulator thickness are given in Appendix 6.1.

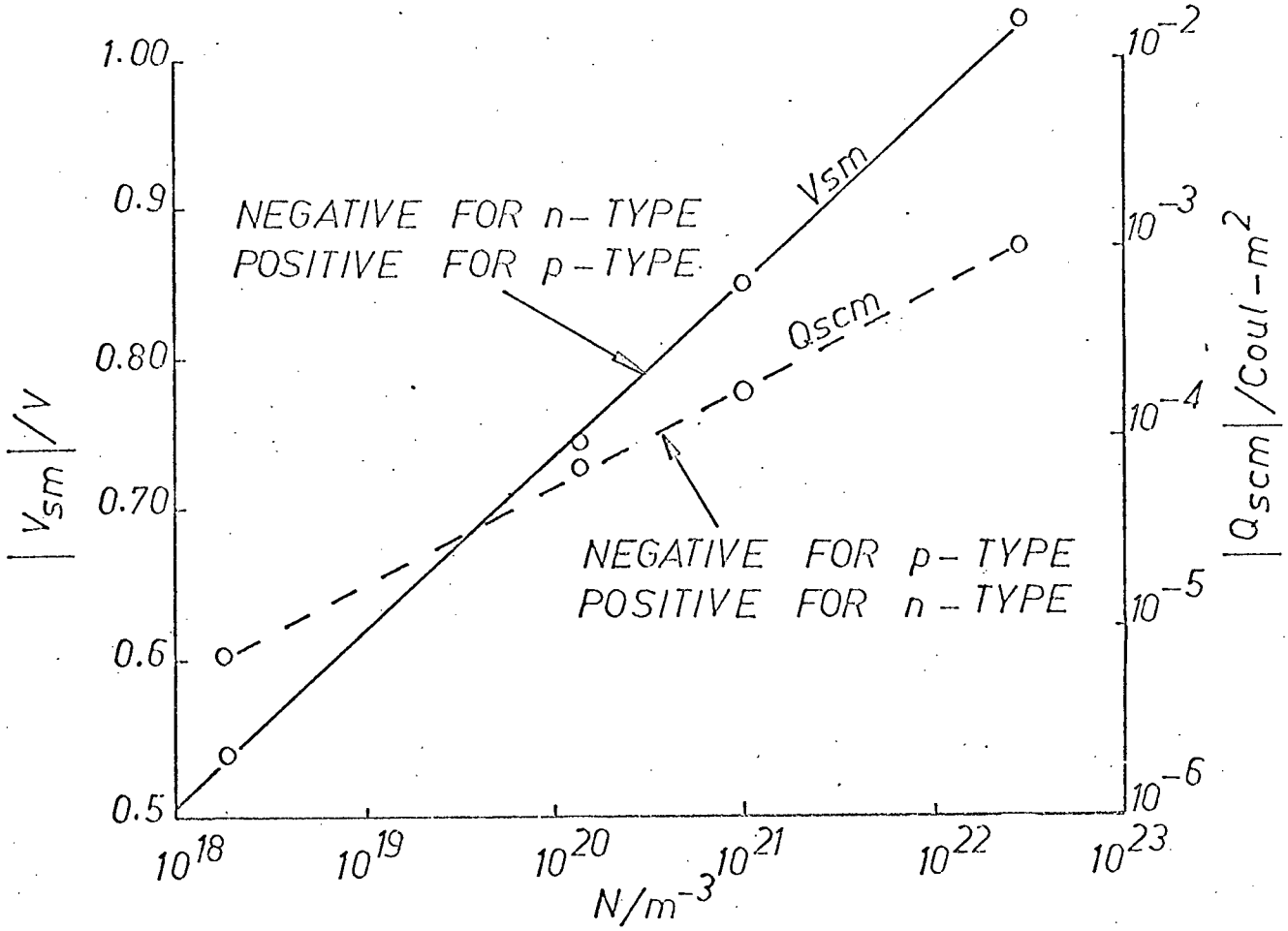

Fig. 6.3 $|Q_{scm}|$, $|V_{sm}|$ versus N for GaAs

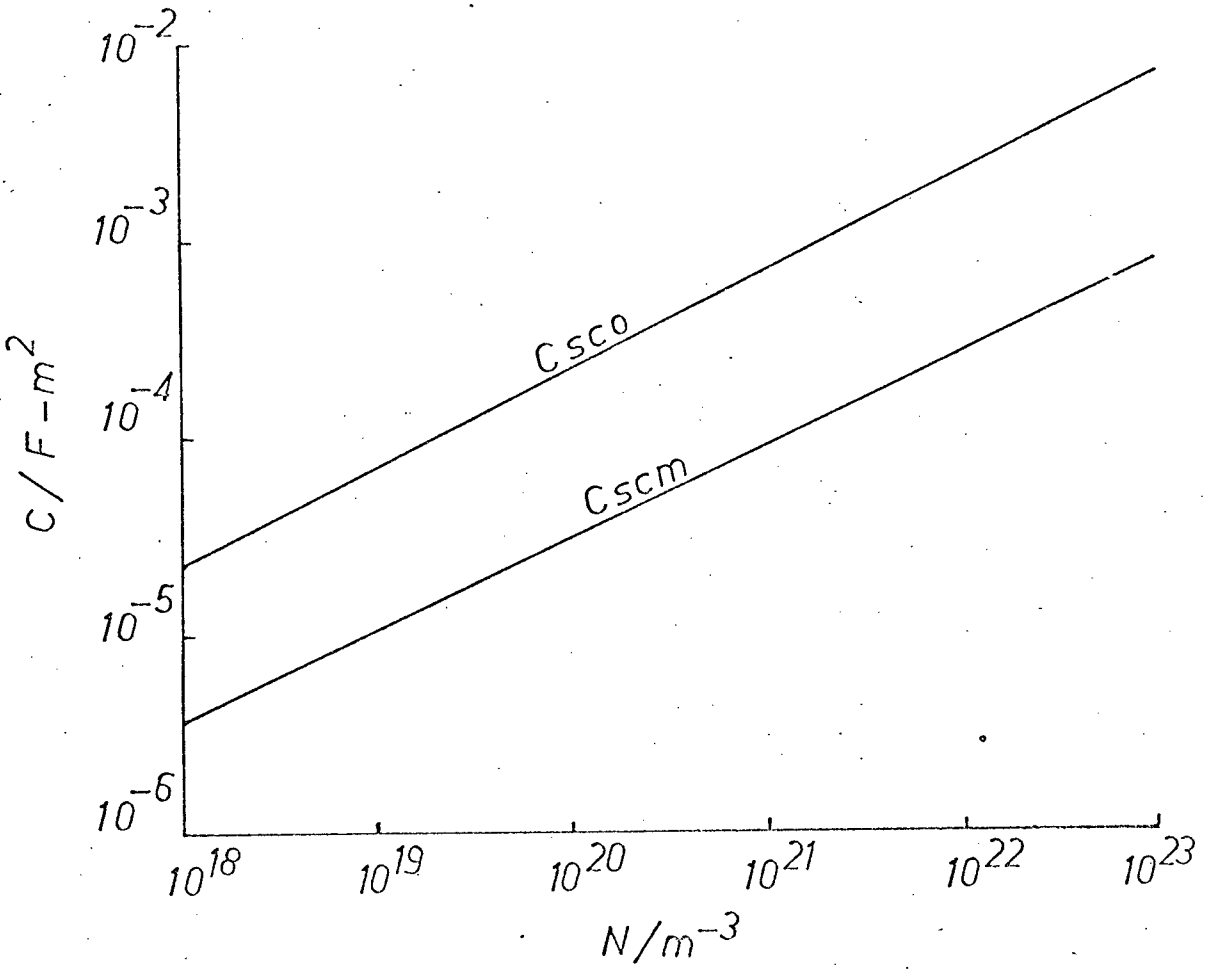

Fig. 6.4 c_{sco}, c_{scm} versus N for GaAs.

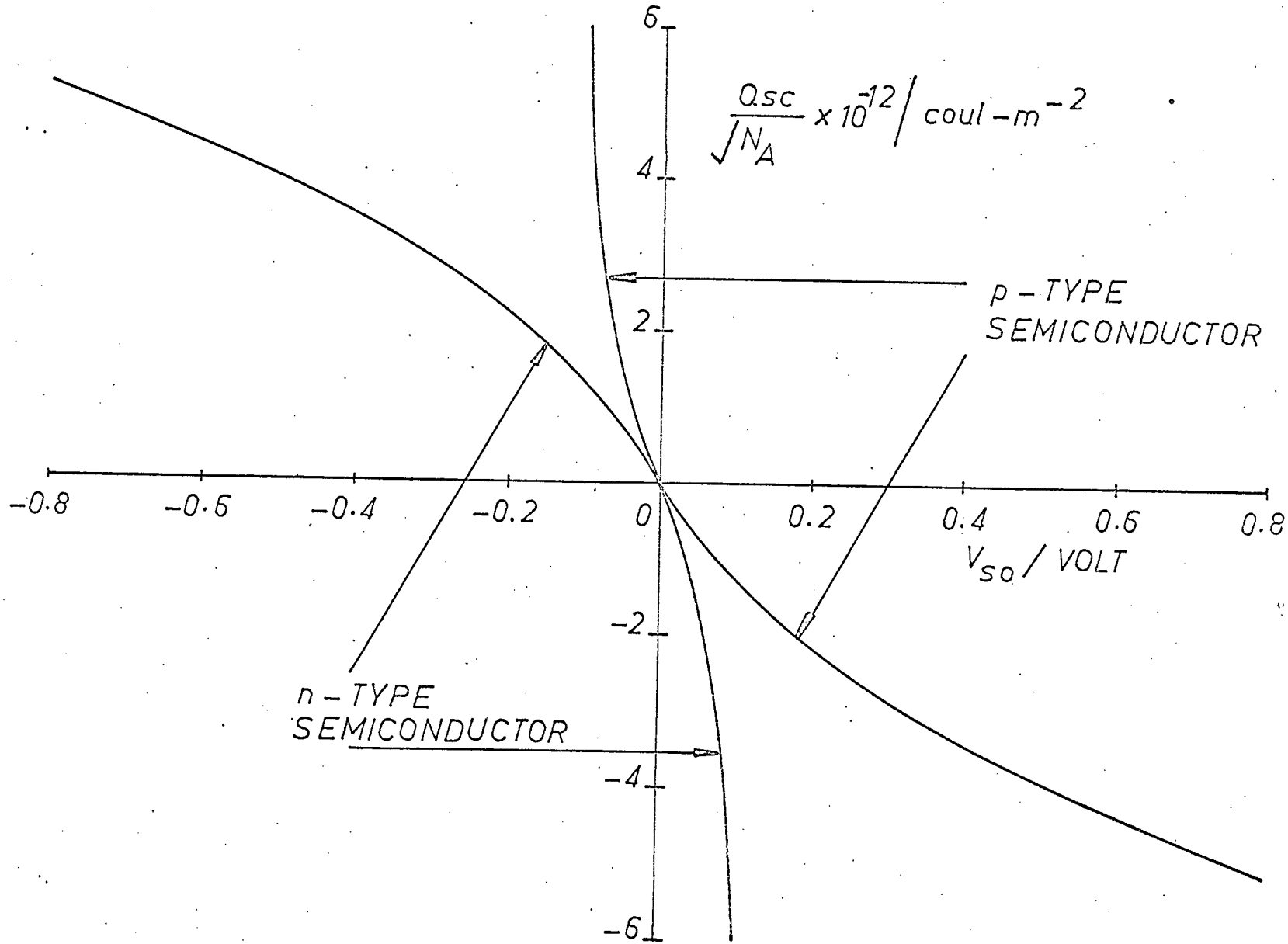

Fig. 6.5 $Q_{sc}/N_A^{1/2}$ versus V_{so} (from Hall and White 1965).

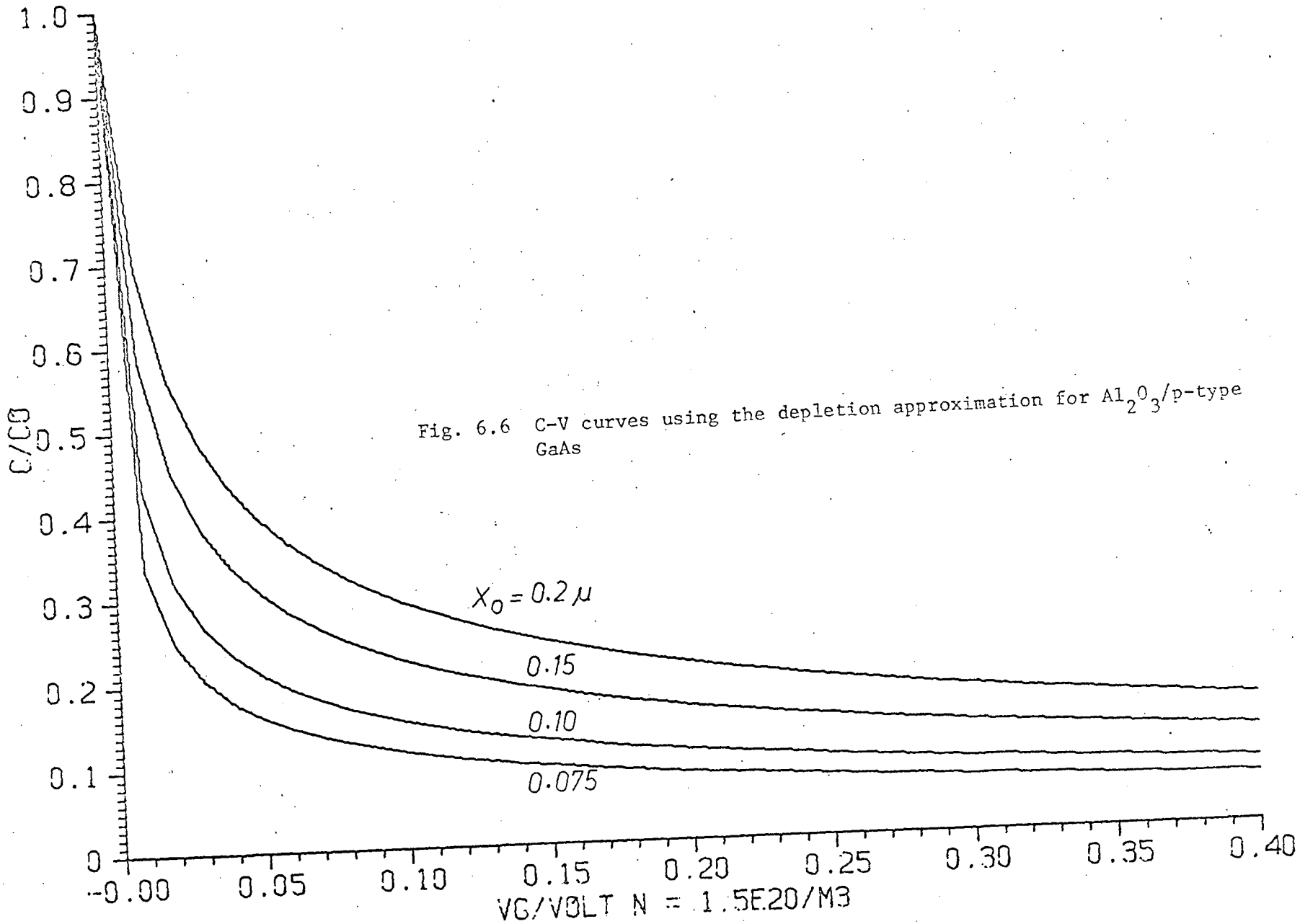

Fig. 6.6 C-V curves using the depletion approximation for Al_2O_3/p-type GaAs

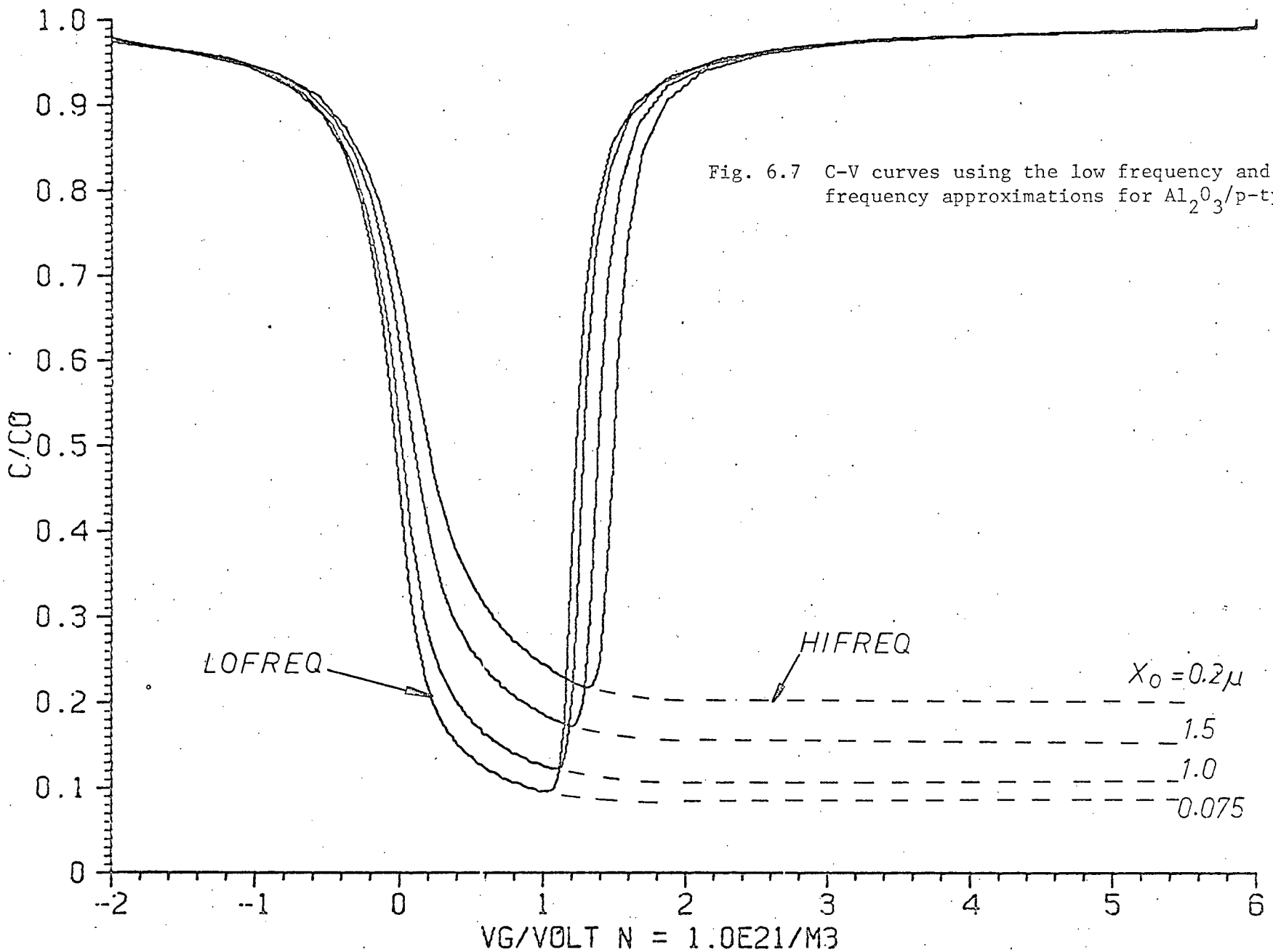

Fig. 6.7 C-V curves using the low frequency and high frequency approximations for Al_2O_3/p-type GaAs.

6.6 Experimental Procedures

Slices of single crystal n-type GaAs were mechanically polished to a 0.3 μ finish and then were subjected to the standard cleaning procedure. After which they were flash-etched in 7 H_2SO_4:H_2O_2;H_2O (by volume) at 80°C. They were then rinsed in doubly-distilled water, in propanol and dried in a stream of N_2 gas. The wafers were immediately introduced into the Veeco vacuum system for the deposition of Al.

Al sources were prepared and evaporated in the same manner and vacuum conditions as described in Chapter 5. The source and samples were allowed to cool for about an hour before breaking vacuum. This may reduce the oxidation of the deposited Al film due to exposure to the atmosphere. The GaAs wafers were then placed on suitable masks for the deposition of Au-Ge contacts on the opposite faces. Alloying of the eutectic has been described elsewhere in the thesis.

Each wafer, except the Al surface, was painted with Apiezon wax which had been dissolved in xylene, and let dried in air. Apiezon wax acts as an insulator against the electrolyte during anodization. The Al film was anodized in a manner similar to that described in Chapter 5. Parallel runs using precleaned glass slides were always done as a means of checking and measuring the dielectric properties and the thickness of the Al_2O_3 films. Au dot counterelectrodes were evaporated onto the Al_2O_3 films. At 1 kHz, loss tangent ranging from 0.006 to 0.010 was obtained.

Capacitances were measured using either the GR 1615A or the Boonton 75 C capacitance bridge, depending upon the test frequency used. The experimental set-up was as described in Chapter 5.

6.7 Results

The measured MIS curves were analyzed using a procedure similar to the one formulated by Hall and White (1965). However, the effects of slow states and contact potential differences, which they neglected, were taken into account in this analysis.

Equation 6.36 can be rewritten as

$$qfN = \frac{c_i c_{nm}}{1 - c_{mn}} + c_{scm} \tag{6.40}$$

where c_{nm}, c_{scm} are the minimum normalized capacitance and minimum space charge capacitance, respectively. The value of c_{nm} and the corresponding V_{gm} can be estimated from the experimental curve.

At zero surface potential, c_{no} can be calculated from

$$c_{no} = \frac{c_{sco} + qfN}{c_{sco} + qfN + c_i} \tag{6.41}$$

The values of c_{scm} and c_{sco} can be determined from the graphs on Fig. 6.4 once the carrier concentration of the semiconductor is known.

Having calculated c_{no}, the corresponding value of V_{go} can be estimated from the experimental curve. From eqn. 6.38 and the known values of V_{go} and V_{gm}

$$qN = \frac{[V_{gm} - V_{go} - V_{sm}]c_i + Q_{scm}}{V_{sm}} \tag{6.42}$$

where V_{sm} and Q_{scm} are the surface potential and surface charge density when $c_{sc} = c_{scm}$. These can be determined from the graphs in Figs. 6.3 and 6.4. The frequency factor is, using eqn. 6.40 and 6.42, given by

$$f = \frac{[c_i c_{nm} - c_{scm}(1 - c_{nm})] V_{sm}}{[1 - c_{nm}][(V_{gm} - V_{go} - V_{sm})c_i + Q_{scm}]} \tag{6.43}$$

By assuming that $V_g = 0$ and that, for the moment, $[-\frac{Q_{sl}}{c_i} + \phi_{ms} + \frac{1}{c_i}\int_o^d \frac{\rho_i(x)}{d}\,dx]$ is negligible, the following normalized expression is obtained.

$$\frac{V_{go} c_i}{\sqrt{N_A}} + \frac{c_i + qN}{\sqrt{N_A}} V_{so} = \frac{Q_{sco}}{\sqrt{N_A}} \tag{6.44}$$

The plot of $\frac{Q_{sc}}{\sqrt{N_A}}$ versus V_{so}, which was adapted from Hall and White (1965), is given in Fig. 6.5. The value of V_{so} is obtained by graphing the LHS expression and reading off the coordinate at its intersection with the graph of $Q_{sco} / N_A^{1/2}$. Thus V_2 can be calculated by using

$$V_2 = [V_{so} + V_{go}] \frac{c_i}{qN} + \frac{kT}{q} \ln \frac{N_A}{n_i} \tag{6.45}$$

The frequency factor, "fast" surface state density and the "filling" level of two MIS capacitors were determined and tabulated. Using these values theoretical C-V curves were computed and plotted by using the FREDEP (frequency dependence approximation) subroutine. These are given in Fig. 6.8 and 6.9. The horizontal displacement between the experimental and the theoretical curves gives

$$V_{fb} - V_{so} = -\phi_{ms} - \frac{Q_{sl}}{c_i} + \frac{1}{c_i} \int_o^d \frac{\rho_i(x)}{d} dx \tag{6.46}$$

where

$$\phi_{ms} = \phi_m - [\chi + \frac{E_g}{2q} - \phi_b] \tag{6.47}$$

The work function of Au is 4.8 eV (Sze 1969). The room-temperature electron affinity and bandgap of GaAs are 4.07 eV and 1.4 eV, respectively (Sze 1969). Using these values and $V_{fb} - V_{so}$ as obtained graphically, the slow states including charges in the oxide, if any, were found to be 9.4×10^{16} m^{-2} eV^{-1} and 1.6×10^{17} m^{-2} eV^{-1}. A comparison between results obtained in this work and those reported in the literature is given in Table 6.1.

From Table 6.1, it can be seen that the "fast" surface state density of Al_2O_3/GaAs interface was comparable to that of pyrolytic SiO_2/GaAs interface and of "free" and "treated" GaAs surfaces. The experimental MIS curves did not exhibit any minima. From the Low Frequency Approximation and the Frequency Dependence Approximation models a minimum in the C-V curve is predicted provided

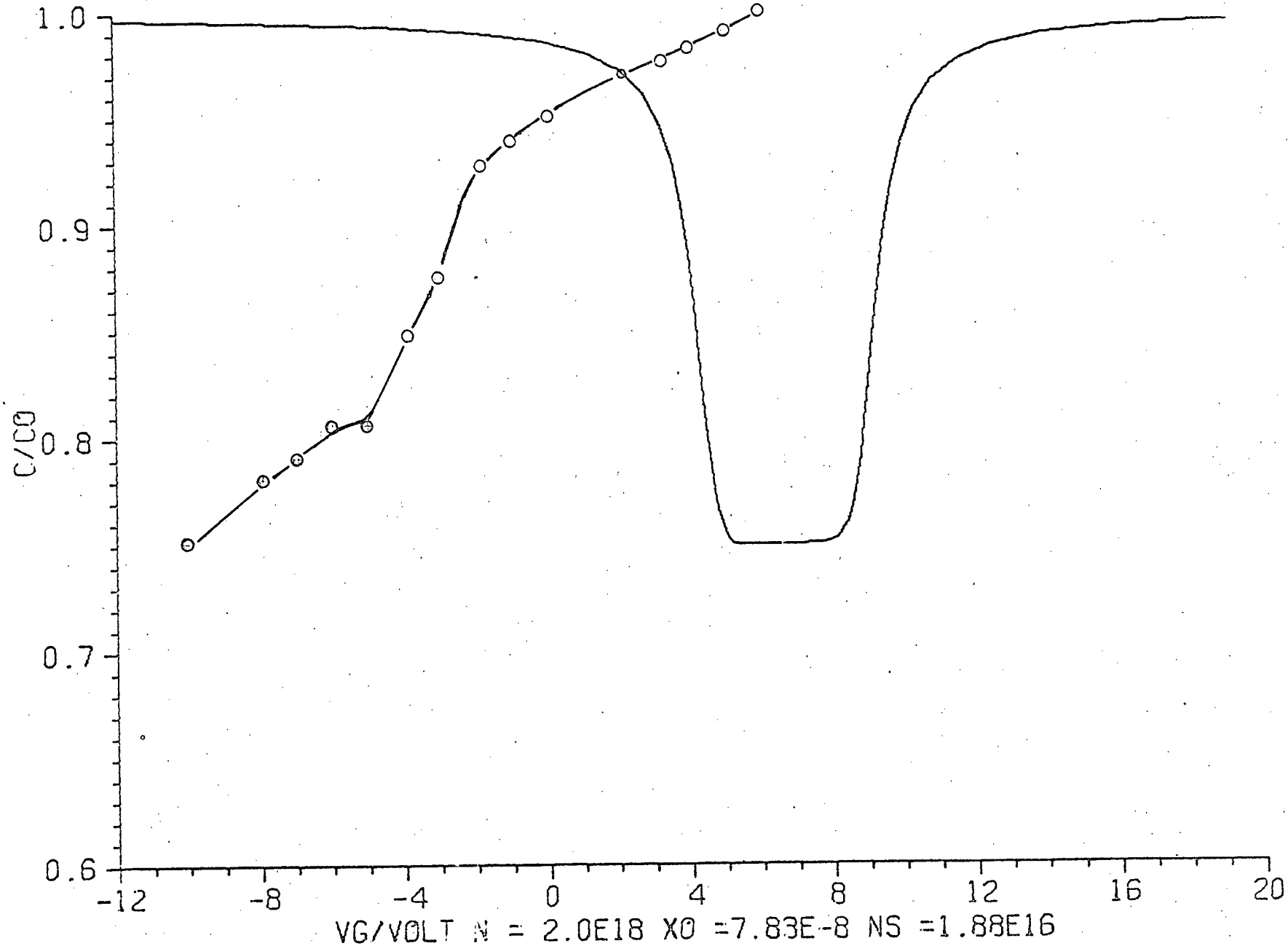

Fig. 6.8 Theoretical FREDEP and experimental C-V curves for sample G13-B.

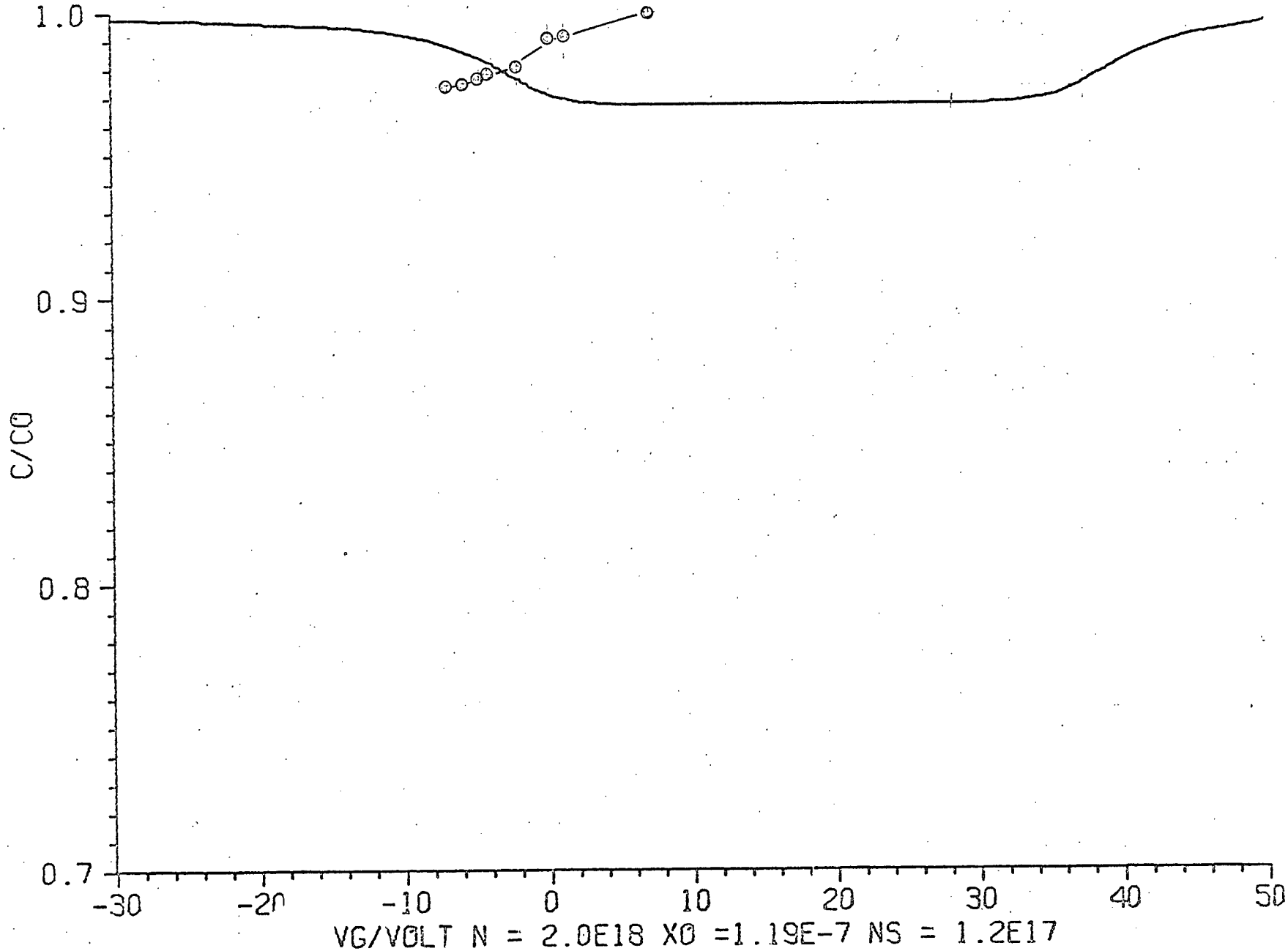

Fig. 6.9 Theoretical FREDEP and experimental C-V curves for sample G15-B.

Substrate	insulator used or surface condition	f	"slow" Surface states	"fast" surface states	V_2 (Volts)	Method(s) used	Reference
p-GaAs	pyrolitic SiO_2	0.86	-	$1.4 \times 10^{16}/m^2$-eV	-1.25	MIS	Hall and White (1965)
n-GaAs	pyrolitic SiO_2	0.79	-	$1.0 \times 10^{16}/m^2$-eV	1.15	MIS	Hall and White (1965)
n and p GaAs	"free"	-	-	$> 10^{16}/m^2$	-	field effect conductance and surface photovoltage	Flinn and Briggs (1964)
n and p GaAs	"treated"	-	-	$\sim 10^{15}/m^2$	-	pulsed field effect	Kawaji and Gatos (1964)
n and p GaAs	"clean" in uhv	-	-	$\sim 10^{17}/m^2$	-	contact potential difference and photoelectric emission	van Laar and Scheer (1967)
n-GaAs (G 13-B)	anodic Al_2O_3	0.95	$9.4 \times 10^{16}/m^2$eV	$1.9 \times 10^{16}/m^2$eV	-2.24	MIS	present work
n-GaAs (G 15-B)	anodic Al_2O_3	0.97	$\sim 1.6 \times 10^{17}/m^2$eV	$\sim 1.2 \times 10^{17}/m^2$eV	$\sim$-0.61	MIS	

Table 6.1 Density of Surface States on GaAs

that the minority carriers in the space charge region are able to follow the applied a.c. signal. Thus, experimental results of the Al_2O_3/GaAs interface implied that the minority carriers did not respond to the applied a.c. signal when the space charge layer was biased in the inversion region. This result agreed with the results of Hall and White (1965, 1966) and Flinn and Briggs (1964). The latter authors measured the field effect conductance of p-type and n-type GaAs. They failed to observe any conductance minimum.

As far as active field-effect devices are concerned, the need for an insulator/GaAs interface with better interfacial properties (e.g. low "fast" surface state density) is indicated. Although GaAs transistors were one of the first III-V compound active devices fabricated, as yet no practical device has been made. It was found that surface states limited the performance of GaAs MIS field-effect transistors (1966 and 1968 Symposia: GaAs)*. Improvements on the properties of the Al_2O_3/GaAs interface are necessary before it can be seriously considered in the fabrication of devices.

---

* A solution to this problem may lie in the use of a reverse-biased Schottky barrier as the gate (Hower, Hooper, Tremere, Lehrer and Bittmann 1968). A disadvantage of using a Schottky gate is that the transistor can be operated only in the depletion mode.

7. CONCLUSION

A new method, the close-spaced sublimation (CSS) method, was developed and used to deposit GaAs films on sapphire. Advantages of the CSS method are as follows. First, the close source-to-substrate spacing produces near-equilibrium conditions, which lends itself to the deposition of stoichiometrically better films. Second, most of the material is deposited on where it is needed. This is economical on source material. Third, because both the source and the substrate holders are independently supported and moveable with respect to each other, films can be deposited on more than one substrate in one pumpdown.

The structural properties of the CSS GaAs films on sapphire were studied using optical and electron microscopy, an electron microprobe and X-ray diffraction techniques. Growth features which resemble equilateral tetrahedrons with their basal planes parallel to the surface of the substrate were observed in most of the films which were deposited on substrates held at 600°C or higher. These growth features appeared to possess a three-fold symmetry which would be consistent with the symmetry properties of the <111> direction of a zincblende structure. An indication of the relative composition of Ga and As in a CSS film was obtained by comparing their respective X-ray counts to those obtained from a single-crystal GaAs standard. The CSS films were found to be stoichiometric within the limits imposed by the probe, which is less than 2 wt %. No gross inhomogeneities and excess Ga were detected. Crystallites increased in size with increasing substrate temperature, from about 0.7μ to 20μ for substrate temperatures from 480 to 670°C. The crystallite size of CSS GaAs films compares favourably with the reported crystallite sizes of GaAs films depostied by using other vacuum techniques.

Results from electron microscope reflection-electron-diffraction (RED) and X-ray diffraction studies indicated that texturing of the films increased with increasing substrate temperature. <111> texture was observed on films

deposited at 600°C or higher. The theory of Kaischew and Bliznakow as applied by Molnar, Flood and Francombe was presented as an explanation for the occurrence of the <111> texture. Single-crystal Laue patterns, with most of the prominent spots consistent with those found in the pattern of (111) GaAs parallel to the substrate, were observed on 630 to 640°C films. No abnormal metastable wurtzite phases were observed in the CSS films. In the case of III-V compounds, nonstoichiometry can lead to the formation of a metastable wurtzite phase.

Lower substrate temperature films, which appeared "dull", had very low (<1 cm^2/V-sec) carrier mobilities while higher substrate temperature films, which appeared "shiny", had higher carrier mobilities. Two types of "shiny" films were observed - the "high ρ" and the "low ρ" films. At room temperature, the "high ρ" films had low Hall mobilities (~2 to 13 cm^2/V-sec) and high resistivities, (4 x 10^2 to 10^5 Ω-cm). At the same temperature, the "low ρ" films had higher Hall mobilities (12 to 42 cm^2/V-sec) and lower resistivities (0.6 to 86Ω-cm). All the as-grown films were p-type. The electrical properties of the films were discussed in terms of the films' polycrystalline structure, deviation from stoichiometry and compensation of impurities. Ionized impurity scattering was the dominant mobility-reducing mechanism. The films were heavily compensated, with free carrier concentrations several orders of magnitude lower than the total impurity concentrations, which were in the order of 10^{19} to 10^{20} cm^{-3}. The total impurity concentration in each film was estimated by using Brooks' formula for ionized impurity scattering. The room-temperature electron mobility of a film that was converted to n-type by postdeposition Ge doping was 77 cm^2/V-sec. Although the carrier mobilities of the CSS films were low, they compare favourably with the carrier mobilities of heteroepitaxial GaAs films deposited by using other vacuum techniques.

A homoepitaxial layer was grown on a semi-insulating GaAs substrate. The room-temperature electron mobility of the as-grown n-type film was 219 cm^2/V-sec. The electron Hall mobility varied with temperature as $T^{3/2}$, which is the form

predicted by Brooks-Herring formula for ionized impurity scattering.

Thin-film insulated-gate field-effect transistors were fabricated using as-grown CSS films. Transistors that operated in the p-type depletion mode with transconductance of 0.1μ-$\mho$ were observed. The effective mobility was 4 cm^2/V-sec. Diodes fabricated on a converted film showed "soft" characteristics. While transistor action and rectification characteristics were observed, the quality of the CSS films needs to be improved before devices with better characteristics can be made.

Evaporated Al films on glass were anodized in ammonium pentaborate dissolved in ethylene glycol. The loss tangent was found to be a slow function of frequency with higher values at lower frequencies. Step response currents followed a t^{-n} law, where n was 0.95 and 0.7 for the discharging and charging currents, respectively. For a linear dielectric response, this corresponded to $\varepsilon''(\omega)$ varying as ω^{n-1}. The d.c. resistivity at low fields was about $10^{13}\Omega$-cm. The breakdown field was about 5×10^6 V/cm.

Capacitances of Au/Al_2O_3/GaAs MIS capacitors were measured as functions of applied d.c. field. Theoretical capacitance-voltage (C-V) curves, based on idealized models, were computed and plotted. The experimental C-V curves were analyzed by using a procedure similar to the one developed by Hall and White. The effects of contact potential differences, charges in the oxide and "slow" surface states, which Hall and White neglected, were considered in this study. "Fast" surface state densities in the order of 10^{16} to 10^{17} /m^2 eV were obtained. These were comparable to the density of surface states at the GaAs surface as obtained by Hall and White and by other authors. The presence of surface states in the insulator/semiconductor interface at such concentration levels would degrade the field-effect action at the interface and render it unsuitable in the fabrication of field-effect devices.

Interesting topics related to the present work which merit further research are given as follows.

A systematic investigation of the H_2-prefiring of the sapphire substrate is important in determining the effects of substrate surface on the properties of CSS GaAs films. How different substrates, in particular semi-insulating GaAs, affect the properties of CSS GaAs films is of interest. The use of semi-insulating GaAs substrates is of less interest from the thin-film circuit point of view.

A necessary condition for obtaining a tunnel diode is that both p-type and n-type regions of a p-n junction must be degenerately doped (dopant concentration of greater than about 10^{18} cm^{-3} for GaAs at room temperature). The high density of dopants in the CSS GaAs films may actually prove to be an asset in the fabrication of tunnel diodes. However, other factors such as the degradation of the tunnel diode due to defects and to diffusion of impurities like Cu must be considered.

Insulating films produced by anodizing a metal film in an oxygen plasma is a relatively new technique. As yet, very little work has been reported on the properties of the plasma-anodized-metal-oxide/GaAs interface. Such studies may yield an insulator/GaAs interface with characteristics suitable for field-effect devices.

BIBLIOGRAPHY

J.A. Aboaf "Deposition and Properties of Aluminum Oxide Obtained by Pyrolytic Decomposition of An Aluminum Alkoxide", J. Electrochem. Soc. vol. 114, 948 (1967).

W. Albers, "Physical Chemistry of Defects", Physics and Chemistry of II-VI Compounds M. Aven and J.S. Prener (editors), Interscience (1967).

R.H. Alderson and J.S. Halliday, "Electron Diffraction" Techniques for Electron Microscopy, D.A. Kay (edit) Blackwell (1965).

J.R. Arthur, "Vapour Pressures and Phase Equilibria In The Ga-As System", J. Phys. Chem. Solids vol. 28, #11, 2257 (1967).

J.R. Arthur, "Interaction of Ga and As_2 Molecular Beams with GaAs Surfaces", J. App. Phys. vol. 39, #8, 4032 (1968).

F. Argall and A.K. Joncher, "Dielectric Properties of Thin Films of Aluminium Oxide and Silicon Oxide", Thin Solid Films vol. 2, 185 (1968).

M.M. Atalla, "Semiconductor Surfaces and Films; The Si-SiO_2 System", Properties of Elemental and Compound Semiconductors, H. Gatos (edit), Interscience (1960).

M.E. Baird, "Determination of Dielectric Behaviour at Low Frequencies from Measurements of Anomalous Charging and Discharging Currents", Rev. Mod. Phys. vol. 40 #1, 219 (1968).

W.J. Bernard and J.W. Cook, "The Growth of Barrier Oxide Films on Al", J. Electrochem. Soc. vol. 106, 643 (1959).

R.W. Berry, P.M. Hall and M.T. Harris, Thin Film Technology, Bell Tel. Lab. Series, North-Holland (1968).

F. Berz, "Variation with Frequency of the Transverse Impedance of Semiconductor Surface Layers", J. Phys. Chem. Solids vol. 23, 1795 (1962).

J. Blanc, R.H. Bube and L. Weisberg, "Electrical Acitivty of Cu in GaAs", J. Phys. Chem. Solids vol. 25, 221 (1964).

J. Blanc, R.H. Bube and L. Weisberg, "Evidence for the Existence of High Concentrations of Lattice Defects in GaAs", Phys. Rev. Letters, vol. 9, 252 (1962).

D.E. Bolger, J. Franks, J. Conrad and J. Whitaker, "Preparation and Characteristics of GaAs", 23, GaAs: 1966 Symposium Proceedings, Inst. of Phys. and Phys. Soc. Conf. Series #3 (1967).

L.S. Birks, Electron Probe Microanalysis, Wiley (1963).

N. Braslau, J.B. Gunn and J.L. Staples, "Metal-Semiconductor Contacts for GaAs Bulk Devices", Solid State Elec. vol. 10, 381 (1967).

H. Brooks, "Theory of the Electrical Properties of Germanium and Silicon", Advances in Electronics and Electron Physics, vol. 7, 85 (1955).

D.S. Campbell, "Methods of Preparing Thin Films", The Use of Thin Films in Physical Investigations, J. C. Anderson (edit) AP (1966).

R. Castaing, P. Deschamps and J. Philibert (editors) X-Ray Optics and Microanalysis (1965).

C. Cherki and R. Coelho, "On Charge Storage in Anodic Tantal Oxide Layers", Phys. Stat. Solidi, vol. 19, K91 (1967).

K.L. Chopra, Thin Film Phenomena, McGraw-Hill (1969).

T.L. Chu, C.H. Lee and G.A. Gruber, "The Preparation and Properties of Silicon Nitride", J. Electrochem. Soc. vol. 114 #7, 718 (1967).

J.W. Colby, "Quantitative Microprobe Analysis of Thin Dielectric Films", private communication.

E.M. Conwell, High Field Transport in Semiconductors, Solid State Physics Supp 9, Academic Press (1967).

E.M. Conwell and V.F. Weisskopf, "Theory of Impurity Scattering in Semiconductors", Phys. Rev. vol. 77 #3, 388 (1950).

R.H. Cox and H. Strack, "Ohmic Contacts for GaAs Devices", Solid-State Elec. vol 10 #12, 1213 (1967).

B.D. Cullity, Elements of X-Ray Diffraction, Addision-Wesley (1959).

F.A. Cunnell, T. Edmond and W.R. Harding, "Technology of GaAs", Solid-State Elec. vol. 1, 97 (1960).

J.E. Davey and T. Pankey, "Structural and Optical Characteristics of Thin GaAs Films", J. App. Phys. vol. 35 #7, 2203 (1964).

J.E. Davey and T. Pankey, "Epitaxial GaAs Films Deposited by Vacuum Evaporation", J. App. Phys. vol. 39 #4, 1941 (1968).

C.J. Dell'Oca, D.L. Pulfrey and L. Young, "Anodic Oxide Films", review article in Physics of Thin Films, in press.

S.S. Devlin, "Transport Properties", Physics and Chemistry of II-VI Compounds, M. Aven and J.S. Prener (editors), Interscience (1967).

R. Dreiner, "The Temperature Dependence of the Field Coefficient for the Anodization of Tantalum", J. Electrochem. Soc. vol. 111, 1350 (1964).

J. Drowart and P. Goldfinger, J. Chim. Phys. vol. 55, 721 (1958) (in French).

D. Effer, "Epitaxial Growth of Doped and Pure GaAs in an Open Flow System", J. Electrochem. Soc. vol. 112, 1020 (1965).

H. Ehrenreich, "Band Structure and Electron Transport of GaAs", Phys. Rev., vol. 120 #6, 1951 (1960).

T. Evans and A. Noreika, "Effect of Gaseous Environment on the Structure of Sputtered GaAs Films on NaCl Substrates", Phil. Mag. vol. 13, 717 (1966)

M.R. Farukhi and E.J. Charlson, "Structural and Electrical Properties of Flash-Evaporated Thin GaAs Films", J. App. Phys. vol. 40 #13, 5361 (1969).

M.M. Faktor, D.G. Fiddyment and G.R. Newns, "Preliminary Study of the Chemical Polishing of α-Corundum Surfaces with Vanadium Pentoxide", J. Electrochem. Soc. vol. 114 #4, 356 (1967).

E. Ferrieu and B. Pruniaux, "Preliminary Investigations of Reactively Evaporated Al_2O_3 Films on Si", J. Electrochem. Soc., vol. 116, #7, 1008 (1969).

J.D. Filby and S. Nielsen, "Single-Crystal Films of Silicon on Insulators", Brit. J. App. Phys. vol. 18, 1357 (1967).

G. Fischer, D. Greig and E. Mooser, "Apparatus for the Measurement of Galvanomagnetic Effects in High Resistance Samples", Rev. Sci. Inst. vol. 32 #7, 842 (1961).

I. Flinn and M. Briggs, "Surface Measurements on GaAs", Surf. Sci. vol. 2, 136 (1964).

D.R. Frankl, Electrical Properties of Semiconductor Surfaces, Pergamon Press (1967).

H. Fröhlich, Theory of Dielectrics, Oxford (1949).

M. Gevers and F. Dupre, "The Relation Between the Power Factor and the Temperature Coefficient of the Dielectric Constant of Solid Dielectrics", Phil. Res. Rept. vol. 1, 279 (1945).

M. Gevers and F. Dupre, "Power Factor and Temperature Coefficient of Solid (Amorphous) Dielectrics", Trans. Farad. Soc. vol. 42A, 47 (1946).

A. Goetzberger, "Ideal MOS Curves for Silicon", Bell System Tech. J. vol. 45 #7, 1097 (1966).

B. Goldstein, "Self and Impurity Diffusion in Gallium Arsenide", Compound Semiconductors, R.K. Willardson and H.L. Goering (editors), Reinhold (1962).

W.S. Goruk, L. Young, F.G.R. Zobel, "Ionic and Electronic Currents at High Fields in Anodic Oxide Films," Modern Aspects of Electrochemistry, vol. 5, Plenum (1966).

R.F. Greene, D.R. Frankl and J.N. Zemel, "Surface Transport in Semiconductors", Phys. Rev. vol. 118, 967 (1960).

A.G. Grove, B.E. Deal, E.H. Snow and C.T. Sah, "Investigations of Thermally Oxi-Oxidized Si Surfaces Using MOS Structures", Solid State Elec. vol. 8, 145 (1965).

A.G. Grove, Physics and Technology of Semiconductor Devices, Wiley (1967).

J.B. Gunn, "Microwave Oscillations of Current in III-V Semiconductors", Solid-State Elec. Comm. vol. 1, 88 (1963).

K.G. Günther, "Interfacial and Condensation Processes Occurring with Multicomponent Vapours", The Use of Thin Films in Physical Investigations, J.C. Anderson (edit) AP(1966).

H. Gutbier, Z. Naturf,vol. 169, 268 (1961) (in German).

R.R. Haering and J.F. O'Hanlon, "Control of the Surface Potential of Evaporated CdS Layers", Proc. IEEE vol. 55, 692 (1967).

R.N. Hall, "Solubility of III-V Compound Semiconductors in Column III Liquids", J. Electrochem. Soc. vol. 110, 385 (1963).

C.E. Hall, Introduction to Electron Microscopy, McGraw-Hill (1966).

R. Hall and J.P. White, "Surface Capacity of Oxide Coated Semiconductors" Solid-State Elec. vol. 8, 211 (1965).

B. Hamon, "An Approximate Method for Deducing Dielectric Loss Factor from dc Measurements", Proc IEE vol. 99, 151 (1952).

A.C. Harkness and L. Young, "High Resistance Anodic Oxide Films on Aluminium", Can. J. Chem. vol. 44, 2409 (1966).

J. S. Harris, Y. Nannichi, G.L. Pearson and G.F. Day, "Ohmic Contacts to Solution-Grown Gallium Arsenide", J. App. Phys. vol. 40 #11, 4575 (1969).

P.B. Hart, P.J. Etter, B.W. Jervis and J.M. Flanders, "Electrical Properties of Epitaxial Silicon Films on α-Alumina", Brit. J. App. Phys. vol. 18, 1389 (1967).

C. Hilsum, "Some Key Feature of III-V Compounds", Semiconductors and Semimetals , vol.1, R.K. Willardson and A.C. Beer (editors) AP (1966).

C. Hilsum and A.C. Rose-Innes, Semiconductor III-V Compounds, Pergamon (1961).

S.R. Hofstein and G. Warfield, "Physical Limitations on the Frequency Response of a Semiconducting Surface Inversion Layer", Solid State Elec. vol. 8, 321 (1965).

L. Holland, Vacuum Deposition of Thin Films, Chapman and Hall (1956).

D.J. Howarth and E.H. Sondheimer, "The Theory of Electronic Conduction in Polar Semiconductors", Proc. Royal Soc. vol. A 219, 53 (1953).

P.L. Hower, W.W. Hooper, D.A. Tremere, W. Lehrer and C.A. Bittmann, "The Schottky Barrier GaAs FET", 1968 Symposium on GaAs, Dallas (1968).

A. Howie, "Interpretation of Micrographs of Metal Foils and Other Objects", Techniques for Electron Microscopy, D.H. Kay (edit) Blackwell (1965).

P. Hudock, "Epitaxial GaAs Films Deposited Under Near-Equilibrium Conditions in Ultra-High Vacuum", Extended Abst. I-3, Electronics Div. vol. 16 #1, Electrochem. Soc. Meeting, Dallas (1967).

L.P. Hunter, Handbook of Semiconductor Electronics (2nd edition), McGraw-Hill (1962).

I. Isenberg, B.R. Russell and R.F. Greene, "Improved Method of Measuring Hall Ceofficients", Rev. Sci. Instrum., vol. 19, 685 (1948).

I.T. Johansen, "Electrical Conductivity in Evaporated Silicon Oxide Films", J. App. Phys. vol. 37, #2, 499 (1966).

B.D. Joyce and J.B. Mullin, "Growth 'Pyramids' in Epitaxial GaAs", Solid State Comm. vol. 4, 463 (1966).

B.D. Joyce and J.B. Mullin, "Pyramid Formation in Epitaxial GaAs Layers", 23, GaAs: 1966 Symposium Proceedings, Inst. of Phys. and Phys. Soc. Conf. Series #3 (1967).

R. Kaischew and G. Bliznakow, Compt. Rend. L'Acad. Bulgure Sci., vol. 1 #2-3, 23 (1948).

C.S. Kang and P.E. Greene, "Tin and Tellurium Doping Characteristics in Gallium Arsenide Epitaxial Layers Grown from Ga Solution", 1968 Symposium on GaAs, Dallas Inst. of Phys. and Phys. Soc. Conf. Series #7 (1968).

D.H. Kay (editor), Techniques for Electron Microscopy, Blackwell (1965).

S. Kawaji and H.C. Gatos, "Gallium Arsenide Surface States", Surf. Sci. vol. 1, 407 (1964).

J. Klerer, "A Method for the Deposition of SiO_2 at Low Temperatures", J. Electrochem. Soc. vol. 108, 1070 (1961).

W. Köster and B. Thomas, Z. Mettalk, vol. 46, 291 (1955) (in German).

F.A. Kroger, Chemistry of Imperfect Crystals, North Holland (1964).

D.F. Kyser and D.B. Wittry, "Cathodoluminescence in Gallium Arsenide", The Electron Microprobe T.D. McKinley, K.F.J. Heinreich and D.G. Wittry (editors), Wiley (1966).

E.N. Laverko, V.M. Marakhonov and S.M. Polyakov, "Structure of Gallium Arsenide Whiskers on Germanium", Sov. Phys. Crist. vol. 10, 611 (1966).

K. Lehovec and A. Slobodskoy, "Impedance of Semiconductor-Insulator-Metal Capacitors", Solid-State Elec. vol. 7, 59 (1964).

R. Lindner, "Semiconductor Surface Varactor", Bell Syst. Tech. J. Vol. 41, 803 (1962).

P. Lublin and W.J. Sutkowski, "Application of the Electron Probe to Electronic Materials", The Electron Microprobe T.D. McKinley, K.F.J. Heinreich and D.B. Wittry (editors), Wiley (1966).

G.W. Mahlman, "Photoconductivity of Lead Sulfide Films", Phys. Rev. vol. 103 #6, 1619 (1956).

H.M. Manasevit, "Single-Crystal Gallium Arsenide on Insulating Substrates", App. Phys. Lett. vol. 12 #4, 156 (1968).

H.M. Manasevit and F.L. Morritz, "Gas Phase Etching of Sapphire with Sulfur Fluorides", J. Electrochem. Soc. vol. 114, 204 (1967).

O. Madelung, Physics of III-V Compounds, Wiley (1964).

A. Many, Y. Goldstein and N.B. Grover, Semiconductor Surfaces, North-Holland (1965).

S. Martinuzzi, Ph.D. Thesis, U. of Marseille (1966).

T.D. McKinley, K.F.J. Heinreich and D.B. Wittry (editors), The Electron Microprobe, Wiley (1966).

M.G. Mier and E.A. Buvinger, "A Comparative Study of Anodized Evaporated and Sputtered Aluminum Oxide Thin Films", Vac. Sci. and Tech. vol. 6 #4, 727 (1969).

R.R. Moest and B.R. Shupp, "Preparation of Epitaxial GaAs and GaP Films by Vapour Phase Reaction", J. Electrochem. Soc. vol. 109 #11, 1061 (1962).

B. Molnar, J. Flood and M. Francombe, "Fibered and Epitaxial Growth in Sputtered Films of GaAs", J. App. Phys. vol. 35 #12, 3554 (1964).

W. von Muench, "Gallium Arsenide Planar Technology", IBM Journal, 438, (Nov. 1966).

E.K. Müller, "Structure of Oriented, Vapor-Deposited GaAs Films Studied by Electron Diffraction", vol. 35 #3, 580 (1964).

H. Nelson, "Epitaxial Growth from the Liquid State and Its Application to the Fabrication of Tunnel and Laser Diodes", RCA Review, vol. 24 (1963).

F.H. Nicoll, "The Use of Close Spacing in Chemical-Transport Systems for Growing Epitaxial Layers of Semiconductors", J. Electrochem. Soc. vol. 110 #11, 1165 (1963).

E.H. Nicollian and A. Goetzberger, "The Si-SiO_2 Interface - Electrical Properties as Determined by the Metal-Insulator-Silicon Conductance Technique", Bell Syst. Tech. J. vol. 46 #6 , 1055 (1967).

T. Pankey and J.E. Davey, "Structural and Optical Characteristics of Thin GaAs Films. II", J. App. Phys. vol. 37 #4, 1507 (1966).

R.L. Petritz, "Theory of Photoconductivity in Semiconductor Films", Phys. Rev. vol. 104 #6, 1508 (1956).

D.L. Pulfrey, P.S. Wilcox and L. Young, "Dielectric Properties of Ta_2O_5 Films", J. App. Phys. vol. 40 #10, 3891 (1969).

E.H. Putley, The Hall Effect and Related Phenomena, Butterworths (1960).

F.D. Rosi, D. Meyerhofer and R.V. Jensen, "Properties of p-Type GaAs Prepared by Copper Diffusion", J. App. Phys. vol. 31 #6, 1105 (1960).

A.G. Revesz and K.H. Zaininger, "The Si-SiO_2 Solid-Solid Interface System", RCA Rev. vol. 29 #1, (1968).

J.L. Richards, P.B. Hart and L.M. Gallone, "Epitaxy of Compound Semiconductors by Flash Evaporation", J. App. Phys. vol. 34, 3418 (1963).

J.L. Richards, "Flash Evaporation", The Use of Thin Films in Physical Investigations J.C. Anderson (edit) AP(1966).

D. Richman, "Dissociation Pressures of GaAs, GaP and InP and the Nature of III-V Melts", J. Phys. Chem. Solids vol. 24, 1131 (1963).

P.H. Robinson, "Transport of Gallium Arsenide by a Close-Spaced Technique", RCA Rev. vol. 24, 574 (1963).

P.H. Robinson and C.W. Mueller, "The Deposition of Silicon Upon Sapphire Substrates", Trans. AIME vol. 236, 268 (1966).

C.A.T. Salama, "Evaporated Silicon Thin-Film Transistors", Ph.D. Thesis, Dept. of Electrical Engineering, U.B.C. (1966).

W.W. Scanlon, "Interpretation of Hall Effect and Resistivity Data in PbS and Similar Binary Compound Semiconductors", Phys. Rev. vol. 92, 1573 (1953).

R. Scheuplin and P. Gibbs, "Surface Structure in Corundum: I, Etching of Dislocations", J. Am. Ceramic Soc. vol. 43, 458 (1960).

J.R. Schrieffer, "Effective Carrier Mobility in Surface-Space Charge Layers", Phys. Rev. vol. 97, 641 (1955).

W. Shockley, Electrons and Holes in Semiconductors, van Nostrand (1963).

J.C. Slater, "Barrier Theory of the Photoconductivity of Lead Sulfide", Phys. Rev. vol. 103 #6, 1631 (1956).

I.N. Stranski and R.Z. Kaischew, Z. Krist. vol. 78, 373 (1931) (in German).

S.M. Sze, Physics of Semiconductor Devices, Wiley (1969).

S.M. Sze and J.C. Irvin, "Resistivity, Mobility and Impurity Levels in GaAs, Ge and Si at 300°K", Solid-State Elec. vol. 11, 599 (1968).

L.M. Terman, "An Investigation of Surface States at a Silicon/Silicon Oxide Interface Employing Metal-Oxide-Silicon Diodes", Solid-State Electronics vol. 5, 285 (1962).

C.D. Thurmond, "Phase Equilibria in the GaAs and GaP Systems" J. Phys. Chem. Solids vol. 26, 785 (1965).

A.C. Tickle, Thin-Film Transistors A New Approach to Microelectronics, Wiley (1969).

J.J. Tietjen and J.A. Amick, "Preparation and Properties of Vapour Deposited $GaAs_{1-x}P_x$ Using Arsine and Phosphine", J. Electrochem. Soc. vol. 113 #7, 727, (1966)

J.J. Tietjen, M.S. Abrahams, A.B. Dreeben and H.F. Gossenberger, "The Origin of Macroscopic Surface Imperfections in Vapour-Grown GaAs", 1968 Symposium on GaAs, Dallas, Inst. Phys. and Phys. Soc. Conf. Series #7, (1968).

N.J. Tighe, "Jet Thinning Device for Preparation of Al_2O_3 Electron Microscope Specimens", Rev. Sci. Inst. vol. 35, 520 (1964).

A.B. Torrens, "Negative Differential Conductivity Effects in Semiconductors", Ph.D. Thesis,Dept. of Electrical Engineering,,U.B.C. (1969).

H.C. Torrey and C.A. Whitner, Crystal Rectifiers, McGraw-Hill (1948).

T.W. Tucker, "The Electrical Properties of Evaporated Silicon Films", M.A.Sc. Thesis, Dept. of Electrical Engineering, U.B.C. (1966).

H.J. van Daal, "Mobility of Charge Carriers in SiC", Philips Res. Rept. Supp. (1965).

L.J. van der Pauw, "A Method of Measuring Specific Resistivity and Hall Effect of Discs of Arbitrary Shape", Philips Res. Rept. vol. 13 #1, (1958).

J. van Laar and J.J. Scheer, "Influence of Volume Dope on Fermi Level Position at Gallium Arsenide Surfaces", Surf. Sci. vol. 8, 342 (1967).

J.R. Volger, "Note on the Hall Potential Across an Inhomogeneous Conductor", Phys. Rev. vol. 79, 1023 (1950).

B.E. Warren and B.L. Averbach, "The Effect of Cold-Work Distortion on X-Ray Patterns", J. App.Phys.,vol. 21, 595 (1950).

A. Waxman, V.E. Henrich, F.V. Shallcross, H. Borkan and P.K. Weimer, "Electron Mobility Studies in Surface Space-Charge Layers in Vapour-Deposited CdS Films", J. App. Phys. vol. 36 #1, 168 (1965).

A. Waxman and K.H. Zaininger, "Al_2O_3-Silicon Insulated Gate Field Effect Transistors", App. Phys. Lett. vol. 12 #13, 109 (1968).

L.R. Weisberg, F.D. Rosi, P.G. Herkart, Properties of Elemental and Compound Semiconductors, Met. Soc. Conf. vol.5, Interscience (1960).

P.K. Weimer, "The Insulated-Gate Thin-Film Transistor", Physics of Thin Films vol. 2, G. Hass and R. Thun (editors), AP (1964)

G.A. Wolff, "Faces and Habits of Diamond Type Crystals", Am. Mineralogist vol. 41, 60 (1956).

E. Yon, W.H. Ko and A.B. Kyser, "Sodium Distribution in Thermal Oxide on Silicon by Radiochemical and MOS Analysis", IEEE vol. ED-13, 276 (1966).

L. Young, Anodic Oxide Films, AP (1961).

K.H. Zaininger and A.S. Waxman, "Radiation Resistance of Al_2O_3 MOS Devices", IEEE vol. ED-16 #4, 333 (1969).

APPENDIX 4.1 CARRIER TRANSPORT IN SEMICONDUCTORS

A4.1.1 The Boltzmann Transport Equation

At steady state, the Boltzmann equation for the distribution function $f(\bar{k},\bar{r})$ of carriers in a solid is given by

$$-\frac{q}{\hbar}[\bar{\mathcal{E}} + \bar{v} \times \bar{B}]\nabla_{\bar{k}} f(\bar{k},\bar{r}) + \bar{v}\cdot\nabla_{\bar{r}} f(\bar{k},\bar{r}) = [\frac{\partial f(\bar{k},\bar{r})}{\partial t}]_{scat} \qquad (A4.1)$$

For solids which have a single spherical energy surface, $\hbar\bar{k} = m^*\bar{v}$, and eqn. A4.1 can be written as

$$-\frac{q}{m^*}[\bar{\mathcal{E}} + \bar{v} \times \bar{B}]\nabla_{\bar{v}} f(\bar{v},\bar{r}) + \bar{v}\cdot\nabla_{\bar{r}} f(\bar{v},\bar{r}) = [\frac{\partial f(\bar{v},\bar{r})}{\partial t}]_{scat} \qquad (A4.2)$$

In the case of semiconductors that are at thermal equilibrium, the distribution function f is

$$f = f_o = \frac{1}{1 + e^{(E-E_F)/kT}} \qquad (A4.3)$$

for degenerate semiconductors or

$$f = f_o = e^{-[(E-E_F)/kT]} \qquad (A4.4)$$

for nondegenerate semiconductors.

When carriers suffer elastic scattering only, the rate of change of $f(\bar{k},\bar{r})$ due to scattering is given by

$$[\frac{\partial f(\bar{k},\bar{r})}{\partial t}]_{scat} = \int\{f(\bar{k}',\bar{r})[1-f(\bar{k},\bar{r})] - f(\bar{k},\bar{r})[1-f(\bar{k}',\bar{r})]\}\, Q(\bar{k},\bar{k}')d\bar{k}' \qquad (A4.5)$$

The transistion probability $Q(\bar{k},\bar{k}')$ measures the rate of transition from state $\bar{k}$ to state $\bar{k}'$. By the principle of microscopic reversibility, $Q(\bar{k},\bar{k}') = Q(\bar{k}',\bar{k})$. The expression for $[\frac{\partial f(\bar{k},\bar{r})}{\partial t}]_{scat}$ given in eqn. A4.5 cannot be simplified any further. It is usual to assume that

$$(\frac{\partial f}{\partial t})_{scat} = -\frac{f-f_o}{\tau} \qquad (A4.6)$$

where τ is the relaxation time. The physical significance of this assumption is that f would approach its equilibrium value exponentially if the external forces which were initially present were suddenly removed. All transport problems are simplified when a relaxation time due to the scattering processes

can be assumed. For most semiconductors, a relaxation time can be assumed provided that the change in energy of the carriers due to scattering is small when compared to their total energy.

A4.1.2 Isothermal Electrical Conductivity

The isothermal electrical conductivity of a uniform material is defined by

$$J_i = \sigma_{ij} \mathcal{E}_j$$

$$\overline{B} = 0 \tag{A4.7}$$

$$\frac{\partial T}{\partial t} = \nabla_{\overline{r}} T = 0$$

For small electric field, $f-f_o << 1$ and terms with $\mathcal{E}^2$ can be neglected. The distribution function f can be obtained by replacing f with f_o in the LHS of eqn. A4.1.

$$f = f_o + \frac{\tau q}{\hbar} \overline{\mathcal{E}} \cdot \nabla_{\overline{k}} f_o \tag{A4.8}$$

The electric current density is given by

$$\overline{J} = -\frac{q}{4\pi^3} \int \overline{v} \, f \, d\overline{k} \tag{A4.9}$$

$$= -q \int_o^\infty \overline{v} \, f(E) N(E) \, dE \tag{A4.10}$$

where

$$N(E) = \frac{1}{4\pi^3} \int \frac{dS}{|\nabla_{\overline{k}} E|}$$

and

$$d\overline{k} = \frac{dS \, dE}{|\nabla_{\overline{k}} E|}$$

In the case of a nondegenerate semiconductor with a single parabolic energy band, the one-dimensional conductivity is

$$\sigma_x = \frac{4 n q^2}{3\pi^{1/2} m^*} \int_o^\infty \tau \eta^{3/2} e^{-\eta} \, d\eta \tag{A4.11}$$

where

$$\eta \triangleq \frac{E}{kT}$$

$$n = \int_0^\infty f(E)\, N(E)\, dE$$

It is usual to assume that

$$\tau = \alpha E^\gamma = \alpha (kT)^\gamma \eta^\gamma \tag{A4.12}$$

Thus, eqn. A4.11 becomes

$$\sigma_x = \frac{4nq^2 \alpha (kT)^\gamma}{3\pi^{1/2} m^*} \int_0^\infty \eta^{\gamma+3/2} e^{-\eta} d\eta$$

$$= \frac{4nq^2 \alpha (kT)^\gamma}{3\pi^{1/2} m^*} \Gamma(\gamma + \tfrac{5}{2}) \tag{A4.13}$$

For the special case where a mean free path, ℓ, can be defined independent of energy, $\ell \overset{d}{=} v\tau$,

$$\tau = \left(\frac{m^*}{2}\right)^{1/2} \ell\, E^{-1/2}$$

$$\alpha = \left(\frac{m^*}{2}\right)^{1/2} \ell, \quad \gamma = -\frac{1}{2}$$

From eqn. A4.13,

$$\sigma_x = n\, q\, \mu_{drift} \tag{A4.13}$$

where

$$\mu_{drift} = \frac{4}{3} \frac{q\ell}{(3\pi m^* kT)^{1/2}} .$$

A4.1.3 Isothermal Hall Coefficient

The isothermal Hall coefficient is defined by

$$R_H = \frac{\mathcal{E}_y}{B_z J_x}$$

$$\frac{\partial T}{\partial t} = \nabla_{\vec{r}} T = 0 \tag{A4.14}$$

$$J_y = 0$$

and

$$\vec{\mathcal{E}} = \mathcal{E}_x \hat{i} + \mathcal{E}_y \hat{j}$$

$$\vec{B} = B_z \hat{k}$$

Equation A4.1 can be solved by assuming a solution of the form

$$f = f_o - \bar{v} \cdot \bar{C} \frac{\partial f_o}{\partial E} \tag{A4.15}$$

and that $f - f_o \ll 1$ and $\Pi(\bar{\mathcal{E}}, \bar{B}, \frac{\partial f_o}{\partial E})$ are negligible. Thus

$$C_x = q\tau \frac{-\mathcal{E}_x + s\mathcal{E}_y}{1 + s^2}$$

$$C_y = -q\tau \frac{[s\mathcal{E}_x + \mathcal{E}_y]}{1 + s^2} \tag{A4.16}$$

where $s \triangleq \frac{q\tau B_z}{m^*}$.

From eqns. A4.10, A4.14, and A4.16,

$$R_H = -\frac{3m^*}{2q^2 B_z} \frac{a_2}{a_1^2 + a_2^2} \tag{A4.17}$$

where

$$a_1 = \int_o^\infty \frac{E\tau}{1 + s^2} \frac{\partial f_o}{\partial E} N(E)\, dE$$

$$a_2 = \int_o^\infty \frac{sE\tau}{1 + s^2} \frac{\partial f_o}{\partial E} N(E)\, dE \tag{A4.18}$$

For a nondegenerate semiconductors with a single parabolic band and if $s^2 \ll 1$ (terms in B_z^2 or higher are negligible) eqn. A4.17 becomes

$$R_H = -\frac{3\pi^{1/2}}{4} \frac{1}{nq} \frac{\Gamma(2\gamma + \frac{5}{2})}{\Gamma^2(\gamma + \frac{5}{2})} \tag{A4.19}$$

The Hall mobility is defined by

$$\mu_H \triangleq |R_H \sigma| \tag{A4.20}$$

$$= \frac{q}{m^*} \alpha (kT)^\gamma \frac{\Gamma(2\gamma + \frac{5}{2})}{\Gamma(\gamma + \frac{5}{2})} \tag{A4.21}$$

For the special case $\gamma = -\frac{1}{2}$,

$$R_H = -\frac{3\pi}{8nq} \tag{A4.22}$$

$$\triangleq -\frac{r}{nq} \tag{A4.23}$$

References

E.H. Putley, The Hall Effect and Related Phenomena, Butterworths (1960).

S. Wang, Solid-State Electronics, McGraw-Hill (1966).

A.H. Wilson, The Theory of Metals, Cambridge (1965).

J.M. Ziman, Principles of the Theory of Solids, Cambridge (1965).

APPENDIX 5.1 POLARIZATION CURRENT OF A DIELECTRIC WITH A UNIFORM DISTRIBUTION OF ACTIVATION ENERGIES

The polarization, P, of a dielectric in which ions make field-assisted thermally-activated jumps between contiguous equilibrium sites separated by a potential barrier of height W is given by (Frohlich 1949)

$$\frac{dP}{dt} = \frac{1}{\tau}(P_s - P) \tag{A5.1}$$

where $\tau = \frac{\tau_o}{2} e^{\frac{W}{kT}}$ (relaxation time of the process) (A5.2)

τ_o = a constant equal to the inverse of the jump frequency

W = activation energy

P_s = static polarization

Assume that only one process with activation energy W is operative and that a sinusoidal field represented by $\mathcal{E} = \mathcal{E}_o e^{j\omega t}$ is applied. From eqn. A5.1 and from

$$D = \varepsilon(\omega)\mathcal{E} = \varepsilon_o\mathcal{E} + P(\omega) \tag{A5.3}$$

the polarization $P(\omega)$ is given by

$$P(\omega) = [\varepsilon(\omega) - \varepsilon_\infty]\mathcal{E} \tag{A5.4}$$

and

$$P_s = (\varepsilon_s - \varepsilon_\infty)\mathcal{E} \tag{A5.5}$$

where

$$\varepsilon_s = \varepsilon(\omega = 0)$$

$$\varepsilon_\infty = \varepsilon(\omega = \infty)$$

The dielectric constant $\varepsilon(\omega)$ is obtained by substituting eqns. A5.4 and A5.5 into A5.1 and

$$\varepsilon(\omega) = \varepsilon_\infty + \frac{\varepsilon_s - \varepsilon_\infty}{1 + j\omega\tau} \tag{A5.6}$$

or

$$\varepsilon' = \varepsilon_\infty + \frac{\varepsilon_s - \varepsilon_\infty}{1 + \omega^2\tau^2} \tag{A5.7}$$

$$\varepsilon'' = \frac{(\varepsilon_s - \varepsilon_\infty)\omega\tau}{1 + \omega^2\tau^2} \tag{A5.8}$$

Equations A5.7 and A5.8 are the Debye equations. Gevers and Dupre (1946) showed that if a nearly flat distribution of activation energies G(W) is present in the dielectric then

$$\varepsilon' = \varepsilon_\infty + (\varepsilon_s - \varepsilon_\infty) \int_o^{W_o} G(W)\, dW \tag{A5.9}$$

$$\varepsilon'' = (\varepsilon_s - \varepsilon_\infty) \frac{\pi}{2} kT\, G(W_o) \tag{A5.10}$$

where W_o is defined by

$$\frac{1}{f} = \frac{\tau_o}{2} e^{W_o/kT} \tag{A5.11}$$

and f is the frequency of the applied field.

The polarization current due to a single relaxation process is given by

$$J_P = \frac{\partial P}{\partial t} \tag{A5.12}$$

Integrating eqn. A5.1 from t = 0 gives

$$P(t) = P_s(1 - e^{-t/\tau}) \tag{A5.13}$$

therefore

$$J_p = \frac{P_s}{\tau} e^{-t/\tau} \tag{A5.14}$$

For a G(W) distribution of activation energies

$$J_p = \int_o^\infty \frac{G(W) P_s e^{-t/\tau}}{\tau}\, dW \tag{A5.15}$$

Since G(W) is assumed nearly flat, it can be evaluated at $W = W_o$ and taken out at the integral sign. From eqn. A5.2, $dW = \frac{kT}{\tau} d\tau$ and by making a change of variable, $u \triangleq \frac{t}{\tau}$, eqn. A5.15 can be simply integrated to give

$$J_p = \frac{kTG(W_o)}{t} P_s \tag{A5.16}$$

If a step field $\mathcal{E} = \mathcal{E}_o\, u(t)$ is applied

$$J_p = \frac{kTG(W_o)\, \mathcal{E}_o u(t)}{t}$$

$$\triangleq \frac{A}{t} \mathcal{E}_o u(t) \tag{A5.17}$$

or, using eqn. A5.10,

$$J_p = \frac{2}{\pi} \frac{\varepsilon''(\omega)}{t} \mathcal{E}_o u(t) \tag{A5.18}$$

APPENDIX 6.1 COMPUTED CAPACITANCE-VOLTAGE CURVES FOR AN IDEAL METAL/Al_2O_3/GaAs MIS CAPACITOR

The following plots are capacitance-voltage (C-V) curves for an ideal metal/Al_2O_3/GaAs MIS capacitor computed by using the equations given in Chapter 6 for the 4 approximations. The acronyms for the different approximations are

(1) DEPLET - the depletion approximation

(2) LOFREQ - the low frequency approximation

(3) HIFREQ - the high frequency approximation

(4) FREDEP - the low frequency approximation modified by the presence of frequency dependent traps.

Dopant concentration in GaAs(N) and insulator thickness (XO) were the parameters used in cases 1, 2 and 3. In case 4, the added parameters were frequency factor (f) and the density of "fast" surface states (NS).

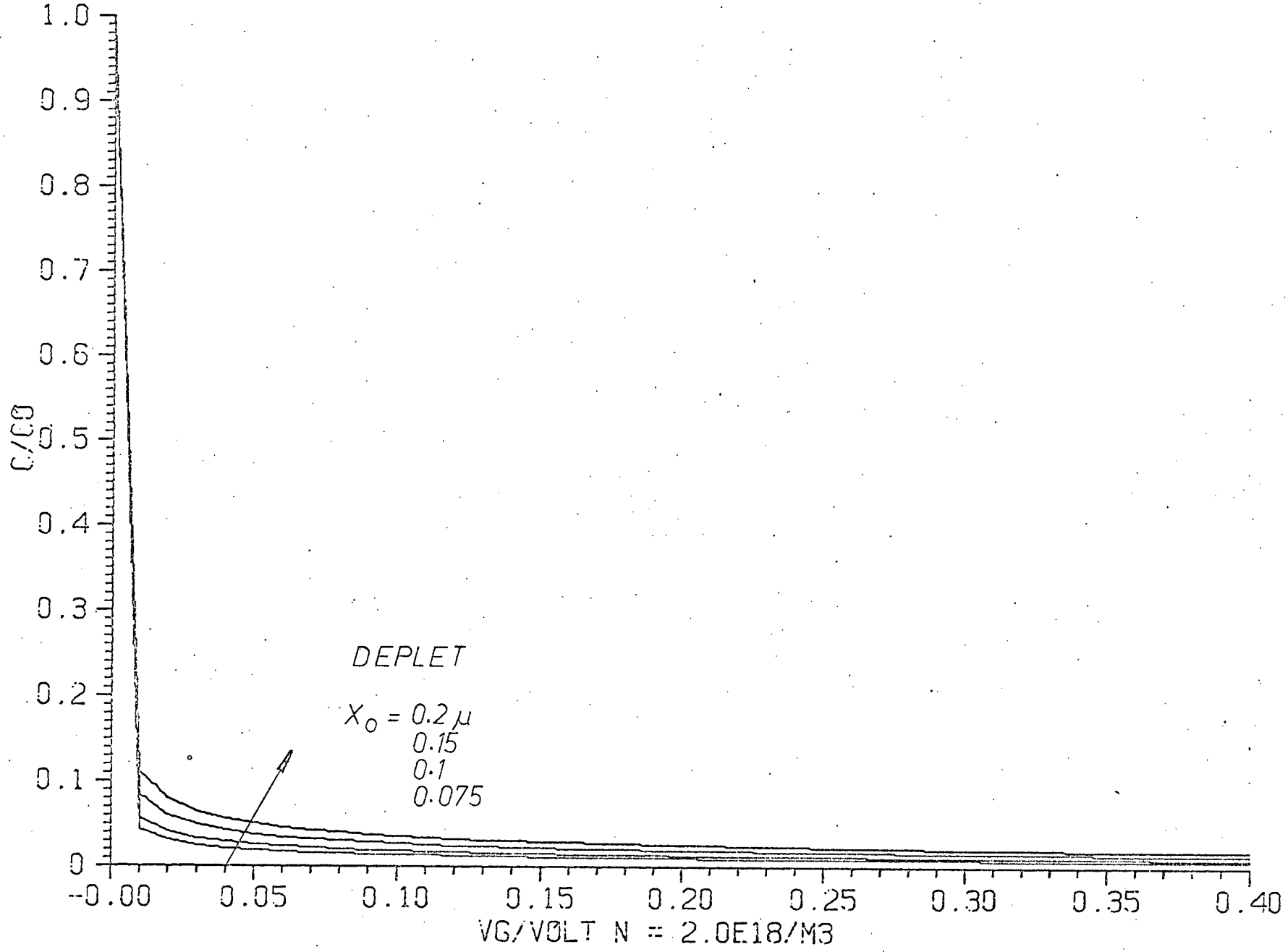
1.0
0.9
0.8
0.7
0.6
0.5
0.4
0.3
0.2
0.1
0
C/C0
DEPLET
X0 = 0.2 μ
0.15
0.1
0.075
-0.00
0.05
0.10
0.15
0.20
0.25
0.30
0.35
0.40
VG/VOLT N = 2.0E18/M3

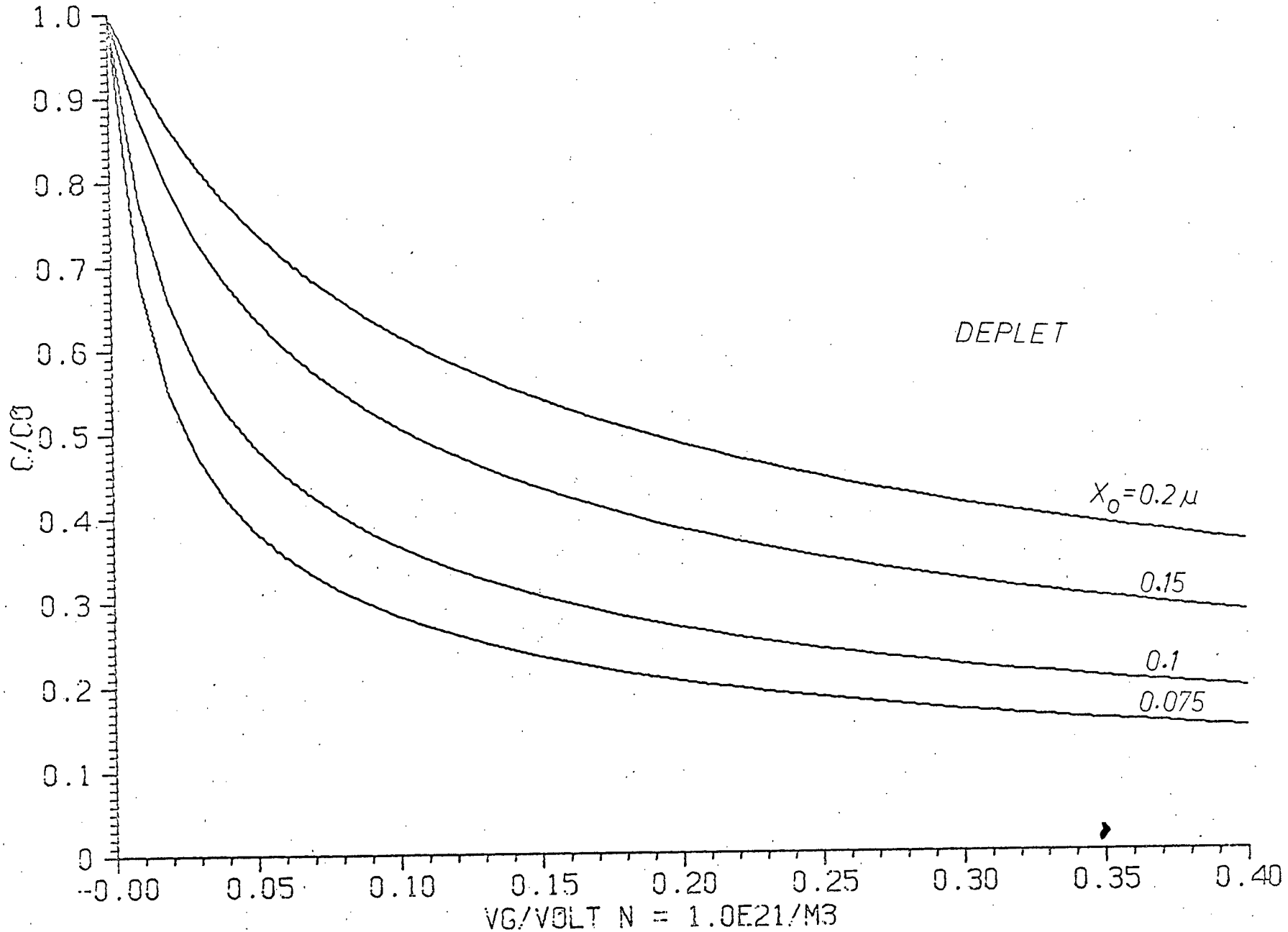
1.0
0.9
0.8
0.7
0.6
0.5
0.4
0.3
0.2
0.1
0
C/C0
DEPLET
X_0=0.2 μ
0.15
0.1
0.075
-0.00
0.05
0.10
0.15
0.20
0.25
0.30
0.35
0.40
VG/VOLT N = 1.0E21/M3

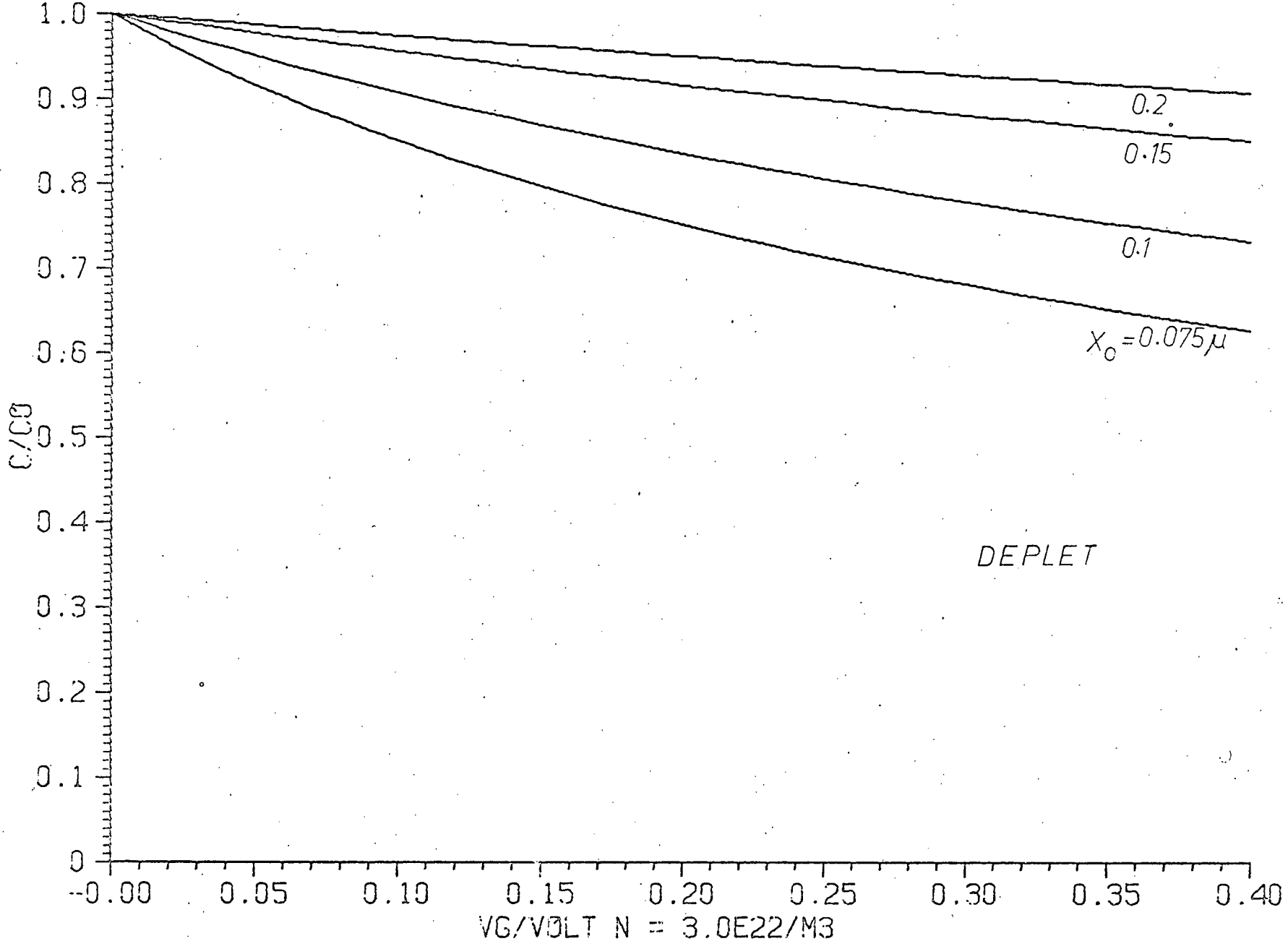
1.0
0.9
0.8
0.7
0.6
0.5
0.4
0.3
0.2
0.1
0
C/C0
0.2
0·15
0.1
$X_0 = 0.075\mu$
DEPLET
-0.00
0.05
0.10
0.15
0.20
0.25
0.30
0.35
0.40
VG/VOLT N = 3.0E22/M3

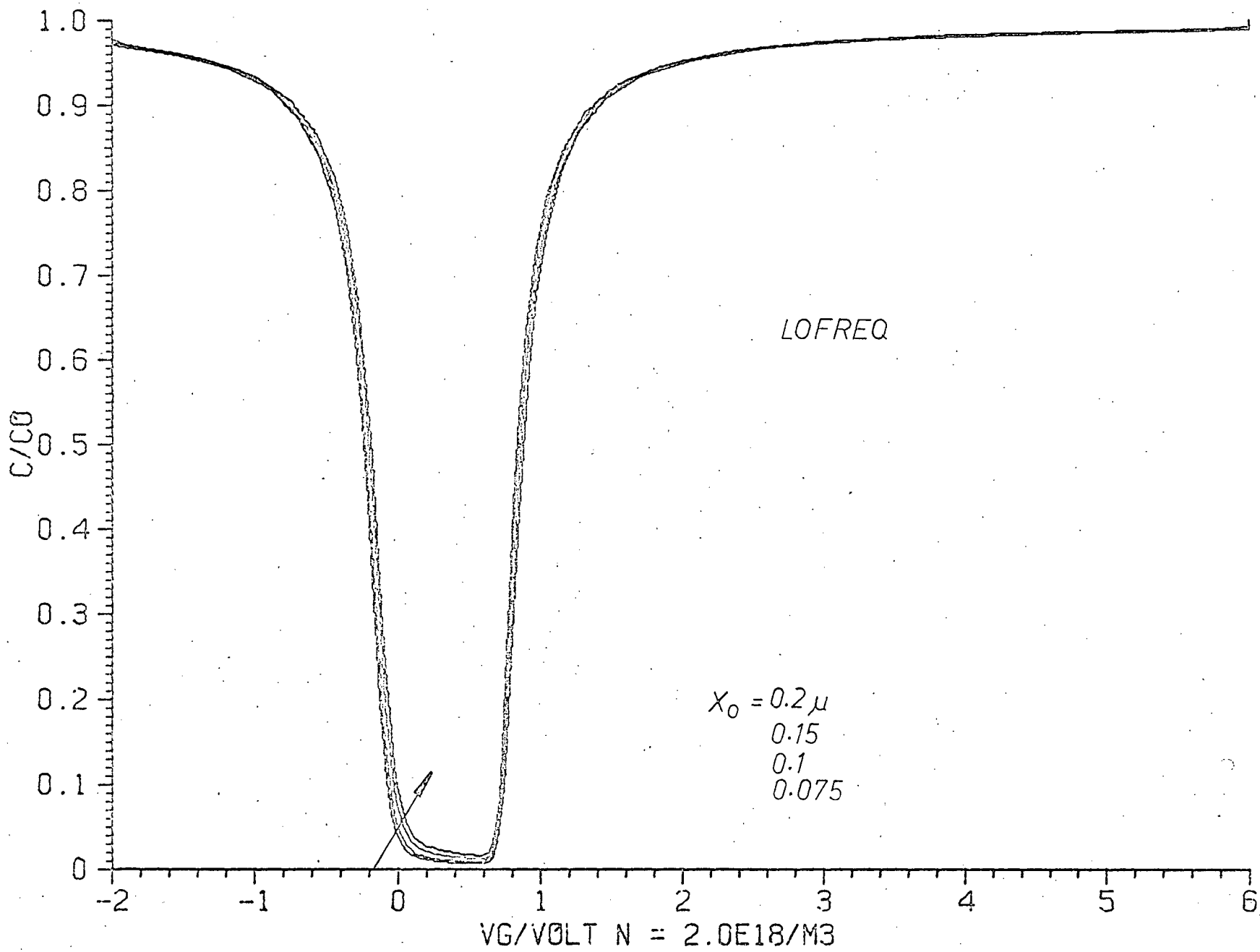
1.0
0.9
0.8
0.7
0.6
0.5
0.4
0.3
0.2
0.1
0
C/C0
-2
-1
0
1
2
3
4
5
6
VG/VOLT N = 2.0E18/M3
LOFREQ
X_0 = 0.2 μ
0.15
0.1
0.075

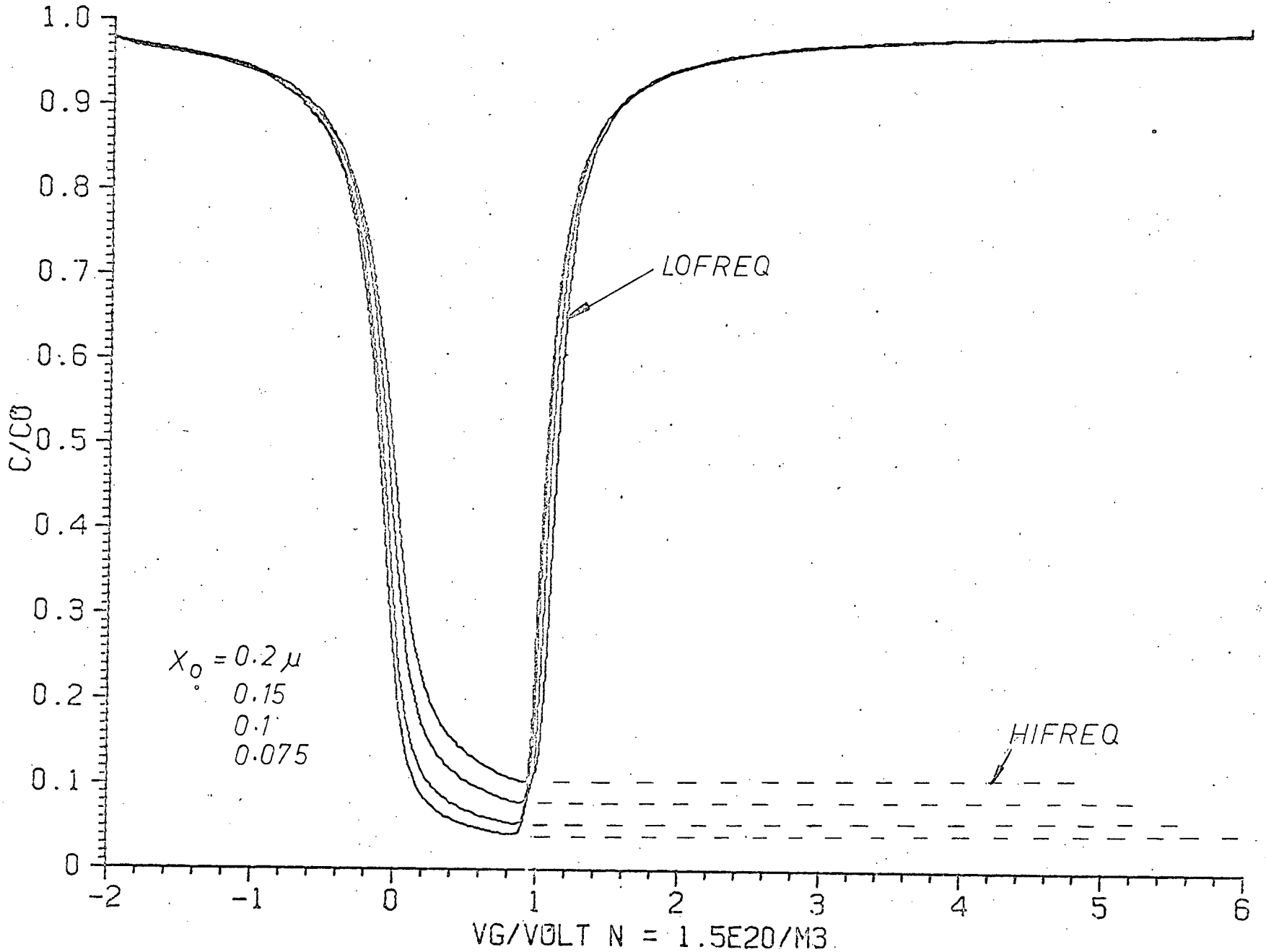
1.0
0.9
0.8
0.7
0.6
0.5
0.4
0.3
0.2
0.1
0
C/C0
LOFREQ
HIFREQ
X_0 = 0.2 μ
0.15
0.1
0.075
-2
-1
0
1
2
3
4
5
6
VG/VOLT N = 1.5E20/M3

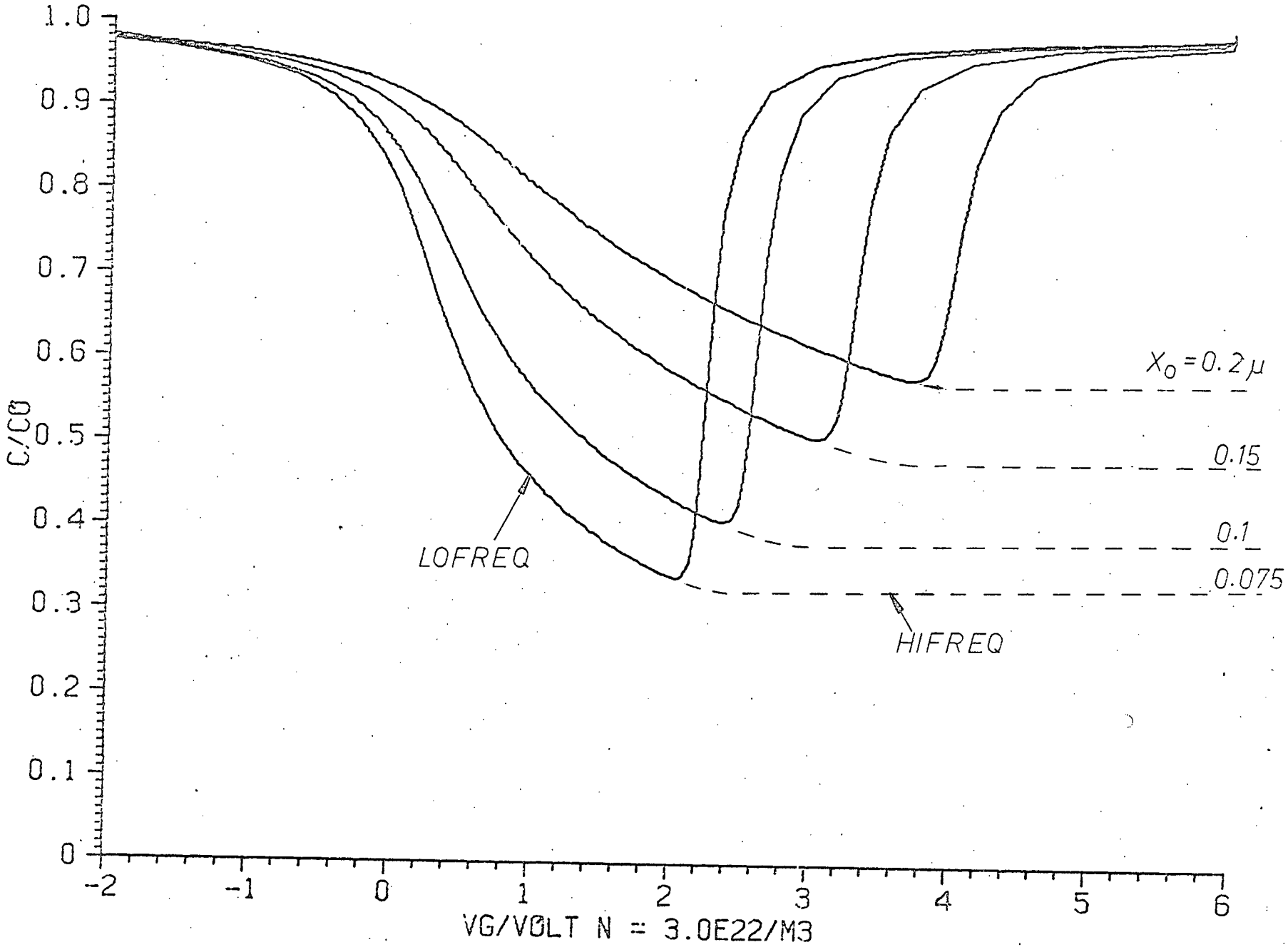
1.0
0.9
0.8
0.7
0.6
0.5
0.4
0.3
0.2
0.1
0
C/C0
-2
-1
0
1
2
3
4
5
6
VG/VOLT N = 3.0E22/M3
$X_0 = 0.2\mu$
0.15
0.1
0.075
LOFREQ
HIFREQ

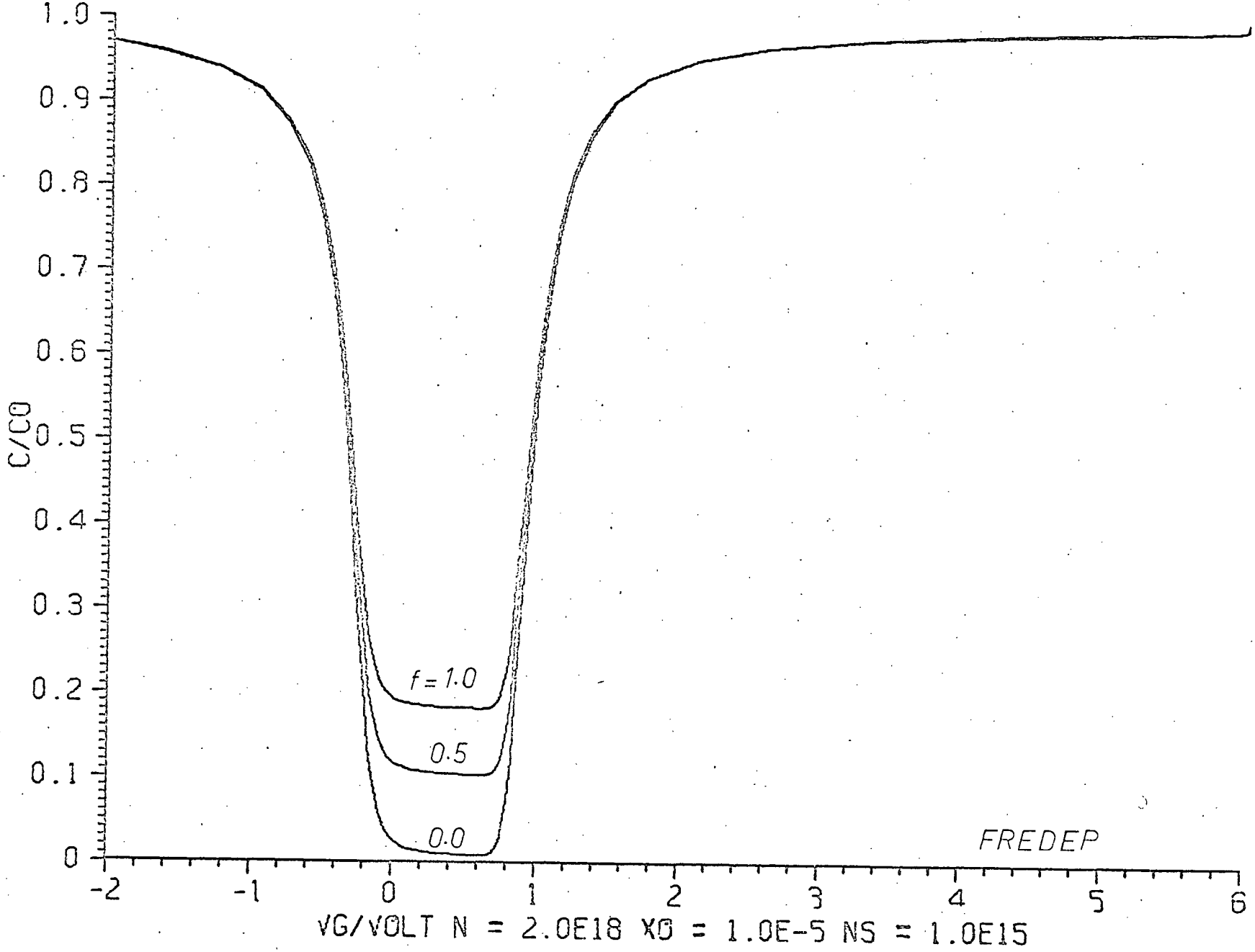
1.0
0.9
0.8
0.7
0.6
0.5
0.4
0.3
0.2
0.1
0
C/C0
f = 1.0
0.5
0.0
FREDEP
-2
-1
0
1
2
3
4
5
6
VG/VOLT N = 2.0E18 XO = 1.0E-5 NS = 1.0E15

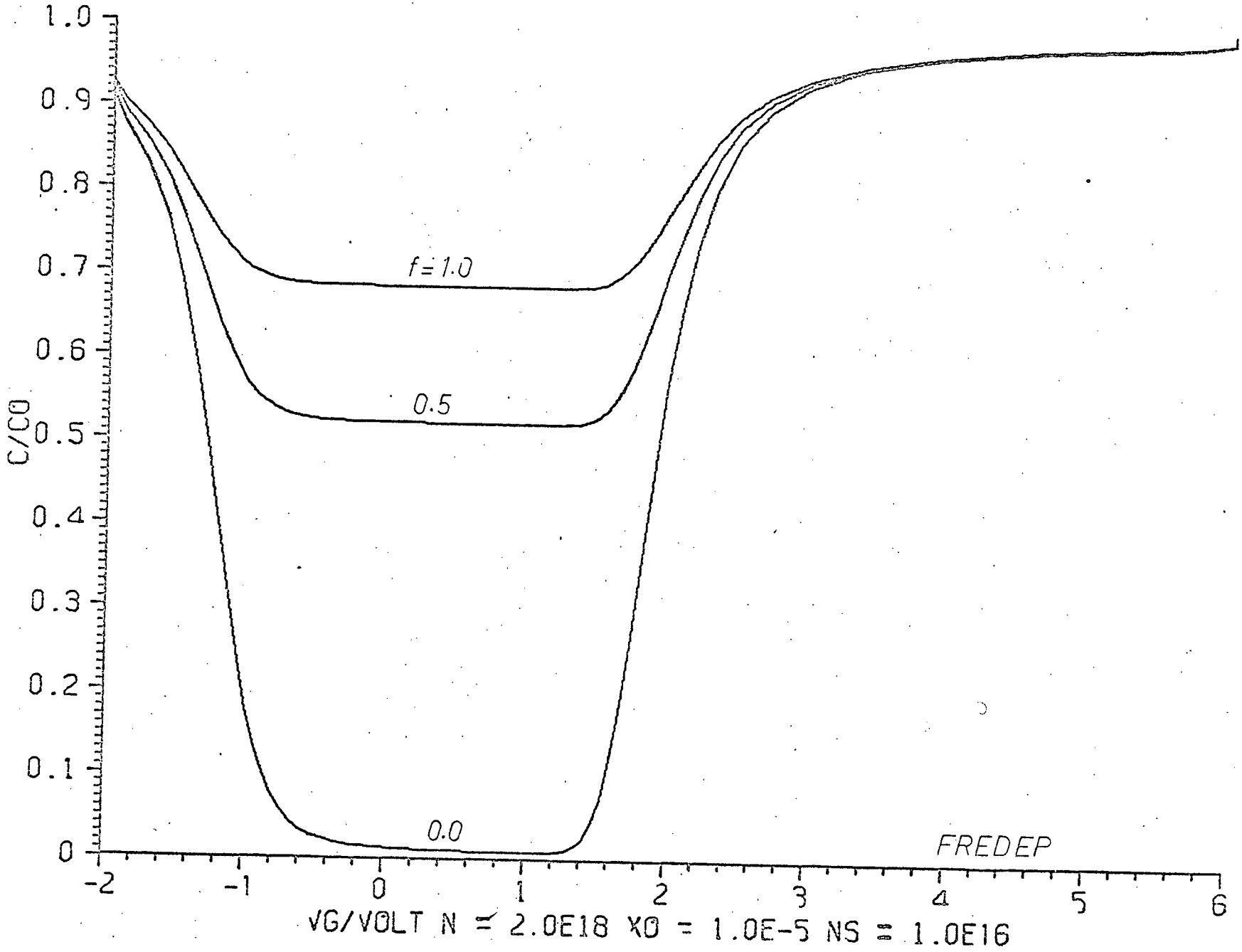
1.0
0.9
0.8
0.7
0.6
0.5
0.4
0.3
0.2
0.1
0
C/C0
f=1.0
0.5
0.0
FREDEP
-2
-1
0
1
2
3
4
5
6
VG/VOLT N = 2.0E18 XO = 1.0E-5 NS = 1.0E16

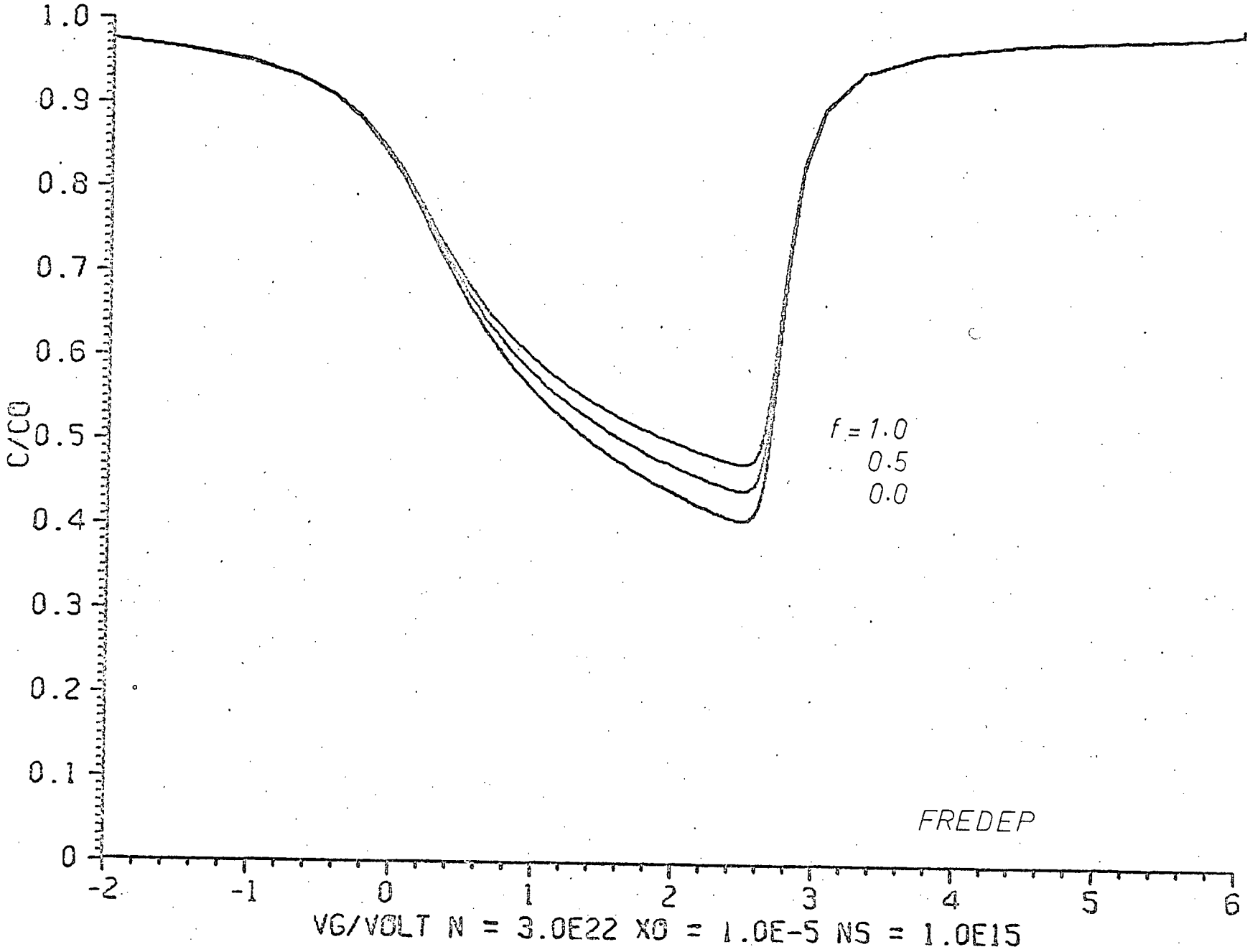
1.0
0.9
0.8
0.7
0.6
0.5
0.4
0.3
0.2
0.1
0
C/C0
f = 1.0
0.5
0.0
FREDEP
-2
-1
0
1
2
3
4
5
6
VG/VOLT N = 3.0E22 XO = 1.0E-5 NS = 1.0E15